NO_x Storage−Reduction Catalysis: From Mechanism and Materials Properties to Storage−Reduction Performance

Sounak Roy and Alfons Baiker*

Department of Chemistry and Applied Biosciences, ETH Zurich, Hönggerberg, HCI, CH-8093 Zurich, Switzerland

Received October 25, 2008

Contents

1. Introduction

Vehicular engines operating under lean burn conditions are becoming more popular than conventional Otto gasoline engines, running at a chemically correct (stoichiometric) air to fuel ratio (≈14.7:1), mainly because of their higher fuel efficiency and thus lower CO_2 emission. However, the toxic NO_x exhaust gas components of lean-burn engines, which operate at air to fuel ratios higher than stoichiometric (>14.7:1), cannot be efficiently removed with the classical three-way catalyst, because NO_x reduction with this system is not efficient under lean operating conditions. Figure 1 illustrates the different sources of NO_x in the U.S. and in European countries.[1,2]

The NO_x emitted from the exhausts have manyfold devastating effects on the atmosphere and ecosystems (such as ozone layer depletion and acid rain) and also on human health. As emerges from Figure 1, NO_x emission from mobile sources contributes almost half of all NO_x produced, and consequently, rigorous legislation was introduced for vehicular emission. Amendments to the U.S. Federal Clean Air Act in 1990 set two standards (Tire 1 and 2) for light duty vehicles. Tire 1 standards were published as a final rule on June 1991 as standards and phased in progressively between 1994 and 1997, and Tire 2 standards were adopted in December 1999 and implemented from 2004 to 2009. California has the most stringent emission regulations, and the regulation Low Emission Vehicles II became effective in 2004. Figure 2a portrays the emission limits of Tire 1 and California Ultra Low Emission Vehicles II.[3] The European Union has the fourth lowest level of emission limits for gasoline and diesel powered passenger cars in effect from 2005 onward, and recently they have approved Euro V (effective from 2009 to 2011) and Euro VI (effective from 2014 to 2015) regulations, under which NO_x emission standards are more stringent (0.175 and 0.08 g km^{-1} for Euro V and Euro VI, respectively) (Figure 2b).[4]

To meet the criteria of changing stringent emission limits, engineers, catalysis researchers, and environmental scientists are challenged to develop more efficient engines and better deNO_x techniques.[5] Under the lean operating conditions, the traditional three-way catalysts are ineffective for NO_x treatment and it is a challenge for researchers to remove NO_x from this oxidizing environment. NO_x can be removed from lean-burn exhaust mainly by three ways: (i) direct decomposition of NO; (ii) selective catalytic reduction (SCR); and (iii) NO_x storage and reduction (NSR). The first one occurs without any reductant. Although direct decomposition of NO is thermodynamically favorable ($NO \rightarrow {}^1/_2N_2 + {}^1/_2O_2$; $\Delta H^\circ_{298} = -86.6$ kJ/mol), the reaction possesses a relatively high activation energy. Cu-Zeolite is so far the best catalyst for NO_x decomposition, but its activity is very poor.[6,7] The second process, SCR, is selectively reducing NO with the reductant (like H_2, hydrocarbons (HC) and NH_3/urea) in the presence of excess oxygen. Problems inherent to HC-SCR are the low activity, narrow temperature window, and insufficient durability.[8,9] On the other hand, urea/NH_3-SCR is a promising alternative in deNO_x catalysis and is preferred for heavy-duty vehicles.[10,11] The adaption of the SCR

* To whom correspondence should be addressed. Fax: +41-44-632-1163. E-mail: baiker@chem.ethz.ch.

10.1021/cr800496f CCC: $71.50
Published on Web 05/20/2009

Sounak Roy received his Ph.D. degree from the Indian Institute of Science, India, in 2008 under the supervision of Professor M. S. Hegde. After completing his Ph.D. studies, he started his postdoctoral work with Professor Alfons Baiker at ETH in Zurich, Switzerland. His research focuses on environmental catalysis, specifically on deNO_x technologies and solid state chemistry.

Alfons Baiker (1945) studied chemical engineering at ETH Zurich and earned his Ph.D. degree in 1974. After several postdoctoral stays at different universities, he finished his habilitation at Stanford University (California) and returned to ETH in 1980, where he started his own research group focusing on heterogeneous catalysis and reaction engineering at the Department of Chemistry and Applied Biosciences. He moved up the ranks to become Full Professor in 1990. His research interests, documented in more than 770 publications in refereed journals and numerous patents, are centered around catalyst design and novel catalytic materials, mechanisms, and kinetics of catalytic surface processes, asymmetric hydrogenation, selective oxidation, environmental catalysis, chiral surfaces, in situ spectroscopy, and the application of supercritical fluids in catalysis. He has supervised over 100 Ph.D. students and 70 postdoctoral fellows. His goal is to further the scientific basis needed for developing environmentally benign chemical processes which make optimal use of raw materials and energy.

technology to diesel engines results in a complex exhaust aftertreatment system consisting of a diesel oxidation catalyst, a NH_3 dosing unit, the SCR catalyst, and finally, a NH_3 oxidation catalyst. For the NH_3 production, urea is usually stored in an additional tank and hydrolyzed after injection into the exhaust pipe. DaimlerChrysler since 2005 has commercialized the urea-SCR based aftertreatment system for meeting the upcoming stringent EPA 2010 and Euro V (2009) emission standards for heavy-duty trucks under the trade name of BlueTec technology. However, carrying urea as an NH_3 source on board is problematic and adding external reductant is not cost-effective. A practical aftertreatment technology for lean burn and diesel engines is NSR, which is becoming the most popular lean-NO_x abatement technology and the catalysis technology of choice. The corresponding catalysts are also known as lean NO_x trap (LNT) or NO_x adsorber catalysts (NAC).

The development and advancement of a catalysis technology depend on the synthesis and characterization of efficient catalytic materials, understanding of the reaction mechanism, and finally proper engineering of the catalytic system. There are a few reviews on NSR, where some aspects of either the overall mechanism or specific features such as sulfur poisoning or thermal deterioration of the catalyst were reported, but only limited effort has been made to relate the materials' properties to the catalytic mechanism and performance.[12−16] To our knowledge, there exists presently no comprehensive review on NO_x storage−reduction catalysis,[17] where the importance of the material properties of the solid catalyst, such as chemical composition, structure, and morphology have been elucidated and related with the mechanism and performance of the storage−reduction process. In this review, at first, a brief overview is provided on the general features and mechanism of NSR catalysts (sections 2 and 3). Later on, in section 4 we thoroughly discuss the role played by the noble metals, storage components, and support oxides in the reaction mechanism. Critical issues such as the local distribution of the red-ox sites and storage components, the role of chemical and structural promoters, and also the importance of the different preparation method of the catalyst will be addressed. The different NSR paths depending on the feed gas composition, the theoretical approach toward evaluation of the mechanism, and reaction engineering aspects such as the influence of different reactor configuration are considered in sections 5, 6, and 7, respectively. Finally, major conclusions are drawn and research needs and some open questions will be addressed.

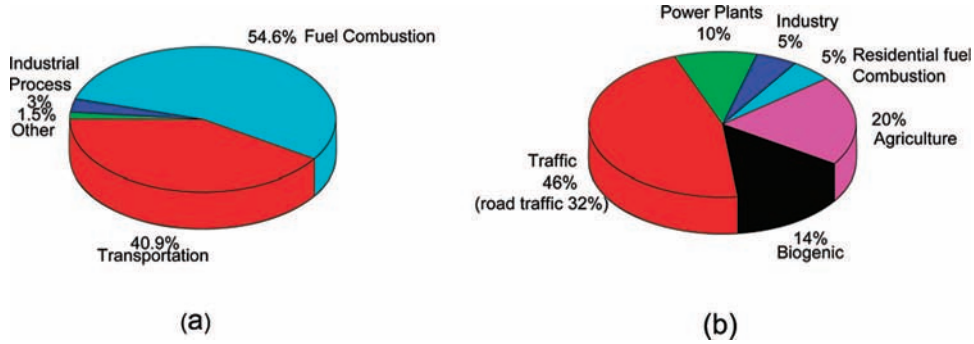

Figure 1. Illustration of emission of NO_x by source category in (a) the USA and (b) European Countries. Redrawn with permission from ref 1. Copyright 2006 American Chemical Society.

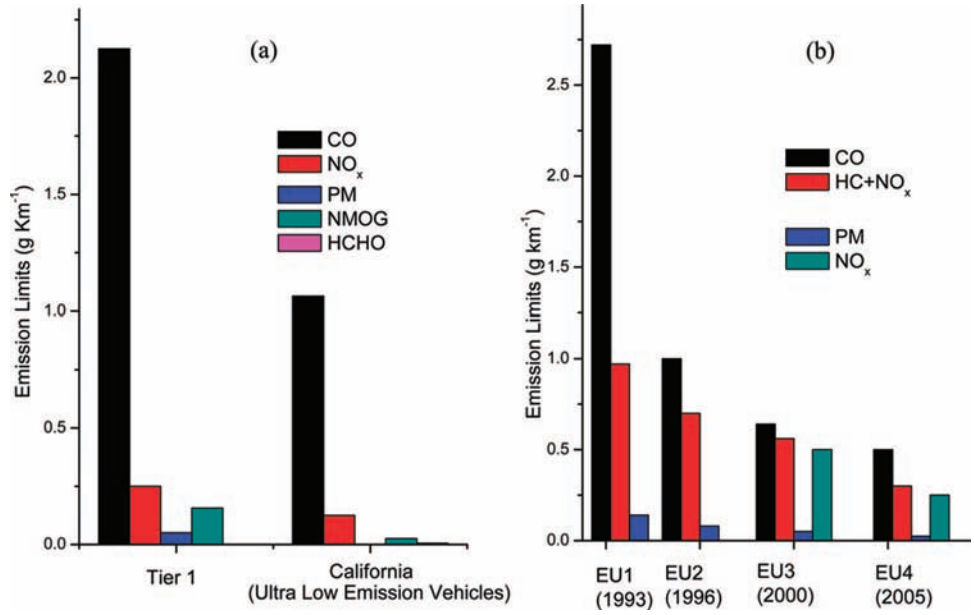

Figure 2. Emission limits for diesel-powered passenger cars in (a) the USA and California and (b) Europe [PM = particulate matter, NMOG = nonmethane-organic-gases, HCHO = formaldehyde].

2. General Features of NSR Catalysts

NO_x storage−reduction catalysts work under cyclic conditions of fuel lean and fuel rich environments. Toyota laboratories brought up this concept of NSR in the mid-1990s.[18−20] Alternating lean/rich conditions are employed during normal driving. Under lean conditions of engines, when oxygen is in excess (i.e., $\lambda > 1$; λ is an alternative way to define the air to fuel ratio during combustion, at stoichiometric conditions of engine $\lambda = 1$, corresponding to an air to fuel ratio of 14.7:1), NO_x is adsorbed on the catalyst, and under rich conditions, when the reductants evolve ($\lambda < 1$), NO_x reduction takes place. Consequently, in principle, an NSR catalyst should have sites for NO_x sorption (alkali metal or alkaline earth metal compounds) and sites for NO_x oxidation/reduction (noble metals).[21] Many of the literature studies have used Ba-based storage materials.[22−24] Generally, the Ba-loading varies from 8 to 20%. Other alkali metals such as Na and K or alkaline earth metals such as Mg, Sr, and Ca are also used.[13,25−27] Thermodynamic evaluation and reaction data demonstrate that the basicity of the alkali/alkaline earth metal components is directly related to the NO_x trapping performance, and thus, the storage component performance was found to decrease in the following order when testing was performed at 350 °C; K > Ba > Sr ≥ Na > Ca > Li ≥ Mg.[13,28] The precious metals are used generally in a very low amount: 1−2% (w/w). Pt,[13] Pd,[29] and Rh[29,30] are commonly in use as NSR catalysts. Besides several other functions (steam reforming or partial oxidation of hydrocarbons, water gas shift, CO oxidation), which will be addressed in section 5, these precious metals are mainly involved in two important steps of the NSR mechanism, one is the oxidation of NO under lean conditions and the other is the reduction of the stored NO_x under rich conditions. Generally, it has been reported in the literature that Pt is a good catalyst for NO oxidation, whereas Pd or Rh show higher NO_x reducing activity.[13] Bimetallic NSR catalysts such as Pd/Rh and Pt/Rh are also applied.[26,31,32] The alkaline earth metal oxides and the noble metals are generally dispersed over high surface area carriers. These supports could be like single oxides (Al_2O_3, ZrO_2, CeO_2, MgO) or mixed metal oxides (MgO−CeO_2, MgO−Al_2O_3). These materials not only have high surface area or large pore volume to disperse the noble and alkali/alkaline earth metals; they also play a role in the adsorption of NO_x, as indicated in several reports. Later we will discuss the role of each functional component in detail (section 4). One of the common NSR catalyst formulations used is Pt−Ba/Al_2O_3.[13,33] We will discuss the mechanism of this particular catalyst in the following section.

3. Mechanistic Views

The chemistry and mechanism occurring during lean and rich periods reported in the literature show overall similar common features. Nevertheless, there exist some divergent views and apparently opposite conclusions regarding the NSR mechanism, which may be due to the partly different experimental conditions applied and variations in catalytic materials prepared by different synthetic routes. For example, the rich regeneration time is a crucial parameter. Storage periods of 1−2 min followed by rich spikes of 3−5 s are typically used in real systems; some researchers practice short regeneration periods;[34−36] however, there are lots of studies regarding long rich regeneration periods compared to those of the real engines.[31,37,38] The exhaust gas composition (different reducing agents such as H_2, CO, and HCs) plays a significant role in the NSR mechanism.[29,39] The presence of CO_2 and water is also a realistic consideration during the rich period.

The NSR mechanism is generally assumed to be a five step mechanism (as depicted in Figure 3):
(a) NO oxidation to NO_2 ($\lambda > 1$);
(b) acidic NO_x sorption as nitrites or nitrates on the basic adsorption sites ($\lambda > 1$);
(c) reductants (such as hydrocarbons, CO, or H_2) evolution ($\lambda < 1$);
(d) NO_x release from the surface ($\lambda < 1$);
(e) NO_x reduction to N_2 ($\lambda < 1$).

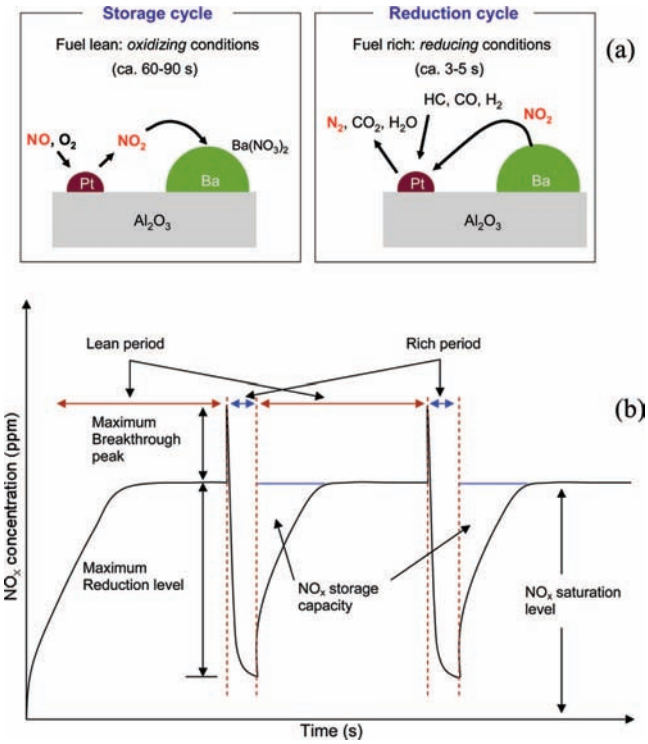

Figure 3. NO_x storage and reduction: (a) pictorial representation of the mechanism; (b) illustrative sketch of lean and rich cycles.

3.1. NO Oxidation

NSR trapping materials are generally more effective in adsorbing NO_2 than NO.[40] Therefore, NO_2 formation is a beneficial precursor step to adsorption, and this NO → NO_2 oxidation, which takes place primarily over the precious metals, is a significant step in the overall mechanism. At lower temperatures, kinetic limitations prevent the NO to NO_2 oxidation from reaching equilibrium, while, above 350 °C, the thermodynamic equilibrium is normally reached.[13,41] Olsson et al. suggested that NO oxidation over Pt−BaO/Al_2O_3 follows the Langmuir−Hinshelwood model and the presence of BaO decreases the rate of NO oxidation compared to that of Ba free catalyst.[42] However, other investigations have found NO oxidation over supported Pt catalysts to follow an Eley−Rideal type mechanism involving dissociative adsorption of O_2 and reaction of NO from the gas phase.[43] NO oxidation over fresh Pt supported on Al_2O_3 was found to be first order with respect to NO and O_2 (for aged catalyst, the order was 0.7 with respect to O_2) and negative first order with respect to NO_2 with an apparent activation energy of 81.8 ± 5 kJ mol^{-1}.[44]

3.2. NO_x Sorption

Much has been published in the early age of NSR on NO_x storage.[19,41,45] Typical NSR formulations are able to accomplish effective removal in a wide operating window. It is believed that NO_x sorption is a sequential process; at the beginning, nitrite is formed followed by nitrate formation. Fridell and co-workers proposed that the storage process involves a three-step mechanism in which NO_2 is at first loosely adsorbed on BaO as a BaO-NO_2 species; this species then decomposes to BaO_2 and NO (which is released to the gas phase), and finally Ba peroxide reacts with the gas-phase NO_2 to give Ba nitrate.[41]

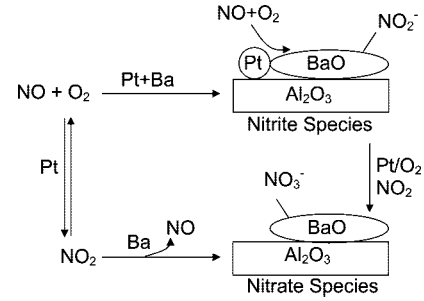

Figure 4. Two different pathways for NO_x oxidation and subsequent adsorption on Pt−Ba/Al_2O_3 catalyst. Redrawn with permission from ref 33. Copyright 2006 Elsevier B.V.

$$BaO + NO_2 \rightarrow BaO{-}NO_2 \quad (1)$$

$$BaO{-}NO_2 \rightarrow BaO_2 + NO \quad (2)$$

$$BaO_2 + 2NO_2 \rightarrow Ba(NO_3)_2 \quad (3)$$

Forzatti et al. have shown that, over Pt−Ba/Al_2O_3, NO in the presence of excess oxygen proceeds through two parallel routes as shown in Figure 4:[33,46,47] (i) the "nitrate route", where NO is oxidized to NO_2 on Pt sites followed by NO_2 spillover on Ba sites to form Ba-nitrates with evolution of gaseous NO; (ii) the "nitrite route", where NO is oxidized on Pt sites and directly stored on Ba neighboring sites in the form of nitrites that are then oxidized to nitrates. The routes changed with the loading of Ba; with higher Ba loading the nitrite route was dominating. This was explained by the close contact of Pt and Ba sites; with increasing Ba loading, the Pt to Ba contacts were more, which lead to predominance of the "nitrite" route. In section 4, the importance of the proximity of Pt and Ba sites will be discussed thoroughly.

The kinetics of NO_2 adsorption over Pt−Ba/Al_2O_3 with the help of mean field model and flow reactor experiments has been successfully explained with the combination of the kinetic model for NO oxidation on Pt−BaO/Al_2O_3 and the model for NO_x storage on BaO/Al_2O_3.[42,48,49] But the model itself did not describe the experimental finding of NO_x desorption at low temperature in the presence of Pt. This was explained by considering the mobility or the forward and reversible spillover of NO_2 between Pt and BaO, which was also supported by the calculated entropy changes. This indicated the importance of the proximity of Pt and Ba sites as well as the importance of spillover and reverse spillover phenomena.[50−53] Reaction 2 accounts for NO slip during NO_x sorption; Kwak et al. in this regard established a different mechanism. They showed that, at the beginning of the NO_x uptake, this spillover process is very fast and provided complete NO_x storage. However, the NO_x uptake goes down when BaO in the vicinity of Pt particles is converted to $Ba(NO_3)_2$. The formation of $Ba(NO_3)_2$ around the Pt particles results in the development of a diffusion barrier for NO_2 and increases the probability of NO_2 desorption and, consequently, the beginning of NO_x slip.[53]

3.3. NO Reduction

The engine periodically shifts to lean/rich conditions. Under rich conditions, the reductants are introduced and the trapping ability of the NSR catalyst is regenerated by reduction of the trapped NO_x. The reductants are generally H_2, CO, or hydrocarbons (e.g., C_3H_6 or C_3H_8). The NO_x reduction largely depends on the reductants introduced. There

are three general methods of introduction of reductants.[13] In the first category, fuel is directly injected into the exhaust. The injected fuel on reaction with NSR catalyst (steam reforming, partial oxidation of hydrocarbons, water gas shift reaction) produces reductants. In the second category, fuel is continuously or periodically processed over an upstream reformer or partial oxidation catalyst, which would result in H_2, CO, and/or smaller hydrocarbon species production. In the third category, intermittent pulses of rich gas from the engines are exhausted to the NSR catalyst and these gases either directly contain the reductant or are processed by the NSR catalyst or an upstream catalyst to form the reductant.

In the regeneration process, the trapped NO_x is released and eventually reduced. As the release and the reduction take place in a very short time, it is difficult to analyze the two steps distinctly. According to Epling et al., there could be two primary driving forces to release NO_x from the surface.[13] First, due to the exothermic oxidation reactions, nitrite and nitrate stability decreases, and with the subsequent decomposition, evolution of NO_x takes place with increasing temperature; second, NO_x is released as a result of the introduction of the reductants. Their further studies demonstrated that the NO_x release also depends on the rate of NO_x diffusion to the precious metal sites and on the rate of NO_x reduction.[38] Depending on the temperature or the regeneration time, different nitrogen-containing byproducts have been observed. When the regeneration time was very small, evolution of NO was not complete and NO and NO_2 were observed in the outlet, whereas, at low temperature (200−300 °C) and long regeneration time, N_2O and NH_3 were detected due to reduction.[38,54] Sakamoto et al. showed that between 230 and 310 °C rate constants for NO_x release and NO_x reduction were about the same; however, above 360 °C, the rate constant for NO_x release was higher than that of NO_x reduction.[55]

The stored NO_x is reduced by the reducing gas evolving under rich conditions of engines, which is actually a very short time of a few seconds. The reductants are generally H_2, CO, or small or long chain hydrocarbons. Variation of reducing gases controls the product selectivity.[56,57] CO or hydrocarbons can reduce the trapped NO_x either directly in the storage component of the catalyst to form N_2,

$$Ba(NO_3)_2 + 5CO \rightarrow N_2 + BaO + 5CO_2 \quad (4)$$

or indirectly by forming H_2 via the water gas shift (WGS) reaction, which eventually reduces NO_x. Similarly, hydrocarbons also can produce H_2 through a steam reforming reaction. H_2 is also present in the exhaust during rich engine operation. The $Ba(NO_3)_2$, which is formed during the lean cycle, reacts with the H_2 and forms the N_2 with the probable reaction stoichiometry:[33]

$$Ba(NO_3)_2 + 5H_2 \rightarrow N_2 + BaO + 5H_2O \quad (5)$$

The selectivity to appropriate products is an important aspect of NO reduction. With the expected N_2, sometimes unselective products such as N_2O and NH_3 are also formed depending on the catalyst.[37]

$$Ba(NO_3)_2 + 3H_2 \rightarrow BaO + 2NO + 3H_2O \quad (6)$$

$$Ba(NO_3)_2 + 4H_2 \rightarrow BaO + N_2O + 4H_2O \quad (7)$$

$$Ba(NO_3)_2 + 8H_2 \rightarrow BaO + 2NH_3 + 5H_2O \quad (8)$$

Clayton et al. depicted the stored NO_x reduction by H_2 comprising five paths (Figure 5); *Path 1* is direct reduction

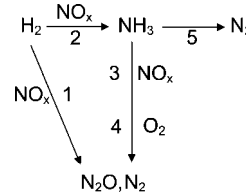

Figure 5. Reaction network comprising five steps during reduction of stored NO_x by H_2. Reprinted with permission from ref 58. Copyright 2008 Elsevier B.V.

of NO_x to N_2 (reaction 5), *Path 2* is reduction of NO_x to NH_3 (reaction 8), *Path 3* is reduction of stored NO_x by NH_3, *Path 4* is oxidation of NH_3 to N_2 ($4NH_3 + 3O_2 \rightarrow 2N_2 + 6H_2O$), and *Path 5* is decomposition of NH_3 to N_2 ($2NH_3 \rightarrow N_2 + 3H_2$).[58] It has been observed that H_2 is a better reductant compared to CO, which in turn is better than C_3H_6 and C_3H_8.[37] The influence of the reducing gas composition on release and reduction of trapped NO_x over various catalysts will be discussed in detail later (section 5).

The above discussion summarizes an overall mechanism for NSR. Although numerous studies have been carried out with the standard catalyst formulation ($Pt-Ba/Al_2O_3$) to evaluate the mechanistic aspect, a practical problem remains, sulfur poisoning.[59−64] Sulfur poisoning of NSR catalysts can generally originate from two different pathways. SO_2 in the exhaust gas can be oxidized on precious metals and reacts with the support, forming aluminum sulfate, or SO_x reacts with the NO_x storage component to form barium sulfate. Because sulfates are more stable than nitrates, they deteriorate the NO_x adsorption, thus deactivating the catalyst. Kim et al. showed BaO, depending on its conditions of activation (i.e., oxidizing or reducing), can form $BaSO_4$ or $BaSO_3$, respectively, even in the absence of Pt.[65] Pt−O bonds and the coordination environment of Pt also play an important role in promoting the formation of sulfate species. With the advancement of the review, we will explore the ongoing research toward desulfurization.

4. Important Catalyst Components and their Role in Storage and Reduction

4.1. Noble Metals

As noble metals play several key roles in the NO_x storage and reduction cycle as well as for sulfur deactivation and for regeneration from sulfur, it is of great interest to investigate their role in detail. In the following section, we will discuss the role of the noble metals in the context of: (i) NO oxidation under lean conditions, (ii) NO_x storage capacity under rich/lean conditions, (iii) NO reduction under rich conditions, and (iv) sulfur tolerance and regenerability. It would not be adequate to compare the role of the noble metals alone in the above-mentioned sections, because there are several reports which show that by changing the supports the catalytic properties of the noble metals may also change. For example, Huang et al. observed that Rh provides better NO_x storage ability for CaO/Al_2O_3 support compared to that of Pt due to higher formation of NO_2.[66] However, several studies on Pt and Rh on Al_2O_3 showed that Rh/Al_2O_3 only can oxidize 30% of NO to NO_2.[67,68] Therefore, we will mostly try to confine the following discussion on the role of noble metals in storage and reduction to the examples of different metals over the same support.

4.1.1. Platinum

Pt loading is generally in the range of 1−2 wt % with dispersion from 20% to 80%.[69−71] The turnover frequency (TOF) of NO oxidation to NO_2 becomes 100 times greater when the Pt dispersion decreases from 82 to 4% on an alumina support.[72] The intrinsic activity of NO reduction by hydrocarbons in an oxidizing environment was found to depend on the Pt particle size and consequently dispersion, which was attributed to the correlation between particle size and the redox properties or strength of the Pt−NO bond.[73] Kim et al. also established that Pt crystallite size plays a critical role in determining the NO_x storage activity (by Ostwald ripening and particle migration and coalescence, the Pt particles sintered in the oxidizing thermal treatment and deteriorated NO_x storage activity).[74] However, detailed investigations have not been carried out on the correlation between Pt dispersion and NSR activity. A combinatorial study concluded that NO oxidation over supported Pt catalyst depends on various factors and the relative order of the importance of the factors was as follows: support > pretreatment > loading > calcination atmosphere > calcination temperature > precursor salt.[75]

NO pulsing experiments over $Pt-BaO/Al_2O_3$ in the absence of O_2 demonstrated that NO decomposed on Pt and also oxidized to NO_2 via oxygen adatoms.[70]

$$NO + Pt \rightarrow NO-Pt \quad (9)$$

$$NO-Pt + Pt \rightarrow N-Pt + O-Pt \quad (10)$$

$$NO-Pt + O-Pt \rightarrow NO_2 + 2Pt \quad (11)$$

Since NO was pulsed over the catalyst, the oxygen accumulation reduced the availability of vacant sites on Pt for NO adsorption or decomposition. But the close proximity of BaO to Pt sites promoted spillover of the oxygen adatoms from Pt to BaO, making the Pt sites free for NO.

$$O-Pt + BaO \rightarrow BaO_2 + Pt \quad (12)$$

Anderson et al. investigated the role of Pt in NO_x storage.[76] As Pt provided atomic oxygen, it facilitated the uptake of NO_x by Ba, resulting in increased NO_x storage in $Pt-BaO/Al_2O_3$ compared to BaO/Al_2O_3. *In situ* FTIR investigations of the adsorption of NO over $PtBaO/Al_2O_3$ showed that, at 350 C, Pt catalyzed the Ba-nitrate and Al-nitrate formation from nitrite species.

$$Ba(NO_2)_2 + 2O-Pt \rightarrow Ba(NO_3)_2 + 2Pt \quad (13)$$

A combined study of EXAFS and TPD showed the presence of two distinct kinds of Pt sites responsible for chemisorption of NO at low temperatures (site 1) and oxidation of NO at higher temperatures (site 2) on the surface of $PtBa/Al_2O_3$.[77]

Under rich conditions, Pt activated the hydrocarbons, promoting the reduction of nitrate species.[78] Abdulhamid et al. prepared $Pt-BaO/Al_2O_3$ by an impregnation method on cordierite with a surface area of around 20 m^2/g.[29,37] Pt had a good H_2 activation ability,[79] and the stored NO_x was reduced at a low temperature of 150 °C. In another work, these authors showed that, when using CO as reducing agent, the interaction between NO_2 and Pt was suppressed due to strong interaction between CO and Pt, and therefore NO_x reduction was deactivated over this catalyst.[80] The authors did not discuss the exact role of the materials or the nature of Pt sites in detail, but similar results were also observed by Szailer et al., who provided a detailed reaction mechanism based on FTIR and time-resolved X-ray diffraction studies.[81] At low temperatures (<150 °C), in the presence of H_2 as a reductant, the activated H_2 reacted with the adsorbed O_2 on the Pt surface, forming H_2O and empty Pt sites, which in turn decomposed the adsorbed surface nitrates. When CO was used as a reductant at low temperature (<150 °C), NCO and CO_2 were formed; however, at higher temperatures (>300 °C), NCO directly reacted with the stored NO_x and formed N_2. Olsson and Fridell showed that during NO oxidation and NO_2 dissociation on Pt/Al_2O_3 or $Pt-BaO/Al_2O_3$, metallic Pt can be oxidized to Pt^{2+} (PtO) or Pt^{4+} (PtO_2) and the catalytic activity decreased.[82] They also concluded that oxidation of Pt is less for Pt/Al_2O_3 compared to that of $Pt-BaO/Al_2O_3$, because Al_2O_3 is acidic in nature as well as electrophilic and the 5d band in Pt donated electron density to the support. Further, electrons are transferred from Pt to oxygen when platinum oxide is formed, and in the case of an acidic support, there was a lower electron density in Pt, which gave less platinum oxide. BaO, on the other hand, is alkaline and influenced platinum in the opposite way; thus, more platinum oxide was formed. Recently, it is believed to be a two-step reduction mechanism of stored NO_x with H_2 over $Pt-Ba/Al_2O_3$, where NH_3 is an intermediate.[58,71,83,84] At very low temperatures (<60 °C), the trapped NO_x is reduced by H_2 to form primarily NH_3 (reaction 8, $\Delta G^\circ = -900$ kJ/mol), and at higher temperatures, the as-formed NH_3 reduces the stored nitrates.

$$3Ba(NO_3)_2 + 10NH_3 \rightarrow 8N_2 + 3BaO + 15H_2O \ (\Delta G^\circ = -625 \text{ kJ/mol}) \quad (14)$$

The catalytic performance and the structural properties related to it are quite dependent on the nature of the metal precursor as well as on the synthetic route. Dawody et al. synthesized $Pt-BaCO_3/Al_2O_3$ from four different Pt precursors: H_2PtCl_6, $Pt(NH_3)_4(OH)_2$, $Pt(NH_3)_2(NO_2)_2$, and $Pt(NO_3)_2$.[85] Among these four catalysts, the one prepared from $Pt(NO_3)_2$ showed the highest NSR activity followed by the catalyst derived from $Pt(NH_3)_4(OH)_2$. Differences in catalytic activities were attributed to different interactions, such as electrostatic interaction and ion-exchange and ligand-exchange interactions between the Pt-precursor solution and the support, and will be discussed elaborately in a latter section (section 4.5). $Pt-BaCO_3/Al_2O_3$, when synthesized by the two-nozzle flame spray pyrolysis method, was composed of primary spherical particles of alumina and barium carbonate that were aggregated to larger particles. Platinum was dispersed on both types of primary particles, whereas the same catalyst synthesized by the conventional wet impregnation method showed $BaCO_3$ deposited on the alumina support, as can be seen from Figure 6.[86,87] This difference in Pt dispersion and the stability of the $BaCO_3$ phase resulted in better NSR activity of flame spray pyrolysis synthesized $Pt-BaCO_3/Al_2O_3$ compared to corresponding catalysts prepared by wet impregnation.

SO_2, which is a detrimental component in the exhaust, when it is introduced in the feed gas, changes the catalytic properties of Pt. Amberntsson et al. surprisingly observed that the presence of SO_2 enhanced the NO_x storage ability on $Pt-BaO/Al_2O_3$.[31] Pt core level spectra of this catalyst had shown Pt in the zerovalent state. Introduction of SO_2 in the feed gas lowers the amount of Pt-oxide formation or reduces the Pt-oxides while forming Pt-sulfite or Pt-sulfate.[88] As we know from Olsson and Fridell's[82] study that metallic Pt shows higher NSR activity, it can be concluded that introduction of SO_2 in the feed gas helped keep Pt in the

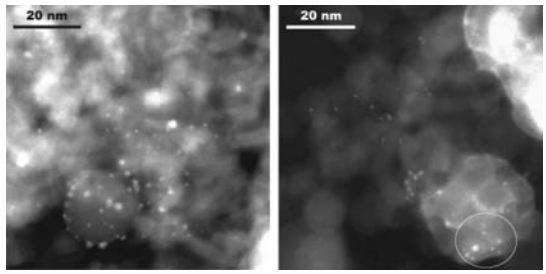

Figure 6. High-resolution STEM images showing Pt particles (bright spots) in wet impregnated Pt−$BaCO_3$/Al_2O_3 (left) and flame synthesized Pt−$BaCO_3$/Al_2O_3 (right). In the flame made catalyst (right), Pt particles are discernible on both Ba-containing (encircled) and Al_2O_3 particles. Reprinted with permission from ref . Copyright 2006 Elsevier Inc.

metallic state, which enhanced the NO_x storage due to higher NO oxidation activity.

Pt is mostly used by the researchers for NSR activity. From the above discussion it emerges that the loading, size distribution, and dispersion of the Pt particles play a significant role in the red/ox mechanism. However, other factors such as precursor salt, oxidation state of Pt, support interaction, and distance from the storage site of Pt have also been identified to be crucial factors for achieving high NSR activity.

4.1.2. Palladium

Recently, investigations have started using Pd as a metal of choice for NSR catalysis because of its manifold catalytic activities.[29,80,89] First of all, Pd exhibits high three-way catalytic activity (i.e. both oxidation and reduction reactions are catalyzed under stoichiometric conditions), and it has been reported that Pd works better than Pt and may be an important alternative to Pt in NSR catalysis.[90−92] Pd also shows a good thermal stability, and the interconversion of the $Pd^{2+} \leftrightarrow Pd^0$ system is easier due to the lower redox potential of Pd^{2+}/Pd^0 compared to Pt^{2+}/Pt, resulting in structural and catalytic activity changes under lean and rich conditions.[91,93] Also, Pd is less expensive compared to Pt and abundant among the precious metals. If carbon-containing reductants were used, Pd−$BaCO_3$/Al_2O_3 always was found to be a better NO_x reduction catalyst compared to its Pt counterpart.[29,80] Salasc et al. carried out a comprehensive comparative investigation between the NSR activities of Pd−BaO/Al_2O_3 and Pt−BaO/Al_2O_3.[89] Both catalysts were synthesized by conventional impregnation methods on cordierite. At relatively low temperature (300 °C), Pd−BaO/Al_2O_3 had a higher NO_x storage capacity than Pt−BaO/Al_2O_3; that is, more NO_x was stored during the lean periods and almost all the NO_x was reduced during the subsequent rich periods. The core level XPS of Pd ($3d_{5/2}$) showed Pd^{2+} and Pd^0 in lean and rich conditions, respectively, whereas Pt ($4f_{7/2}$) showed only metallic Pt under both reaction conditions. The better NSR activity of the Pd catalyst was attributed to the easier convertibility of $Pd^{2+} \leftrightarrow Pd^0$. Transient reactor and *in situ* FTIR studies using C_3H_6 as a reductant over Pd−BaO/Al_2O_3 showed a higher NSR catalytic activity compared to Pt−BaO/Al_2O_3.[94] Between 250 and 375 °C, the Pd catalyst showed higher overall NO_x reduction efficiency due to (i) higher activity for the oxidation/activation of propylene and (ii) higher activity for the formation of surface nitrite species. The interaction of the noble metal with the storage component and support oxide also plays a crucial role for the catalytic activity, which we will discuss thoroughly in section 4.6. Briefly, when Pd was deposited on $Ba_xAl_{2y}O_{x+3y}$/Al_2O_3/NiAl(110), Pd nucleated at the $Ba_xAl_{2y}O_{x+3y}$ nanoparticles and covered them. However, when the Ba component was deposited on the Pd/Al_2O_3/NiAl(110), isolated $Ba_xAl_{2y}O_{x+3y}$ nanoparticles were formed without having any contact with Pd.[95] These structural differences resulted in different IR spectra of Pd/$Ba_xAl_{2y}O_{x+3y}$/Al_2O_3/NiAl(110) and $Ba_xAl_{2y}O_{x+3y}$/Pd/Al_2O_3/NiAl(110) taken after NO_2 sorption due to the decreasing surface area of Pd and its modification by $Ba_xAl_{2y}O_{x+3y}$.

Although it is well-known that Pt group metals produce NH_3 during reduction of NO_x by H_2, Rh has shown a promising effect in this regard. Rh not only showed the lowest NH_3 formation during reduction of NO_x, it also showed the highest reduction capability of NO_x among Pt, Pd, and Rh.[29,96] The NO_x storage capacity of Rh−BaO/Al_2O_3, however, was lowest compared to that of Pd and Pt due to lack of NO_x spillover from Rh to storage sites.[29] This difference between Rh, Pd, and Pt was explained by the different abilities of Pt, Pd, and Rh to dissociate NO, forming surface atomic nitrogen. Various other promising noble metals such as Ag and Ir have shown efficient NO_x reduction abilities in the presence of excess O_2. Ag, under lean conditions, can store NO_x as nitrites and nitrates, which are reduced by H_2.[97−99] Ir-based catalysts have been reported to be good catalysts for NO_x reduction;[100−102] however, almost no significant investigations are reported in the literature regarding catalytic usage of Ir in NSR.

4.1.3. Bimetallic Systems

There are several reports on NSR catalysts containing only Pt or Pd or Rh as a metal on support. As mentioned above, depending on the reaction conditions and the feed gas stream, different metals behave differently. For example, Pt-containing catalysts show better sulfur tolerance, whereas Pd shows higher NO_x storage ability as well as better reduction activity compared to Pt.[13,89] Therefore, currently, the role of bimetallic catalysts in NSR is an important topic of investigation.[103−108]

Pt−Rh−BaO/Al_2O_3 and Pd−Pt−BaO/Al_2O_3 showed some interesting results compared to the monometallic catalysts. The NO_x storage ability as well as oxidation under lean conditions followed the order Pt−BaO/Al_2O_3 > Pt−Rh−BaO/Al_2O_3 > Rh−BaO/Al_2O_3.[31] XPS analysis helped explain this order of NO_x storage. The Pt^0 and Rh^0 in the catalyst converted to Pt^{2+} and Rh^{3+} under lean conditions. It was observed that the surface concentration of Rh increased by 35%, whereas for Pt it decreased by 70%. This explains the observation that the NO oxidation rate under lean conditions is lower for catalysts containing both Pt and Rh compared to the Pt only samples. Also, with an increase in Pt loading, the NO_x storage ability was increased. It was suggested that this behavior is probably due to more Pt being in contact with the Ba, providing more accessible storage area in the catalyst. Again, increasing the amount of Pt also increased the number of sites for adsorption of NO_x. On the other hand, Rh-containing catalysts showed higher NO reduction ability than Pt only catalysts (the rich cycle period was as long as 5 min). Interestingly, catalysts containing both metals showed higher overall efficiency than the corresponding monometallic catalysts. In a recent work on Pt- and Rh-containing Ba/Al_2O_3 catalysts, where the rich period was only 1.2 s, it was found that over Pt−Ba/Al_2O_3 and Pt−Rh−Ba/Al_2O_3 the rate of regeneration during the rich phase was not sufficiently fast to fully remove all the NO_x stored in the previous lean

phase, resulting in deteriorating performance of the catalysts,[32] whereas, on the contrary, over Rh−Ba/Al_2O_3 the rate of regeneration was sufficiently fast. The authors concluded that the rate of storage was likely to be limiting the performance of the monometallic Rh-containing catalyst rather than the rate of regeneration. However, the Rh-containing catalyst had a poor activity for NO_x storage. Over this 0.5%Pt−0.8%Rh−BaO/Al_2O_3 catalyst during 60 s of lean period at 350 °C, the amount of NO_x storage was about 75%, whereas the monometallic Pt-containing catalyst showed almost complete NO_x storage. In another investigation, Lesage et al. have shown that, over 2%Pt−1%Rh−BaO/Al_2O_3, the amount of NO_x species stored was 285 μmol/g of catalyst (at 300 °C) and 590 μmol/g of catalyst (at 400 °C), respectively.[26] However, in this case the nitration was of 1 h duration.

In a DFT study on oxidation of NO with atomic oxygen involving Pd and Pt monolayers above the late transition metals (Ru, Rh, and Ir), and 1B metals (Cu, Ag, and Au), it was proposed that the two factors: (i) geometric effect (which arises due to lattice strain introduced by the epitaxial placement of Pt on the (111) surface of host metals), and (ii) electronic effect (due to the bonding between Pt and the host metal, which necessarily has a different electronic configuration than Pt) conspire to alter the reactivity.[109,110] The calculations proposed Pt/Ir as a promising system because Pt would remain at the surface even when exposed to reactants and this catalytic system also seems to have a lower activation energy for NO oxidation.

Though these are promising observations, so far, too few investigations have been carried out for a conclusive assessment of the possible beneficial role of bimetallic systems for NSR applications. This is particularly true for metal alloys whose possible potential is as yet largely unexplored.

4.2. Storage Components

In section 3 we have discussed the overall general mechanism of storage of NO_x over the Ba-component of the catalyst. As a storage component, generally alkali metals or alkaline earth metal compounds are common in use because of their high basicity. Several studies have been devoted to NO_x storage over the alumina supported Ba component,[19,20,33,46,47] and the burning questions related to the storage component are as follows: (i) What is the optimum loading of the Ba component in the NSR catalyst and what is the exact nature of the Ba component therein? (ii) What are the natures of the sorbed NO_x species on the Ba component? Does particle size play any role in storage? (iii) Does the storage occur just on the surface layer or throughout the bulk? Or are only the Ba sites near to Pt associated with the storage process? What happens if there is no Pt? (iv) What is the role played by *in situ* produced oxides such as BaO_2 or Ba-aluminate in the storage step? (v) How to regenerate the sulfated Ba-containing catalysts and which other alkaline earth metals or alkali metals can overcome the limitations of Ba? In order to investigate how NO_x molecules are adsorbed onto a NO_x-trap catalyst, extensive studies have been performed using various powerful analytical tools (FTIR, Raman, X-ray diffraction, LEED, STM, XPS, IRAS). In the following section, focus will be on the above-mentioned questions related with the storage components (alkaline earth metals and alkali metals) over primarily Al_2O_3 support.

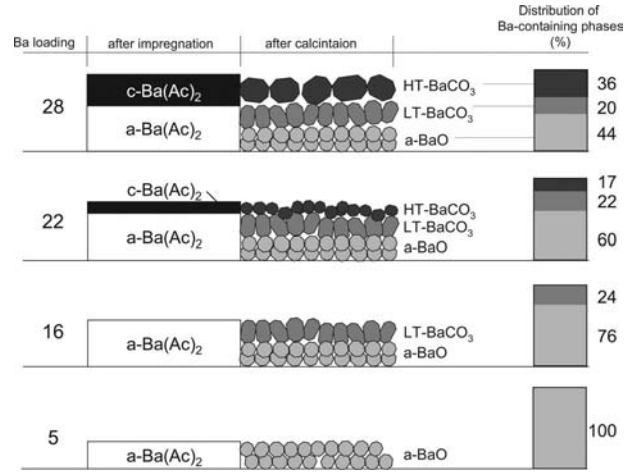

Figure 7. Schematic presentation illustrating the effect of Ba-loading and calcination on the distribution of Ba-containing phases. BaO and orthorhombic (HT, high temperature) and monoclinic (LT, low temperature) $BaCO_3$ were observed. The prefixes a and c refer to amorphous and cyrstalline phases, respectively. The bars on the right side indicate the quantity of respective phases (%). Different phases are marked by different gray tones. Reprinted with permission from ref 127. Copyright 2005 Elsevier B.V.

4.2.1. Earth Alkaline Metals

Although lots of investigations have been carried out, the composition of the storage material in the trapping process is still ill-defined. Epling et al.[13] show that it is difficult to draw general conclusions concerning the activity of Ba phases because samples with different Ba-loading were used in the various studies: e.g. 8 wt % of BaO/$BaCO_3$,[111] 8.3 wt % of Ba,[112] 9 wt % of Ba,[113] 16 wt % of Ba,[114] 17 wt % of Ba,[46,85] 9−18 wt % of Ba,[115] and more than 20%.[116] The distribution and dispersion of Ba-containing species and consequently the influence on the reactivity can be distinctly influenced by the Ba-loading.[117] According to Lietti et al., BaO, $Ba(OH)_2$, and $BaCO_3$, all three kinds of Ba-components, are present in wet impregnation synthesized Pt−Ba/Al_2O_3 catalysts.[118] The storage of NO_x occurs first at BaO and then at $Ba(OH)_2$ in 3% O_2/He atmosphere, and finally the carbonates are replaced by nitrates, in line with the greater basicity of the former compound. Researchers have observed either the presence of only BaO,[119,120] or only $BaCO_3$,[80,121−123] or both BaO and $BaCO_3$ together in as-prepared Pt−Ba/Al_2O_3 catalysts.[124−126] Frequent observation of $BaCO_3$ as the primary phase may be attributed to its high temperature stability; at a temperature as high as 1300 °C, it decomposes to give BaO and CO_2. At lower temperature, bulk carbonate undergoes two polymorphic transformations at 800 °C (orthorhombic ↔ hexagonal) and 968 °C (hexagonal ↔ cubic). Compared to BaO or $Ba(OH)_2$, bulk $BaCO_3$ because of its crystallinity could be easily identified by transmission electron microscopy from the characteristic lattice fringe (3.72 Å) of the most intense diffracting crystallographic plane (111). It could also be easily identified by XRD. Pt−Ba/Al_2O_3 synthesized from the $Ba(Ac)_2$ precursor with different Ba loading via the wet-impregnation method showed that the thermal stability of the Ba-containing phases depends on their interaction with the alumina support and the presence of dispersed platinum (Figure 7).[127] The following Ba-containing phases have been identified: amorphous BaO confined to the interface with the alumina support, monoclinic $BaCO_3$ being in intimate contact with BaO, and orthorhombic $BaCO_3$ showing bulklike properties. At low

Ba loading (<5 wt %), the Ba-containing phase exists exclusively as BaO. With 9−28 wt % Ba loading, the relative amount of monoclinic $BaCO_3$ is limited to 5−6 wt %, whereas the amount of orthorhombic $BaCO_3$, appearing at higher loading (>16 wt %), grows proportionally to the Ba-loading. It is clear that, in the presence of water (real exhaust gas), BaO is prone to transform to $Ba(OH)_2$. Frola et al. also demonstrated that with increasing Ba loading a well-dispersed $BaCO_3$ phase (up to 10% Ba loading) converted into a bulky orthorhombic $BaCO_3$ phase (more than 10% Ba loading).[128] After a few cycles of heating at 350 °C in NO_2 and subsequent evacuation at 550 °C (conditioning treatment), the $BaCO_3$ initially present evolved to $Ba(NO_3)_2$ and then decomposed into a well-dispersed nanosized BaO phase. Thermodynamic calculations proposed that $BaCO_3$ is a relatively inactive compound in the storage process, and they favor BaO as active component due to the higher stability of carbonates compared to $Ba(NO_3)_2$, and there are thermodynamic limitations to the storage process if it is represented as[129]

$$BaCO_3 + 2NO_2 + {}^1/_2O_2 \rightarrow Ba(NO_3)_2 + CO_2 \qquad (15)$$

However, the predictive value of such thermodynamic considerations has to be considered with caution, because they refer to bulk properties and do not take into account interfacial contact of the dispersed components, which may greatly alter the stability of the different phases. The nature of the $BaCO_3$ and its stability at higher temperature was studied by exposing $Pt-Ba/Al_2O_3$ to CO, CO_2, and CO + O_2 at room temperature up to 500 °C.[130] Barium carbonate species readily formed under all conditions and were stable in vacuum up to 500 °C. At elevated temperatures, some of the bidentate carbonate species transformed to unidentate species. Residual hydroxide species on the catalyst resulted in bicarbonates. Formate species were formed when CO was used but decomposed at moderate temperatures, forming more carbonate species in the process. Broqvist et al. concluded from first-principles calculations and ab initio studies that introduction of NO_2 on a hexagonal $BaCO_3$ surface made the decarbonation energetically relevant, while forming $NO_2-BaO-NO_2$ units, on the decarbonated surface.[131] The interaction of NO_x species on the BaO (100) plane was totally electrostatic.[132,133] The chemisorption was initiated by NO_2 adsorption in the form of a nitrite over a Ba^{2+} site. This generated an electron hole among the surrounding surface oxygen atoms. The second NO_2 either could act as surface oxidant, forming a surface nitrite−peroxide pair by releasing NO(g), or could bind to a surface oxygen to form a formal surface nitrate. For nitrates, the preferred orientation during the simulations was a lateral structure with the N atom over a surface anion. Nitrate diffusion between anion sites was found to occur via a tumbling motion, involving a molecular configuration with nitrate oxygen atoms coordinated toward surface Ba cations. Castoldi et al. studied NO_x storage with different Ba loadings (in the range 0−30% w/w) in $Pt-Ba/Al_2O_3$ catalysts.[116] The increase in the Ba loading resulted in a strong increase of the NO_x adsorption; at 350 °C with 23% w/w Ba loading, the highest NO_x adsorption was 8×10^{-4} mol /g catalyst. They proposed that the addition of Ba increased the number of Pt−Ba neighboring species, which could favor the NO_x storage process. However, with more than 10% Ba loading, the morphological properties and the noble metal dispersion of the catalyst were negatively affected. It is commonly believed

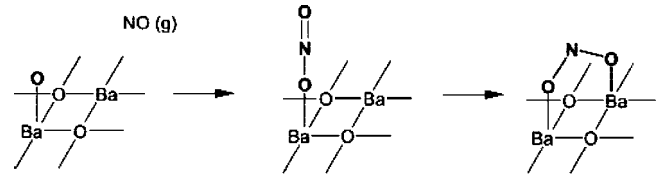

Figure 8. Formation of linear and bridged Ba nitrites by molecular adsorption of NO. Reprinted with permission from ref 111. Copyright 2003 Elsevier Science (USA).

that NO_2 formation is the precursor step to adsorption, and NO → NO_2 conversion takes place over the noble metal. The analysis of the storage phase showed that with higher Ba content, NO_2 concentration decreased. This could happen because Ba coverage exceeds the monolayer capacity of the support and Pt sites were masked. As the spillover process plays a key role, the enhancement of NO_x storage on BaO due to intimate Pt−BaO contact has also been supported by other researchers.[51] NO_x adsorption as nitrates without the assistance of Pt sites and molecular O_2 had been proposed to occur via a disproportionation reaction (combination of reactions 1, 2, and 3).[112]

$$3NO_2 + BaO \leftrightarrow Ba(NO_3)_2 + NO \qquad (16)$$

This stoichiometry implies that, for every two molecules of NO_2 stored on the surface, one molecule is released in the form of NO. NO_x uptake on noble metal free BaO/Al_2O_3 has been proposed to take place via two steps, a small complete uptake followed by a larger but slower process, which generated one NO for every three NO_2 lost.[113]

The interaction of NO or NO_2 with BaO has been studied by several groups, and surface species such as bidentate nitrite, N-coordinated nitrite and ionic nitrites (indicative vibrational bands at 1220, 1225, and 1330 cm^{-1}, respectively),[134−136] monodentate nitrate (1291, 1542 cm^{-1}),[137] and bidentate nitrates (1214, 1573, 1200−1320, 1540−1650 cm^{-1}) have been identified.[134,137] Sedlmair et al. investigated the surface species and the reaction intermediates during NO_x storage on a commercial $Pt-Ba/Al_2O_3$ catalyst (both BaO and $BaCO_3$ were identified).[111] They proposed sequential reaction steps during the sorption of NO_x. Initially, NO was adsorbed in the form of Ba nitrite with a linear as well as bridged geometry (Figure 8). When the catalyst was exposed to NO, two negative bands at 1456 and 1297 cm^{-1} were observed, which were attributed to the decomposition of $BaCO_3$ during NO sorption (however, the carbonate decomposition phenomenon was not observed with NO_2 sorption). The Ba-nitrites (linear nitrite, 1422; monodentate nitrites, 1340, 1440; bridged bidentate nitrites, 1230, 1300 cm^{-1}) could form by replacing the Ba carbonates (Figure 9a). The nitrite bands around 1200 cm^{-1} were observed to decrease with increasing exposure, while new bands at 1429 cm^{-1} and above appeared. The bands at 1429 and 1332 cm^{-1} were attributed to monodentate nitrates, whereas all bands above 1500 cm^{-1} were assigned to nitrate species on Al_2O_3. This led to the conclusion that, after a certain NO exposure, the NO was oxidized on Pt, spilt-over, and sorbed on BaO or Al_2O_3 as nitrates. The thermal stability of the formed NO_x species increased in the order Al nitrites (linear, N-coordinated) < Ba nitrites (linear, monodentate) < Al nitrates (bridging bidentate, chelating bidentate) < Ba hyponitrites < Ba nitrates (monodentate). The formation of strong nitrite bands with very weak nitrate bands followed by the intense nitrates bands has also been supported by other research on powder samples as well as thin films.[47,138] At room temper-

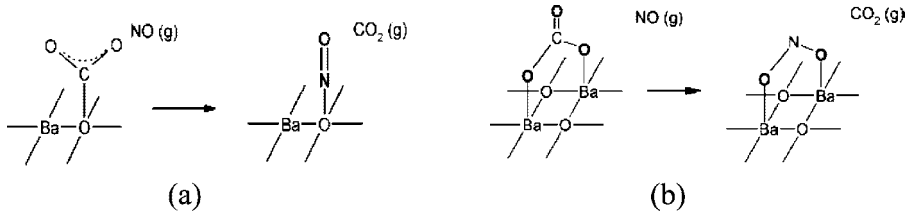

Figure 9. Replacement of Ba carbonates with linear (a) and bridged (b) Ba nitrites. Reprinted with permission from ref 111. Copyright 2003 Elsevier Science (USA).

ature, the geometry of the nitrite was considered aligned parallel to the surface because of its weak intensity.[138] However, since a few nitrates were also observed from the very beginning of the run, a disproportionation reaction of NO_2 was proposed. Recently, investigations were carried out on the nature of sorbed NO_x species as a function of reaction temperature or BaO particle size. NO_2 adsorption on a thick BaO film led to the formation of nitrates with a rate proportional to the sample temperature.[139] With the increase in sample temperature, the agglomeration of $Ba(NO_3)_2$ particles increased on the BaO surface and opened up new, unreacted BaO sites for reaction with NO_2. Interestingly, in a fairly recent investigation combining DFT and IRAS, the authors showed that on BaO supported on Al_2O_3 film, both monodentate and bridged nitrates are present and their ratios depend on the BaO particle size, NO_2 exposure, and reaction temperature, whereas only bridged nitrates were predominant over the Al_2O_3 film.[140] They further showed that the thermal dependence of these nitrates is also affected by the particle size: the nitrates of the small particles had lower thermal stability and vice versa.[141] An elaborate discussion will be given in section 6.2.

So far we discussed the solid state chemistry of the Ba component changing with the loading and temperature as well as issues such as the different NO_x species trapped by the Ba component. Now the question comes about the role of the surface and bulk Ba components in the catalyst. Szanyi et al. proposed that, upon NO_2 adsorption, the morphology of a BaO/Al_2O_3 catalyst changes and there are two kinds of nitrate species. Surface nitrates, which are associated with a monolayer BaO on the alumina support, and a bulklike nitrate that forms on this thin BaO layer.[142] In another investigation from the same group, on BaO deposited on θ-Al_2O_3 film on a NiAl(100) model system (vide section 6.2 for synthesis of this model catalyst and experimental details of the surface science techniques), the authors again observed two different kinds of nitrate species, which decomposed at 350 and 520 °C, hailing from surface and bulk Ba sites.[143,144] The interaction of NO_2 with $BaAl_{2x}O_{1+3x}$ nanoparticles on Al_2O_3/NiAl(110) at higher temperatures (330 °C) showed that the nitrate formation was not restricted to the particle surface but also involved the multilayer.[145,146] In a more recent study, they clarified the formation of bulk nitrates and surface nitrates; the surface nitrates were formed on Al_2O_3-supported $(BaO)_x$ species (monomers, dimers, and/or small clusters) that are bound to Al^{3+} sites.[147] Bowker in a recent review also supported the involvement of both the surface and bulk Ba species in the storage mechanism.[148] Szanyi et al. further observed a cyclic morphological change of the active Ba-containing phase using time-resolved X-ray diffraction and energy dispersive X-ray spectroscopy.[149] During preparation by an incipient wetness method using an aqueous $Ba(NO_3)_2$ solution, large $Ba(NO_3)_2$ crystallites on the alumina surface were formed. Upon thermal treatment, these large $Ba(NO_3)_2$ crystallites decomposed, forming nanosized BaO particles. During room temperature NO_2 uptake, nanosized (<5 nm) $Ba(NO_3)_2$ particles formed, and heating at higher temperature (300 °C) resulted in larger $Ba(NO_3)_2$ crystals (15 nm). At higher temperatures, and in the absence of NO_2, the average size of $Ba(NO_3)_2$ particles increased further and eventually the component decomposed into BaO, regenerating the surface.

Thermodynamic calculations show favorable formation of BaO_2 up to 600 °C. During the storage of nitrates at elevated temperatures, many of the researchers identified oxidation of BaO to BaO_2 as an intermediate step.[48,113,150,151] According to Fridell et al., BaO is first oxidized to BaO_2, which is then able to store NO_2 as nitrate without need for additional oxygen.[151] Exposure of BaO to NO_2 at cryogenic temperature resulted in the formation of nitrite−nitrate pairs, suggesting that the activation energy of the ion pair formation is very low. Upon heating the nitrite−nitrate pair-covered BaO, nitrites decomposed first, leaving one O atom behind that took part in the formation of BaO_2.[152] The thus-formed BaO_2 was present even after all the nitrates were decomposed. Although the formation of BaO_2 from BaO is thermodynamically allowed under storage conditions, the corresponding reactions starting with bulk $BaCO_3$ are highly unfavorable. Unfortunately, to the best of our knowledge, there have not been many reports on the direct experimental observation of BaO_2 formation (Figure 10).[152]

The formation of spinel $BaAl_2O_4$ is one of the key mechanisms responsible for the lowering of the performance during thermal and hydrothermal aging.[120,126] Thermal aging (oxidizing treatments at 1000 °C) of Pt−20 wt %BaO/Al_2O_3 catalyst showed significant sintering of Pt particles and formation of $BaAl_2O_4$, leading to a decrease of bulk NO_x adsorption sites.[119] Reducing treatments at 1000 °C lead to the formation of $BaAl_2O_4$ but, at most, minimal growth in Pt particle sizes.[120,153] Szailer reported the formation of $BaAl_2O_4$ as a function of Ba loading on Al_2O_3 support. At low concentration of Ba (2 and 8 wt % of Ba in Al_2O_3), there was no structural change in the surface BaO phase, even up to thermal aging of 1000 °C, whereas with 20 wt % Ba loading, formation of $BaAl_2O_4$ was observed already at 800 °C.[119] The authors concluded that, at lower Ba loading, only a monolayer of BaO is formed, while, at higher Ba loading, bulk BaO forms, which reacts with Al_2O_3 and results in $BaAl_2O_4$. The formation of a Ba-aluminate phase depending on the Ba concentration in Al_2O_3 has also been reported by other researchers. Balint et al. demonstrated that, at higher Ba loading on γ-Al_2O_3, $BaAl_{12}O_{19}$ was formed; however, this particular phase was not found with lower Ba content samples.[154] Diffusion experiments using $BaCO_3-Al_2O_3$ couples have further evidenced the formation of various Ba-aluminate phases via the intermediate $Ba_3Al_2O_6$ with excess of Ba, as a function of the distance of diffusion.[155] Most of the authors concluded that the NO_x storage capacity is reduced due to formation of this Ba-aluminate at higher temperatures.[156−158] On the other hand, there are reports

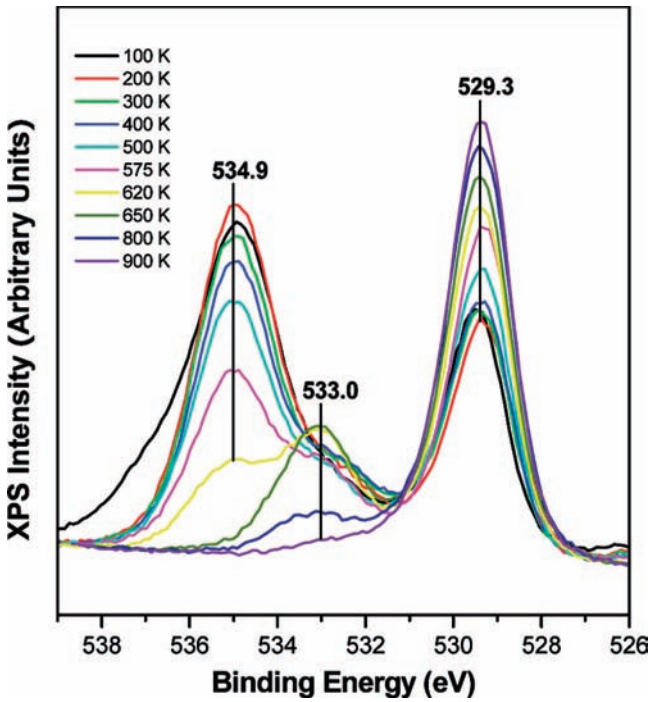

Figure 10. XPS data of the O 1s region after adsorption of NO_2 at cryogenic temperature on a thick BaO film and subsequent annealing. The peak at around 533.0 eV is due to formation of BaO_2. The intensity of this peak reached its maximum after heating the sample to 350 °C, and it remained constant until all the ionic NO_x species desorbed. Reprinted with permission from ref 152. Copyright 2007 American Chemical Society.

where $BaAl_2O_4$ had been shown as a potential NO_x adsorber.[77,159,160] Interestingly, Yi et al. demonstrated that, at low BaO coverage (<1 ML), BaO forms a barium-aluminate-like surface phase. Upon exposure of this phase to NO_2, nitrite species form initially, and then, Ba ions are pulled out from the barium-aluminate-like surface at higher NO_2 exposures, resulting in the formation of ionic barium nitrates.[161] $BaAl_2O_4$ was considered as a better NO_x adsorber compared to BaO because strongly held carbonates were formed on BaO, which was not the case with $BaAl_2O_4$, where the competition of formation of nitrates and carbonates is always in favor of the nitrates. $BaAl_2O_4$ also showed better sulfur resistance behavior. Therefore, the exact role of the spinel in NSR catalysis is still not completely resolved. Arena et al. in this context reported that this apparent discrepancy might be related to the differences between the nonstoichiometric surface $BaAl_2O_4$-like phase and crystalline $BaAl_2O_4$.[162] In the nonstoichiometric phase, the substitution of $[Al-O-Al]^{4+}$ with two Ba ions would create surface charged oxygen species, and therefore, it is likely that this phase would be more active in NO_x storage compared to the crystalline one.

One of the major drawback using Ba as a storage material is its high susceptibility toward sulfur. As $BaSO_4$ is thermodynamically more stable than $Ba(NO_3)_2$, the formation of the sulfate species hinders the NO_x sorption, and also the degree of deactivation of the NO_x storage capacity was found to be proportional to the amount of SO_2 to which the BaO based catalyst had been exposed.[163] Limousy et al. have shown that sulfur species on support material can migrate on barium sites, giving stable S-bound species.[164] Sedlmair et al. proposed two different mechanistic pathways for SO_2 deactivation over $Pt-Ba/Al_2O_3$.[165] Under lean conditions (exposure to SO_2 and O_2), surface sulfates are formed on the Ba storage component, which subsequently migrate into the bulk phase. These species are hardly reducible by C_3H_6 up to 550 °C and block permanently Ba sites, which in turn leads to a decrease of NO_x storage capacity during successive cyclic treatments. A second pathway of deactivation by sulfur species occurs during fuel-rich (reducing) conditions. Sulfides seem to be formed on the Pt particles, which block the metal surface and, thus, hinder the further reduction function of the metal, as revealed by the lower reducibility (higher hydrogen reduction temperature) of the noble metal. Schreier et al. have found that the amount of desorbed sulfur compounds during lean/rich regeneration cycles increased with decreasing λ value (0.99−0.94) at constant temperature and with increasing temperature (660−720 °C) at constant λ value.[166] Elbouazzaoui et al. studied the regeneration of the $Pt-Ba/Al_2O_3$ catalyst from sulfur deactivation.[167] They found three types of sulfates, Al-sulfate, surface Ba-sulfate, and bulk Ba-sulfate. The reduction of the Al-sulfate and surface Ba-sulfate was promoted by Pt, whereas Pt was not effective in the reduction of bulk Ba-sulfate. During regeneration of the sulfated $Pt-Ba/Al_2O_3$ catalyst, under H_2/Ar up to 800 °C, they observed surface Ba-sulfates to be reduced to sulfides directly or by reaction between H_2S produced during reduction.

$$BaSO_4 + 4H_2 \rightarrow BaS + 4H_2O \quad (17)$$

or

$$BaSO_4 + 4H_2 \rightarrow BaO + H_2S + 3H_2O \quad (18)$$

$$BaO + H_2S \rightarrow BaS + H_2O \quad (19)$$

However, when CO was introduced in the feed gas composition of regeneration, all sulfur was eliminated but the initial NO_x storage capacity was not recovered because the storage material formed Ba-aluminate. In another catalyst-regeneration investigation, Kim et al. synthesized sulfated $Pt-BaO/Al_2O_3$ (primarily $BaSO_4$) with two different Ba loadings (8 and 20 wt %) and observed that desulfation was easier with the less Ba loaded sample.[168] They found that some of the Ba species in $Pt-BaO(20)/Al_2O_3$ were inaccessible to the SO_2 adsorption because of diffusion limitations in the formation of sulfate species in the interior region of the particulate Ba phase. Surface $BaSO_4$, originally from the "monolayer" $BaO/BaCO_3$ phase in $Pt-BaO(8)/Al_2O_3$, was more readily (i.e., at lower temperature) and completely removed as gaseous H_2S than the bulk sulfates in $Pt-BaO(20)/Al_2O_3$. At high temperature, desulfation of both samples led to residual sulfur in a reduced form, primarily as fairly large BaS particles.

Apart from using Ba as a storage component, there are plenty of reports on other alkaline earth metals such as Mg, Ca, or Sr. The high affinity of Ba for sulfating makes the other alkaline earth metals popular. Different storage behavior and NO_x conversions were observed by replacing Ba with Mg, Ca, and Sr on noble metal based Al_2O_3.[169−171] Han et al. proposed that for effective removal of NO_x a good capacity for NO_x storage is required.[169] $Ba(NO_3)_2$ or $Sr(NO_3)_2$ species, which were formed on $Pt-BaO/Al_2O_3$ and $Pt-SrO/Al_2O_3$, respectively, were more favorable as the storage form than other monodentate and bidentate nitrate species formed on $Pt-CaO/Al_2O_3$. They also showed that NO_x conversion was highest with $Pt-BaO/Al_2O_3$ followed by $Pt-SrO/Al_2O_3$, whereas $Pt-CaO/Al_2O_3$ had the least NO_x conversion ability among the three. However, by changing the noble metals (from Pt to Pd and Rh) on CaO/Al_2O_3, the amount of NO_x

conversion as well as the storage amount could be changed.[170] Huang et al. also proposed from FTIR data that with an increase in intensity of nitrate bands the storage property increases and the order was CaO/Al_2O_3 < $Pd-CaO/Al_2O_3$ < $Pt-CaO/Al_2O_3$ < $Rh-CaO/Al_2O_3$. The basicity of the alkaline earth materials shows a strong correlation with the storage property; the amount of bulk nitrate increases with the basicity of the alkaline earth oxide, while the amount of surface nitrates decreases along this series.[27,172]

Takeuchi and Matsumoto proposed that, with an increase in the basicity of NO_x storage material, the amount of the stored NO_x can also be increased, and in comparison with Ba and Mg, Ba will be a better storage material than Mg.[171] However, promising storage activity at lower temperature (200 °C) was observed when Ba was partially replaced with Mg.[121,173] $17\%Ba-1\%Pt/Al_2O_3$ and $1.5\%Mg-8.5\%Ba-1\%Pt/Al_2O_3$ were prepared using the wet impregnation method, and X-ray diffraction patterns of the catalysts showed the presence of BaO and $BaCO_3$ phases with an around 20 nm $BaCO_3$ particle size. During preparation of the catalysts, addition of alkaline earth metals lead to a progressive occlusion of pores. At lower temperature (200 °C), the NO_x storage capacity was higher with $1.5\%Mg-8.5\%Ba-1\%Pt/Al_2O_3$ compared to $17\%Ba-1\%Pt/Al_2O_3$, while at higher temperatures (300 and 400 °C) the trend was reverse. However, the Mg−Ba catalyst exhibited high resistance to the deactivation by SO_2. The behavior of the Mg−Ba catalyst suggested a synergistic effect of the two elements and a better interaction with the support.

4.2.2. Alkali Metals

Using alkali metals as a storage component is a comparatively newer concept and also getting popularized.[174−176] Among the alkali metals, potassium is mostly used as a storage component in NSR catalysts.[177−179] Toops et al. have quantified the amount of adsorbed NO_x on $Pt-K/Al_2O_3$ catalyst by a DRIFT study. Potassium on an Al_2O_3 surface replaced the OH groups by OK, and the phases had a fractional surface area of 1.1% for the 1.7 nm-sized Pt, 34% for pure Al_2O_3, and 65% for the alkalized-Al_2O_3. The addition of K to the catalyst increases the adsorption capacity to 6.2 μmol of NO_x/m^2, and the primary storage form on K is a free nitrate ion.[178] Recently, Toops and Pihl studied the effect of SO_x on the cycling lean/rich NSR activity of $Pt-K/Al_2O_3$ at three different temperatures (200, 300, and 400 °C) and concluded that, during initial sulfation, NO_x conversion was directly linked to the lean phase storage capacity (storage capacity was reduced) and did not hamper the reduction kinetics in the rich phase because the amount of unconverted NO_x decreased or was constant with sulfation time.[180] Sulfur interactions with the catalyst had a distinct temperature dependence. At 300 °C, SO_2 initially adsorbed near Pt before interacting with other sites further away from Pt. At 400 °C, SO_2 either preferentially adsorbed near Pt and then quickly diffused along the surface to other less proximal sites or it directly adsorbed on sites further away from Pt. Potassium on Al_2O_3 in the regeneration step of NSR also showed a higher rate of NO reduction compared to its Ba counterpart.[181]

Investigations have been carried out on potassium as a potential storage component on other than Al_2O_3 support. Lesage et al. have shown by using K instead of Ba that the amount of NO_x stored could be enhanced significantly even at lower temperatures. At 200 °C, K-containing catalyst showed 560 μmol of NO_x per g of catalyst, whereas the Ba-containing catalyst did not show any storage property.[26] Furthermore, using K instead of Ba, due to increased basicity of the storage sites, delayed nitrate release during rich steps and consequently delayed the production of NH_3 and isocyanate, thus achieving complete N_2 selectivity. Under lean conditions over the catalyst $Pt-K-Mn/Al_2O_3-CeO_2$, initially NO oxidized to NO_2 and got adsorbed on K sites such as KNO_2, which then involved NO_2 as oxidant, and finally oxidized to KNO_3.[25] The authors observed two different periods during NO_x storage. The first one was complete NO_x adsorption (i.e., surface nitration) with carbonate decomposition, and the second one was NO_2 diffusion in the bulk phase. They proposed two different kinds of K present in the catalyst surface as well as bulk K. The enhanced storage property was also correlated with the structure of the catalyst, which will be discussed in section 4.3.2. Liu et al. in a fairly recent investigation of $Pt-K/TiO_2-ZrO_2$ also came to the same conclusion of two different K sites; however, they discriminate the K sites based on the distance from the noble metal Pt.[182] A comparatively new concept of coupling catalysis and solid-state electrochemistry for the electrochemically assisted $Pt-K/Al_2O_3$ catalyst showed some interesting results.[183] Under negative polarization, NO_x was stored on the catalyst surface in the form of KNO_3. Under positive polarization, the catalyst was regenerated, and the stored nitrates were efficiently desorbed and reduced to N_2. K ions electrochemically transferred to Pt played a double role in the NSR process, as a promoter for NO oxidation and as storage sites. This ability of the electrochemical catalyst to work under wet conditions demonstrated the potential practical uses of this novel system. However, a serious practical problem with using K as storage material is that KNO_3 melts at 334 °C and decomposes around 400 °C. Table 1 provides an overview of current NO_x storage results in the literature.

From the investigations available so far, it emerges that besides the type of storage material, several other factors are decisive for NO_x storage behavior, such as loading, crystallinity and dispersion, interfacial contact with support, proximity of the noble metal component, thermal stability, and reactivity with components of the exhaust gas, such as CO_2, H_2O, and sulfur compounds.

4.3. Supports

The noble metals and the storage materials are dispersed over a support; the support not only helps in dispersing the noble metals but also plays a significant role in the NSR mechanism. Depending on the support, the dispersed noble metal particles show different stability and catalytic activity (see section 4.1). As concerns the effect of the support on the storage properties, in many cases, single-site sorption models on Ba sites have been used to explain the observed chemistry or trends in data. However, there are plenty of reports which deal with involvement of the support as: (i) a storage material, (ii) a hindrance toward agglomeration, and (iii) prevention of formation of mixed oxides with the primary storage materials. We will discuss the role of the support materials in detail in the following sections.

4.3.1. Single Oxides

FTIR investigation of alumina samples exposed to $NO_2 + O_2$ below 300 °C revealed that Al_2O_3 is an important

Table 1. Overview of the Current NO_x Storage Data Reported in the Literature

catalyst	feed	adsorption amount[a] (temp)	ref
2%Pt−17%BaO/Al_2O_3	NO + O_2	0.11×10^{-3} (300 °C)	Mahzoul et al.[266]
1%Rh−5%CaO/Al_2O_3	NO	0.28×10^{-3} (300 °C)	Huang et al.[170]
1%Pt−5%CaO/Al_2O_3	-do-	0.18×10^{-3} (300 °C)	-do-
1%Pd−5%CaO/Al_2O_3	-do-	0.097×10^{-3} (300 °C)	-do-
Pt−16.5%Ba/Al_2O_3	NO + O_2	0.177×10^{-3} (200 °C)	Lietti et al.[118]
-do-	-do-	0.581×10^{-3} (300 °C)	-do-
-do-	-do-	0.407×10^{-3} (350 °C)	-do-
-do-	-do-	0.324×10^{-3} (400 °C)	-do-
9%$BaCO_3$/Al_2O_3	NO + O_2 + CO_2	0.34×10^{-3} (400 °C)	Rodrigues et al.[129]
Pt−20%BaO/Al_2O_3	NO_2	0.363×10^{-3} (300 °C)	Olsson et al.[48]
-do-	-do-	0.375×10^{-3} (400 °C)	-do-
9%BaO/Al_2O_3	-do-	0.260×10^{-3} (400 °C)	Cant and Patterson[113]
11%BaO/TiO_2	-do-	0.277×10^{-3} (200 °C)	Despres et al.[197]
Pt−10%Ba/Al_2O_3	-do-	0.7×10^{-3} (400 °C)	Anderson et al.[76]
Pt−Mg−Al−O (Mg/Al = 1)	NO	0.401×10^{-3} (350 °C)	Cheng et al.[211]
Pt−Mg−Al−O (Mg/Al = 2)	-do-	0.469×10^{-3} (350 °C)	
Pt−Mg−Al−O (Mg/Al = 3)	-do-	0.505×10^{-3} (350 °C)	
1%Pt−20%$BaCO_3$/Al_2O_3	NO_2	0.67×10^{-3} (350 °C)	Nova et al.[46]
-do-	NO+O_2	0.46×10^{-3} (350 °C)	-do-
Pt−Rh−16.3%Ba/Al_2O_3	-do-	0.285×10^{-3} (300 °C)	Lesage et al.[108]
-do-	-do-	0.59×10^{-3} (400 °C)	-do-
Pt−4.5%K/Al_2O_3	NO + O_2	0.79×10^{-3} (250 °C)	Toops et al.[178]
Pt−Na_2O/TiO_2	-do-	0.66×10^{-3} (300 °C)	Yamamoto et al.[198]
-do-	NO + O_2 + SO_2	0.57×10^{-3} (300 °C)	-do-
Pt−Mn−K/Al_2O_3−CeO_2	NO + O_2	0.56×10^{-3} (200 °C)	Lesage et al.[25]
-do-	-do-	0.865×10^{-3} (300 °C)	-do-
-do-	-do-	0.98×10^{-3} (400 °C)	-do-
0.1%Pt−MgO/CeO_2	NO + O_2	0.014×10^{-3} (400 °C)	Costa et al.[227]

[a] The amount of NO_x stored is reported in mol g^{-1} of catalyst.

storage compound forming surface nitrate species with various coordination (monodentate, bridged, and bidentate nitrates) modes to the surface.[137] When the same gas mixture was introduced to BaO/Al_2O_3 samples, bidentate and bridged nitrates formed on Al_2O_3 at the Al_2O_3−BaO interface and also there was indication of nitrate groups moving from Al_2O_3 to BaO during storage. However, some other investigations demonstrated that only with longer exposure were bridged and chelating nitrates on Al sites formed and that the thermal stabilities of the Ba-nitrates/nitrites were higher than those of the corresponding ones of Al.[111,113]

As we have discussed earlier, sulfation is a major drawback of Ba/Al_2O_3 based catalysts; there are two strategies to overcome this problem. One is to replace the storage material Ba by another alkali or alkaline earth material, which we have discussed in sections 4.2.1 and 4.2.2, and the second one is to make use of support materials that either do not form any mixed oxides with the storage material or form mixed oxides that easily decompose in the presence of CO_2 or NO_x.

CeO_2 as a support is one such example.[184−186] Contradictory reports exist in the literature about the role of CeO_2 in NSR catalysis; inertness of CeO_2 toward NO_x adsorption has been reported by Svedberg et al.,[187] whereas some beneficial role of CeO_2 has also been reported.[126,156,188−192] DRIFT studies have demonstrated that, over BaO/CeO_2, NO storage as nitrites on Ce(IV) sites reduced it to Ce(III).[188] A favorable aspect of using CeO_2 as a support is formation of highly instable $BaCeO_3$. $BaAl_2O_4$ formation is a high temperature (more than 850 °C) phenomenon, whereas $BaCeO_3$ forms at slightly lower temperature (800 °C).[126] Interestingly, $BaCeO_3$ is transformed to $Ba(NO_3)_2$/CeO_2 in the presence of NO_2/H_2O already at 300−500 °C. Also, the presence of CO_2 leads to decomposition of barium cerate, which has important consequences for the catalyst aging under NO_x-storage conditions. After on-board reactivation treatment, the thermally aged Pt−BaO/CeO_2 showed a promising improvement in NO_x storage compared to that of a conventional Pt−BaO/Al_2O_3 catalyst.[156] The nature of Pt also changes in the CeO_2-supported catalyst compared to the Al_2O_3-supported catalyst during thermal aging.[189] Casapu et al. demonstrated by means of X-ray absorption spectroscopy that, on CeO_2-supported catalysts, the behavior of Pt resembles that in a mechanical mixture of $BaCO_3$ and PtO_2, with $BaPtO_3$ formed at relatively low temperature (600−700 °C). Above 800 °C, $BaPtO_3$ reacted with $BaCeO_3$ to form a double perovskite Ba_2CePtO_6. Both perovskites kept the Pt well-dispersed and could be reduced with H_2 at relatively low temperatures, thus restoring the catalytically active Pt species. Exposure of the Pt−Ba/CeO_2 catalyst to reducing H_2 atmosphere in the temperature range 300−500 °C lead to a moderate increase of Pt particle size, which beneficially influenced the regeneration activity.[190,191] On the contrary, in Al_2O_3 based catalyst, with an increase in temperature, there was no formation of Pt−Ba oxide; only sintering of Pt particles took place. Pt−BaO/CeO_2 showed better sulfur resistance compared to the Pt−BaO/Al_2O_3 (Figure 11d).[193] After reductive desulfation at 600 °C, the Pt−BaO/CeO_2 catalyst was almost unchanged (Figure 11a and b), whereas ∼5 nm Pt clusters were formed on the Al_2O_3-supported catalyst (Figure 11c), confirming again weaker interaction between Pt and the support material.

ZrO_2 is also an alternative promising support to CeO_2. Piacentini et al. demonstrated that low temperature $BaCO_3$ (monoclinic) is more efficient for NO_x adsorption compared to the high temperature $BaCO_3$ (orthorhombic-whiterite).[86] Monoclinic $BaCO_3$ (at lower Ba loading) supported on ZrO_2 was more efficient than that supported on Al_2O_3, leading to higher NO_x sorption.[125,194] They also showed that the concentration of monoclinic $BaCO_3$ was poorest over SiO_2. In a separate study, with different Ba loading over ZrO_2 and Al_2O_3, they found that, at higher Ba loading, Al_2O_3 and ZrO_2

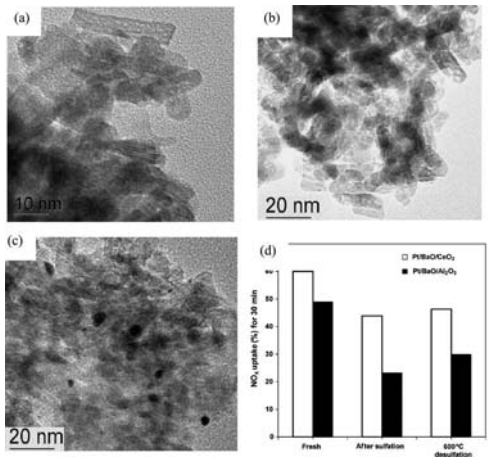

Figure 11. TEM images of (a) Pt−BaO/CeO_2 after calcination at 500 °C; (b) Pt−BaO/CeO_2 after desulfation; and (c) Pt−BaO/Al_2O_3 after desulfation. (d) NO_x uptake profile of Pt−BaO/CeO_2 and Pt−BaO/Al_2O_3. Sulfation was carried out by treating the sample at 250 °C with 25 ppm SO_2 in the lean gas mixture for 3 h. Reactants consisted of a continuous flow of 200 ppm NO, 10% CO_2, and 10% H_2O balanced with He with either rich (1330 ppm C_3H_6, 4% CO, and 1.33% H_2) or lean (12% O_2) gas added over 0.1167 g of catalyst at a total flow rate of 300 cm^3/min. Reprinted with permission from ref 193. Copyright 2008 Elsevier B.V.

afforded about similar NO_x storage behavior.[195] However, the surface area of the ZrO_2 was lower than that of Al_2O_3, and blocking of the Pt sites occurred, resulting in poor reduction of stored NO_x.

TiO_2, due to its lower acidity compared to Al_2O_3, should form instable sulfates, and this led researchers to make use of TiO_2 as a support in NSR catalysis.[196] Despres et al. observed formation of three different nitrate species (surface nitrates on BaO and TiO_2 as well as bulk nitrate on BaO) during NO_2 adsorption on BaO/TiO_2 at 200 °C.[197] Surface nitrates on TiO_2 were decomposed at 370 °C during TPD. Yamamoto and co-workers synthesized a series of alkali and alkaline earth metal oxides supported on Pt/TiO_2; 1%Pt−10%M_xO_y/TiO_2, where M = Li, Na, K, Cs, Sr, Ba.[198] The NO_x sorption capacity among these catalysts in both SO_2-free and SO_2-containing atmospheres obeyed the following order: K > Na > Cs > Sr > Ba > Li. TiO_2 in all the samples was present as mixed phases of anatase and rutile, and after calcination at 450 °C, formation of Li_2TiO_3, $SrTiO_3$, and $BaTiO_3$ over Pt−Li_2O/TiO_2, Pt−SrO/TiO_2, and Pt−BaO/TiO_2, respectively, was observed, which could be responsible for the low NO_x sorption observed over these catalysts.

In situ Raman spectroscopy investigation on NO_2 storage and reduction on BaO supported on MgO put a new mechanistic view on sorption of NO.[135,136] 14 mol % BaO on MgO below 400 °C was found to form barium−nitro species, which eventually transformed into nitrite and nitrates. Above 400 °C, crystalline BaO_2 was observed. However, the role of MgO was not elucidated.

4.3.2. Mixed Oxides

Mixed oxides were also being used as supports in NSR catalysis, and promoting as well as demoting effects have been observed. Pt−BaO/Al_2O_3 with additives such as WO_3, MoO_3, V_2O_5, and Ga_2O_3 has been examined for catalytic activity. When tested for NO oxidation to NO_2, WO_3, and MoO_3, additives lead to the best performing catalyst in the absence or in the presence of SO_2.[199] However, the NO_x storage capacity was poorer for Pt−$BaO/MoO_3−Al_2O_3$ than for Pt−BaO/Al_2O_3 in presence of SO_2. $Al_2O_3−CeO_2$ mixed oxide has cut a mark for sulfur resistance.[200,201] When 2−3% Co was added to Pt−BaO/Al_2O_3 catalyst (Co mainly existed as Co_3O_4), the NO_x storage capacity was higher compared to the Co free counterpart.[202] A promoting effect of Co_3O_4 has also been supported by others.[203] Addition of 5% Co increased the NO_x storage capacity of a 1% Rh−15%Ba/Al_2O_3 catalyst by 50% and that of a 1% Pt−15% Ba/Al_2O_3 by 100%. This promotional effect of Co was 2-fold: (i) the high oxidizing ability of Co, present in the form of Co_3O_4, allowed to reduce the noble metal content to 0.25%, and (ii) provided extra oxidation sites for NO to NO_2 conversion and a large contact area for NO_2 spillover to Ba storage sites. Cu addition to Pt−BaO/Al_2O_3 improved the sulfur tolerance of the material, which was believed to be caused by formation of the bimetallic phase, Pt−Cu.[204] Lesage et al. demonstrated that by utilizing $Al_2O_3−CeO_2$ they could enhance the storage of NO_x.[25] The Pt−K/Mn-$Al_2O_3−CeO_2$ catalyst was prepared by the wet impregnation method and showed two distinct structures: poorly crystalline round shaped particles with various amounts of Ce and Al, and needle shaped crystallites made of $AlKMn_3$ oxides and Al_2K oxides. The $AlKMn_3$ oxides of Holloandite structure with K atoms in the tunnel generally slowed down the NO_x diffusion resulting in higher storage (Figure 12).

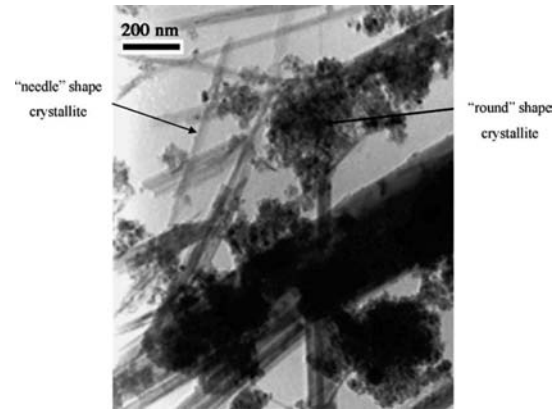

Figure 12. TEM image evidencing the shape of the crystallites in the Pt−K/Mn/$Al_2O_3−CeO_2$ sample. Reprinted with permission from ref 25. Copyright 2007 Elsevier B.V.

Ample investigations have been performed with Mg−Al supports. Hydrotalcites, layered double hydroxides of general formula $[M^{z+}_{1-x}M^{3+}_x(OH_2)]^{b+}[A^{n-}_{b/n}]mH_2O$ (M = metal, A = anion and B = x or $2x−1$, respectively, for $z = 2$ or 1), are very attractive catalyst supports, and Pt and Cu doped Mg−Al hydrotalcite (Mg^{2+}/Al^{3+} = 1.3:1, 2:1, 3:1) showed interesting characteristics as novel NSR catalysts, with improved low-temperature activity (<200 °C) and better resistance to deactivation by SO_2 compared to the conventional Pt−Ba/Al_2O_3 catalyst.[205−210] Fornasari et al. observed that the sample with the lowest Mg/Al ratio (Mg^{2+}/Al^{3+} =1.3:1) showed the best activity at temperatures <200 °C but deactivated almost completely at 500 °C.[205,207] They concluded that (i) the presence of the cubic Mg(Al)O mixed oxides was responsible for the higher activity, while formation of the spinel $MgAl_2O_4$ deactivated the NO_x storage activity, and (ii) the presence of Cu had no substantial effect on NO_x storage but the addition of Cu lead to resistance to deactivation by SO_2 and also prevented conversion of Mg(Al)O mixed oxides to $MgAl_2O_4$. However, conflicting

results have been reported in the literature about the Mg/Al ratio, the importance of the spinel structure for storage, as well as the role of transition metals in hydrotalcites. Cheng and co-workers demonstrated that the amount of the NO_x storage increased with increasing Mg/Al atomic ratio and that the highest amount of NO_x storage occurred when $Mg^{2+}/Al^{3+} = 3:1$.[211] Takahashi et al. synthesized Pt−K/$MgAl_2O_4$, which crystallized in a pure spinel structure and showed a considerable amount of NO_x storage over the spinel phase even at higher temperature.[212] Co as a transition metal played a significant role in Co_xMg_{3-x}/Al hydrotalcite-like compounds (where $x = 0.0, 0.5, 1.0, 1.5, 2.0, 2.5, 3.0$).[213] When more Co was incorporated to replace Mg in the hydroxide layers, the derived oxide contained more spinel (with chemical formula $Co^{2+}_{4/3}Co^{3+}_{5/3}AlO_{16/3}$) and less MgO. NO_x adsorption over these catalysts was different at different temperatures. At 100 °C, NO_x storage was highest when the Co concentration was less ($x = 0.5$), and at 300 °C, NO_x storage increased with an increase in Co concentration, resulting in the highest storage amount at $x = 2.5$. The Co^{3+} helped in NO_x adsorption via the reactions:

$$NO + Co^{3+} - O^{2-} \rightarrow Co^{2+} - NO_2^- \quad (20)$$

$$NO_2 + Co^{3+} - O^{2-} \rightarrow Co^{2+} - NO_3^- \quad (21)$$

Higher NO_x adsorption was due to a migration process of NO_3^- and NO_2^- from Co to adjacent Mg/Al to form relatively stable Mg/Al nitrates and nitrites. Yu et al. had studied NO_x trapping catalysis further by adding one more transition metal such as Fe or Mn or rare earth metals such as La and Zr.[214,215] The incorporation of the fourth element facilitated the two stage reduction of $Co^{3+} \rightarrow Co^{2+}$ and $Co^{2+} \rightarrow Co^0$ and helped in oxidizing nitrites to nitrates and storing them. As the incorporation of the fourth element increased the activity due to the combination of the redox properties of these metals and the acid−base properties of the hydrotalcite, Palomares et al. incorporated 1% of Pd, Pt, Ru, and V in Co_xMg_{3-x}/Al and observed the best results with 1% V.[210] Yamazaki et al. demonstrated that, among the first row transition metals (Fe, Co, Ni) in Pt−Ba/Al_2O_3 catalyst, the aged Pt−Ba−Fe/Al_2O_3 had the highest NO_x purification activity.[216] They came to the conclusion that the Fe compound inhibited the growth in the size of $BaSO_4$ particles formed on the Pt−Ba−Fe/Al_2O_3 catalyst under oxidizing conditions in the presence of SO_2 and promoted the decomposition of $BaSO_4$ and desorption of the sulfur compound under reducing conditions. Although the Fe component favored the reduction of the $BaSO_4$ phase, Luo et al. showed that the coexistence of Pt and Fe was detrimental for the NO_x storage and sulfur removal as compared with Pt−Ba/Al_2O_3 catalyst.[217] Mn $2p_{3/2}$ XP spectra of Mn−Ba/Al_2O_3 catalyst showed the presence of MnO_2 and Mn_2O_3 as well as formation of $BaMnO_3$ due to reaction between BaO and MnO_2 during the calcination process.[218] MnO_2 and Mn_2O_3 on the surface catalyzed the oxidation of NO, and Mn−Ba/Al_2O_3 in combination with Pt−Ba/Al_2O_3 catalyst showed promising regeneration activity.

Other than Al_2O_3, CeO_2 based compounds such as CeO_2-ZrO_2 gained importance as support in NSR catalysis. Pt−Ba/$Ce_xZr_{1-x}O_2$, synthesized by flame spray pyrolysis, exhibited two different structures of $BaCO_3$ and $Ce_xZr_{1-x}O_2$.[219] At $x > 0.5$, orthorhombic $BaCO_3$ was found, whereas, at $x < 0.5$, there was more monoclinic $BaCO_3$. Pt−Ba/$Ce_{0.7}Zr_{0.3}O_2$ was studied against conventional Pt−Ba/Al_2O_3 with regard to sulfur resistance and regeneration.[220] Crystallized $BaSO_4$ was detected on sulfated Pt−Ba/Al_2O_3 catalyst after aging at 600 °C under oxidizing conditions, whereas the same was observed on Pt−Ba/$Ce_{0.7}Zr_{0.3}O_2$ only after aging at 800 °C. The sulfates elimination under rich conditions was more efficient on Pt−Ba/$Ce_{0.7}Zr_{0.3}O_2$: 85−90% of sulfur was eliminated at 550 °C on Pt−Ba/$Ce_{0.7}Zr_{0.3}O_2$ while only 55% was eliminated on Pt−Ba/ Al_2O_3.

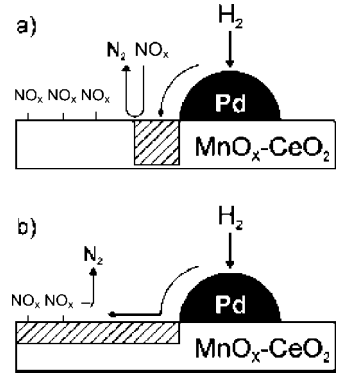

Figure 13. Possible two models for the spillover-assisted NO−H_2 reaction over Pd/$Ce_{1-x}Mn_xO_2$ catalyst. Reprinted with permission from ref 224. Copyright 2003 American Chemical Society.

First row transition metal (such as Mn, Fe) doped CeO_2 is being used as support as well as storage materials for NSR catalysis. Machida et al. synthesized a solid solution of $Ce_{1-x}Mn_xO_2$ in a pure fluorite structure until $x = 0.5$ (with an increase in concentration of Mn, there was formation of Mn_2O_3) and observed NO_x adsorption at low temperature.[221] The low temperature NO_x adsorption was attributed to adjacent pair sites with different characters, i.e., NO oxidation over MNO_x and adsorption over CeO_2. 1% Pd supported on the $Ce_{1-x}Mn_xO_2$ showed efficient selective reduction of sorbed NO_x.[222,223] The authors proposed two possible models for the NO−H_2 reaction over Pd/$Ce_{1-x}Mn_xO_2$ considering significant reactions between spilt-over hydrogen and NO_x adsorbates stored on the surface of $Ce_{1-x}Mn_xO_2$ (Figure 13).[224] The first model (a) is the reaction between gaseous NO_x and the anion vacancy created by spilt-over hydrogen. The reaction would take place in the vicinity of the boundary with Pd, where anion vacancy must be most abundant. On the other hand, the second model (b) is based on the direct reduction of NO_x adsorbates by spilt-over hydrogen. This process requires continuous H_2 supply to NO_x-saturated $Ce_{1-x}Mn_xO_2$, which would expand the reduced area on the surface of $Ce_{1-x}Mn_xO_2$ and consequently convert a large number of NO_x adsorbates into N_2. $CeO_2-Fe_2O_3$ as a support in the aged Pt−Ba/$Al_2O_3-CeO_2-Fe_2O_3$ catalyst at 750 °C also showed better NSR activity when using CO as a reducing agent at a relatively low temperature (up to 300 °C) compared to the Fe_2O_3 free catalyst.[225]

The alkaline earth metals are also used with CeO_2 as a support. Costa and Efstathiou showed that over 0.1%Pt/$MgO-CeO_2$ (CeO_2/MgO = 1:1), two structurally different NO_x adsorbed precursor intermediates ("active NO_x" species) were formed within the metal−support interface region, whereas "inactive NO_x" species were populated on both the metal and support surfaces.[226−228] The reduction mechanism followed the H_2 spillover process from Pt metal to $MgO-CeO_2$ support interface. Figure 14 shows the interface formed between MgO and CeO_2 crystals.

TiO_2 has been blended in widely with other single oxide supports, such as Al_2O_3 or ZrO_2, and showed promising

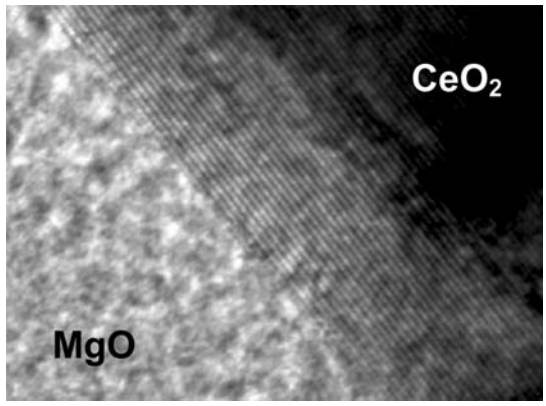

Figure 14. HRTEM image of 0.1 wt % Pt/MgO−CeO_2 prepared by the sol−gel synthesis where the distinct interface formed between MgO and CeO_2 crystals. NO_x adsorption and catalytic sites have been created along the interface of the two oxides. Reprinted with permission from ref 227. Copyright 2007 American Chemical Society.

sulfur tolerant properties when applied as support for NSR catalysis.[229−237] A combination of 33 mol % TiO_2 and 67 mol % lithium-doped Al_2O_3 was selected by Matsumoto et al. to optimize the acidity of the support, and this catalyst minimized the amount of SO_x deposit after the sulfur poisoning test.[230] Takahashi and co-workers obtained the best NO_x removal activity above 500 °C with Pt−K/70%ZrO_2−30%TiO_2 compared to pure TiO_2 or ZrO_2 support (below 400 °C, TiO_2-rich supports were superior for NO_x removal, whereas ZrO_2-only supports had a poor activity over the entire temperature range).[231] The authors found that TiO_2 had a high resistance to K_2SO_4 formation, while ZrO_2 suppressed the solid phase reaction with K. Nanocomposites of Al_2O_3 and TiO_2−ZrO_2 had higher thermal stability compared to that of the physical mixture of Al_2O_3 and TiO_2−ZrO_2 when thermally treated at 900 °C (Figure 15a and b). In the nanocomposite oxide, the particle size of the primary TiO_2−ZrO_2 particles was less than 30 nm on average, whereas aggregation of the TiO_2−ZrO_2 particles in the physically mixed oxide was observed. This phenomenon was attributed to the Al_2O_3 particles acting as a diffusion barrier to the TiO_2−ZrO_2 particles in the nanocomposite. This behavior was also reflected in their NO_x storage capacity, as can be seen from Figure 15c and d.[235] Zou et al. doped Al_2O_3 into TiO_2−ZrO_2 oxide (by sequential impregnation), which improved both the NSR and sulfur-resistance performance of the catalyst Pt−K/TiO_2−ZrO_2.[238] ZrO_2 reacted with TiO_2, $ZrTiO_4$ was formed, and Al_2O_3 doping increased the specific surface area and decreased the Ti content.

Perovskite-type oxides of general formula ABO_3 (where A is usually a rare earth metal coordinated by 12 oxygen atoms and B is usually a transition metal surrounded by six oxygen atoms in octahedral coordination) have been investigated for their role in NSR catalysis. Casapu et al. demonstrated that the formation of $BaPtO_3$ or double perovskite Ba_2PtCeO_6 kept Pt well dispersed, and it could be reduced with H_2 at relatively low temperatures, thus restoring the NSR catalytic activity of Pt.[189,191] With A = Ca, Sr, or Ba and B = Sn, Zr, or Ti, Hodjati et al. studied the NO_x adsorption−desorption and reached the conclusion that, for A sites, the NO_x adsorption−desorption order was Ba > Sr > Ca and, for B sites, Sn > Zr > Ti.[239,240] Using Sn in the B site, they observed little amount of SnO_2 and $BaCO_3$ or $SrCO_3$ phases, whereas, for Zr and Ti, pure perovskite phase was formed. The key factors which control the absorption of NO_2 were the bonding energy between the element B and the oxygen atom and the electropositivity of the element A. However, when $BaSnO_3$, the best perovskite obtained, was exposed to SO_2 and NO_2 together, the competition between the formation of nitrate and sulfate favored the latter, leading eventually to deactivation. Calcined $BaFeO_3$ and $BaFeO_{3-x}$ type perovskite phases showed better sulfur tolerance activity at low SO_2 concentration.[241]

Zeolites have also been reported as possible NO_x adsorbents.[242,243] The zeolite structure, the silica to alumina ratio, and the cation counterbalancing the negative charge of the zeolite framework were found to be important parameters. Alkali metal exchanged zeolite Y uniquely showed trapping of NO and NO_2 as N_2O_3 molecules.[244−246] These N_2O_3 molecules compete with the water molecules on specific adsorption sites.

$$Na_x(H_2O)_y + NO + NO_2 \rightarrow Na_x(H_2O)_{y-3}(N_2O_3) + 3H_2O \quad (22)$$

N_2O_3 can be desorbed as NO and NO_2 by displacing the equilibrium in the above equation as a result of changing the partial pressure (by flushing the adsorbent bed with water-containing gas). When SO_2 was in the feed gas, formation of sodium and hydrogen sulfite was found to poison the N_2O_3 adsorption capacity; however, that could be minimized by high temperature and low oxygen concentration during desorption.[247] Experiments with NO at 200 °C show that this molecule cannot be stored on Cu/ZSM-5.[248] On the other hand, NO_2 may be stored over a wide temperature range from both dry and humid feeds. The adsorption of nitrogen dioxide involves a disproportionation reaction yielding two stored nitrate species and one molecule of NO released to the gas phase:

$$3NO_2 + [CuO] \leftrightarrow NO + Cu(NO_3)_2 \quad (23)$$

Unfortunately, these works do not address the reduction of the stored NO_x. However, combination of Pd/Al_2O_3 as oxidation−reduction component, Pt/Rh−Ba/Al_2O_3 as NSR component, and Cu/ZSM-5 as NO_x storage component showed higher activity than the individual catalysts, which was attributed to the additional synergic effect of this combination.[249] The Pd catalyst upstream of the NSR catalyst improved the NO_x storage ability by NO_2 formation under oxidative atmosphere. The stored NO_x was reduced to NH_3 on the NSR catalyst, and the generated NH_3 was adsorbed on Cu/ZSM-5 downstream of the NSR catalyst under a reductive atmosphere and subsequently reacted with NO_x on the Cu/ZSM-5 under an oxidative atmosphere. Interestingly, Corbos et al. showed that the NO_x removal activity almost doubled with the Pt−Rh−Ba/Al_2O_3 and Cu/ZSM-5 mixed catalyst compared to a system where Pt−Rh−Ba/Al catalyst is situated upstream and Cu/ZSM-5 downstream of the gas flow.[250] They found Cu/ZSM-5 enhanced the formation of NCO species on alumina during rich conditions, which were further hydrolyzed to NH_3 under lean conditions to act as a reductant for NO_x.

4.4. Promoters

In section 4.2 we have discussed the use of other storage components and support oxides which are applied in place of/with conventional Ba and Al_2O_3 for improving the resistance against sulfur deactivation in terms of suppressing

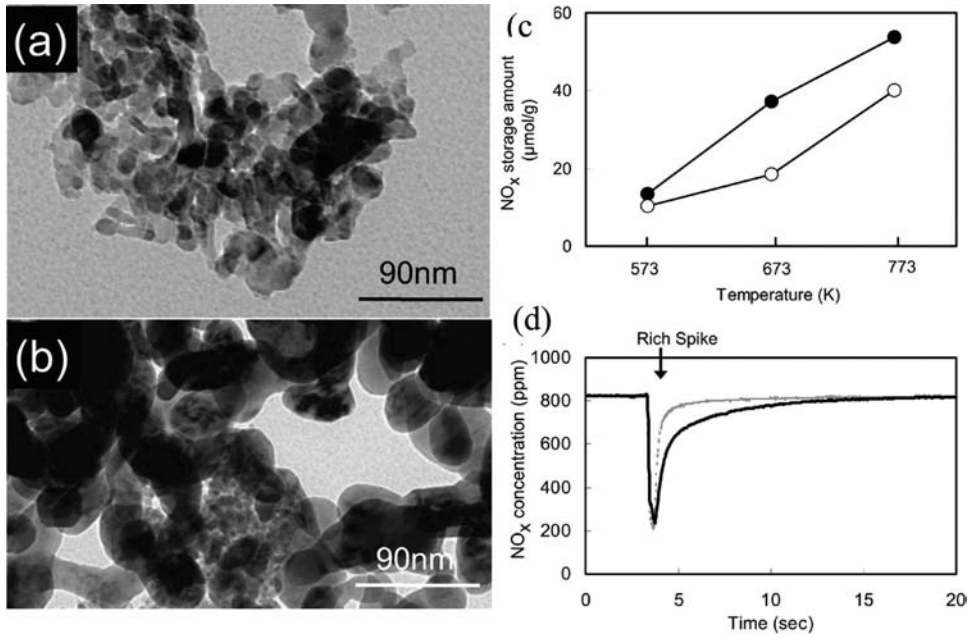

Figure 15. Left panel: TEM micrographs of a nanocomposite of Al_2O_3 and TiO_2-ZrO_2 (a) and a physical mixture of Al_2O_3 and TiO_2-ZrO_2 (b) after thermal treatment at 900 °C for 5 h. Right panel: NO_x storage performance of a nanocomposite of Al_2O_3 and TiO_2-ZrO_2 (●) and the physical mixture (○) after the thermal aging test (c), and the NO_x outlet profile of the nanocomposite of Al_2O_3 and TiO_2-ZrO_2 (dark line) and the physical mixture (broken line) under the lean/rich cycle (d). The lean and rich atmospheres were switched every 2 min. Lean conditions: 0.065% C_3H_6, 800 ppm NO, 6.6% O_2. Rich conditions: 0.34% C_3H_6, 5.6% CO, 1.9% H_2, 50 ppm NO. Under both conditions: H_2O (3%) and CO_2 (11%) were present. The gas flow rate was 1000 cm^3/min, and the gas hourly space velocity was 30,000 h^{-1}. Reprinted with permission from ref 235. Copyright 2007 Elsevier Inc.

formation of $BaSO_4$ or mixed oxides such as $BaAl_2O_4$. However, this addition of foreign components affects the catalytic behavior in various ways, including thermal stability (as a structural promoter) and electronic promotion (as a chemical promoter). It is often difficult to differentiate clearly between structural promoters and chemical promoters.

In NSR catalysts, Ba is added to Al_2O_3 primarily for its storage property. However, much evidence showed that the addition of Ba to Al_2O_3 increases the thermal stability of Al_2O_3. At higher temperature, there can be textural changes in Al_2O_3 which may result in loss of surface area and porosity; sintering can affect the size and distribution of metal particles or structural changes, such as a phase transition from $\gamma \rightarrow \alpha$-$Al_2O_3$ at 1200 °C, may occur. Balint et al. demonstrated that synthesis of Al_2O_3 using combined microemulsion and hydrothermal techniques followed by calcination at 1100 °C produced the α phase, with a very low surface area and large particle size, whereas addition of Ba in the synthesis remarkably increased the surface area with stabilization of the γ phase.[154] However, with higher Ba loading, $BaAl_{12}O_{19}$ was formed. Enhanced thermal stability of Al_2O_3 with addition of Ba compared to the other alkaline earth metals had also been shown by other authors.[251,252] Addition of large cations such as La had shown a promising effect on the thermal stability of the Al_2O_3 support. A long time ago, Schaper et al. had shown that sintering of γ-Al_2O_3 proceeds via surface diffusion and that addition of La_2O_3 decreased the rate of sintering by forming surface $LaAlO_3$ layers, thereby inhibiting the diffusion of ions Al^{3+} and O^{2-} and increasing the transformation temperature by 100 °C.[253] Later, many other researchers revealed the enhanced thermal stability of Al_2O_3 with introduction of rare earth doping elements such as La, Ce, Zr, Gd, and Pr; however, to our knowledge, no NSR catalysis has been carried out with these materials.[251,254] Rare earth metals behaving as chemical promoters along with structural promotion had also been shown by researchers.[255,256] 1%Pt−16%Ba supported on $Al_2O_3-Ce_{0.75}Zr_{0.25}O_2$ showed better hydrothermal stability and higher Pt dispersion compared to conventional $Pt-Ba/Al_2O_3$ catalyst.[257] During the calcination, barium ions migrated over the surface of the catalyst, which showed a good NO_x storage−reduction behavior. Lin et al. showed that Ce, along with Ba, was a better storage material compared to La ($Pt_{2.5}Ce_{30.5}Ba_{33.4}Al_{100}$ had a storage capacity of 1020 × 10^{-6} mol/g at 30 min, while $Pt_{2.5}La_{30.5}Ba_{33.4}Al_{100}$ had a storage capacity of 341 × 10^{-6} mol/g).[255] A further advantage of using CeO_2 compared to Al_2O_3 as a support is the lower stability of formed $BaCeO_3$ (which does not become a hindrance to NO_x sorption like $BaAl_2O_4$), which we have discussed in section 4.3.1. When the rare earth oxides (La_2O_3, Nd_2O_3, Pr_6O_{11}) were used without Ba on CeO_2-ZrO_2 support, they enhanced Pt dispersion and sulfur tolerance compared to the $Pt-Ba/Al_2O_3$ catalyst.[256] Among the rare earth oxides, La_2O_3 doped CeO_2-ZrO_2 showed the highest NO_x sorption at low temperature (200 °C) as well as at higher temperature (400 °C). A promoting effect for NSR activity of TiO_2-ZrO_2 with K as storage component at different calcination temperatures has been observed by Liu and coworkers.[258] $Pt-K/Ti_{0.5}Zr_{0.5}O_2$ ("third-generation NSR catalyst" as called by the authors) calcined at 500 °C showed the largest surface area but the lowest storage capacity. When calcination temperature had been increased to 650 and 800 °C, the NO_x storage capacity of the catalyst was greatly improved, but its sulfur-resisting ability decreased. The interactions between large amount of surface hydroxyl groups and K_2CO_3 at different temperatures were supposed to be responsible for this behavior. An interdependent and combined promoting effect of Co and Rh was demonstrated by Kim et al.[30] Chemically promoting the NO_x storage efficiency by Co was discussed in section 4.3.2. The kinetics of 2% cobalt loading over $Pt-BaO/Al_2O_3$ demonstrated the highest NO_x uptake during the lean cycle, while the reduction

efficiency during the rich cycle was inferior. In contrast to this, Rh lowered NO_x uptake during the lean cycle but enhanced the efficiency of NO_x reduction during the rich cycle.

Thus, the addition of foreign metal oxides to the prototypical Pt−Ba/Al_2O_3 catalyst could result in higher NO_x storage efficiency or a higher rate of reduction of sorbed NO_x, as proved in many instances. The distinction between structural and chemical promotion is often ambiguous because both effects were observed. In any case, the addition of transition metal oxides to Al_2O_3 or CeO_2 supports showed significant promotional effects. High red/ox properties of Co and Mn in Al_2O_3 and in CeO_2 catalyzed NO oxidation, or the presence of Fe or Cu promoted desulfurization (vide section 4.3.2). On the other hand, the presence of rare earth oxides promoted NSR catalytic activity chemically as well as structurally.

4.5. Preparation Methods

Different synthesis methods are adopted for the preparation of solid catalysts. Interestingly, the distinct synthetic routes (which lead to variation in noble metal dispersion and particle size, surface area, crystalline nature, and structural and morphological diversities), different precursor materials, aging, and calcination temperature play an important role in the resulting catalytic behavior of the solid materials.[259,260] For example, Uy et al. found a higher NSR activity for freshly prepared Pt−Ba/Al_2O_3 compared to thermally aged catalyst.[158] The sintering, loss of surface area, oxide formation, and separation of Ba and Pt sites in the thermally aged catalysts were considered possible reasons for its low catalytic activity. Pt−Ba/Al_2O_3 synthesized by three different methods, (i) successive impregnation of Ba and Pt, (ii) coaddition of Pt and Ba, and (iii) Ba precipitation followed by Pt impregnation, did not result in significant differences in rapid NO_x storage as well as in the surface area of the catalysts.[261] On the contrary, the pretreatment of the catalysts under N_2 before thermal aging gave rise to a higher dispersion of Pt and Ba and proximity of the duo, which led to remarkable improvement of the NO_x storage performance. We have discussed earlier the different activities of Pt−Ba/Al_2O_3 on monolith catalysts prepared from four different Pt precursors.[85] The catalyst prepared from $Pt(NO_3)_2$ had significantly higher NO_x storage and reduction activity as well as the highest surface area (96 m^2/g) and Pt dispersion (16%). The pH of the $Pt(NO_3)_2$ solutions in the synthesis of Pt−Ba/Al_2O_3 was ∼3. In this acidic medium, the Pt complexes in the $Pt(NO_3)_2$ solution and the $BaCO_3/Al_2O_3$ surface both were positively charged and had a repulsive electrostatic interaction to prevent agglomeration and precipitation, which led to higher Pt dispersion and consequently higher NSR activity. On the contrary, BaO/Al_2O_3 catalysts, made of different nitrate and acetate precursor salts via impregnation method, showed NO_2 uptake behaviors which were proportional to the BaO content but virtually independent of the preparation method.[262]

In the following section, we will discuss the possible effect of the catalyst preparation route on the catalytic behavior. Syntheses of monolith catalysts are different from those of the powder ones. Monolith supports of cordierite, $2MgO·2Al_2O_3·5SiO_2$ of cylindrical shape with ∼60 channels/cm^2, are impregnated with the catalyst washcoat.[58,263] The catalyst is generally deposited on the cordierite by stepwise impregnation by dip coating. Al_2O_3 is dispersed first with the help of boehmite, followed by Ba and noble metals. In order to achieve a higher degree of Pt and Ba dispersion, increasing hydrothermal stability, many synthetic methods, such as coprecipitation,[77,213,215,235,264] flame-made synthesis,[86,87,219] and sol−gel,[162,241,265] and wet impregnation methods[20,32,71,94,113,116,127,149,167,169,173,266−268] are employed.

Wet impregnation is the most commonly used and conventional synthetic route for NSR catalysts, and most of the monolith catalysts are prepared by this process. It is a stepwise process of impregnating Pt and Ba on an Al_2O_3 support. A recent investigation on changing the order of impregnation of Pt and Ba on Al_2O_3 revealed that the storage capacity at higher temperatures was higher for the catalysts prepared by impregnating Ba on Al/Pt (Al/Pt/Ba) than by impregnating Pt on Al/Ba (Al/Ba/Pt), and at 400 °C the storage was increased by as much as 54% (the optimum storage temperature for the Al/Pt/Ba was around 300−400 °C, and the corresponding temperature for the Al/Ba/Pt samples was 200−300 °C.)[269] The authors suggested that the reason for the shift in temperature is that Ba was better utilized when added to the catalyst after the Pt impregnation than before. The negative effect of the Pt precursor (Pt-$(NO_3)_2$) on Ba during the preparation of Al/Ba/Pt samples was attributed to lowering of the dispersion of the Ba. This might have lowered the amount of storage sites available and possibly also decreased the interfacial area between Ba and Pt for the Al/Ba/Pt samples compared to the Al/Pt/Ba. Preparation by impregnation showed a beneficial effect compared to that by coprecipitation. Li et al. synthesized Pt−MgO/Al_2O_3 from $Mg(NO_3)_2·6H_2O$ and $H_2PtCl_6·6H_2O$ as precursors by incipient wetness impregnation as well as by the coprecipitation method.[270] The results showed that the preparation methods exert significant influence on the structural properties and the adsorption abilities for NO_x. The coprecipitated Pt−MgO/Al_2O_3 had only a hydrotalcite structure, while, in the impregnated catalyst, MgO had two kinds of structural patterns: one was a monolayer dispersion on Al_2O_3, and the other was the excessive bulk MgO. This led to Pt−MgO/Al_2O_3 samples prepared by impregnation with larger specific surface areas. FTIR results showed different mechanisms for NO_x storage on the duo, which was attributed to the higher NO_x storage capacity for the wet impregnated catalyst. On the coprecipitated Pt−MgO/Al_2O_3, after about 15 min, NO was first transferred into bridged nitrite species, and then the nitrite species were oxidized by the oxygen atoms spilling over from Pt sites on the catalyst surface to monodentate and bidentate nitrate species. On the other hand, over the impregnated catalyst, after 10 min, in addition to the above process, NO was first oxidized to NO_2 over Pt sites of the catalyst, and then NO_2 species reacted with O_2 to form monodentate nitrate species.

A proven method for producing homogeneous ceramic powders is sol−gel processing. Stable dispersions, or sols, of small particles are formed from precursor chemicals such as metal alkoxides or other metal organics. Arena et al. synthesized Pt−Ba/Al_2O_3 by the sol−gel method and studied its reactivity as a function of the preparation method and also compared the reactivity with that of a reference sample prepared by wet impregnation.[162] 1%Pt−15%BaO/Al_2O_3 was made from H_2PtCl_6, $Ba(CH_3COO)_2$, and Al(O-i-Pr)$_3$ by the sol−gel procedure using acid (HCl 37%) for the gelification. Figure 16 shows the comparison of NSR activity between the catalysts synthesized by the sol−gel and wet impregna-

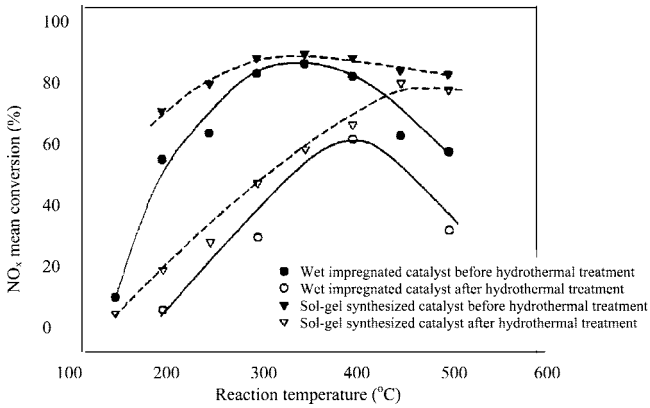

Figure 16. Mean NO_x conversion of sol−gel derived and wet impregnated catalyst before and after hydrothermal treatment. The hydrothermal aging treatment was carried out in a fixed bed reactor at 800 °C (6 h) feeding a mixture of air saturated with water at 60 °C (about 10% water in air). The NSR activity was studied using a series of cyclic sequences of feed changes from lean conditions (120 s: 5% O_2, 10.8% CO_2, 954 ppm NO, remaining He) to rich conditions (6 s: 3.3% CO, 1.1% H_2, 6000 ppm C_3H_6, 5% O_2, 10.8% CO_2, 954 ppm NO, remaining He). Space-velocity was set to 60,000 h^{-1}. Reprinted with permission from ref 162. Copyright 2005 Elsevier B.V.

tion methods before and after the hydrothermal treatment (hydrothermal treatment was at 800 °C for 6 h with 10% water in air). The sample prepared by the sol−gel method before the hydrothermal treatment showed a similar maximum NO_x conversion as the wet impregnated sample. The higher activity of the sol−gel derived catalyst compared to the impregnated one at low and higher temperatures suggested a higher dispersion of the NO_x storage component in the sol−gel derived catalyst. The interesting result was the activity of the catalysts before and after the hydrothermal treatment. After the hydrothermal treatment, the sol−gel derived catalyst showed improved NO_x conversion activity at higher temperatures. The authors suggested the presence of two different types of NO_x storage sites in the sol−gel derived catalyst. At lower temperature, $BaCO_3$ surface species were responsible for NO_x storage, whereas, at higher temperature, $BaAl_2O_4$ was the active NO_x storage component. However, the authors could not place any experimental evidence against their hypothesis. Conflicting results are also available in the literature exhibiting better NSR activity of wet impregnation prepared Pt−Ba/Al_2O_3 compared to corresponding samples prepared using the sol−gel method.[268] BaO in ZrO_2 derived from the sol−gel method showed poor NO_x storage activity compared to BaO in CeO_2−ZrO_2 prepared by wet impregnation. However, this comparison is doubtful because the structural environment of BaO was different in the two catalysts. The sol−gel method has also proven its superiority to the coprecipitation method in the synthesis of NSR catalysts.[265] Haneda et al. synthesized CeO_2−ZrO_2 by two different procedures: the sol−gel method and the coprecipitation method. CeO_2−ZrO_2 synthesized by the sol−gel method showed formation of a solid solution with a single cubic fluorite structure, whereas coprecipitated CeO_2−ZrO_2 showed the presence of separate phases of CeO_2 (cubic) and ZrO_2 (tetragonal). NO_x uptake by the sol−gel synthesized catalysts showed an order of magnitude higher storage capacity than that of the corresponding coprecipitated catalyst (2.19×10^{-4} compared to 0.21×10^{-4} mol of NO g^{-1} CeO_2−ZrO_2 prepared by coprecipitation methods). The NO_x removal proceeded through the oxidation of NO to NO_2 and subsequent adsorption as NO_3^- species on Ce^{4+}−O^{2-} pair sites. However, no great difference in NO_2 coverage was observed between CeO_2−ZrO_2 prepared by sol−gel and coprecipitation methods (0.48 layers and 0.41 layers, respectively), suggesting that the properties of the sorption sites on both sorbents were similar but the storage amount in sol−gel synthesized catalyst was high due to high NO oxidation activity to NO_2. The improved oxygen storage capacity enhances the oxidation ability. As the sol−gel synthesized catalyst consists of a complete solid solution, its enhanced NO oxidation activity was attributed to the formation of O_2^- species, which is a more efficient oxidant than any other surface oxygen species. Homogeneous mixing of Ce ions and Zr ions in the solid solution was considered to be one of the important factors for the high NO_x sorption capacity of the sol−gel synthesized catalyst compared to the corresponding coprecipitated catalyst.

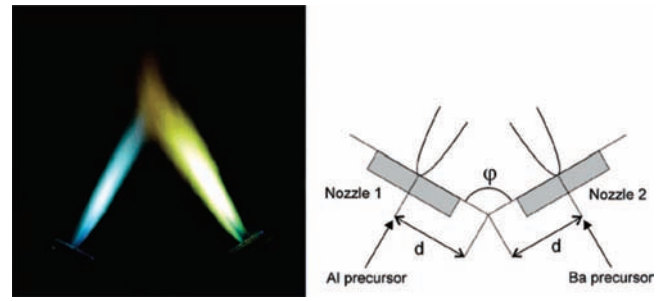

Figure 17. Schematic of the FSP setup using two separate nozzles. The image shows two flames producing Pt/Ba/Al_2O_3 (blue flame (left): Al; yellow-greenish flame (right): Pt and Ba). The angle between the two nozzles φ was fixed at 120°, and the internozzle distance between the angle tip and each nozzle center (d) was varied symmetrically between 6 cm. Reprinted with permission from ref 87. Copyright 2006 American Chemical Society.

Flame spray pyrolysis has cut a mark in the synthesis of NSR catalysts. Flame spray pyrolysis is a one step process involving the combustible precursor solutions. Single-nozzle as well as two-nozzle flame syntheses have been applied.[271] The latter allows a better control of the distribution of the different constituents in the resulting material. A typical setup for two-nozzle flame synthesis is shown in Figure 17. Crucial are the positions of the two nozzles, which greatly influence the temperature and concentration fields in the flame. Strobel et al. used a setup with a fixed angle φ of 120° and a distance d = 6 cm between the nozzles. The precursor mixture contained Al(III) tri-*sec*-butoxide as Al precursor and Ba(II) 2-ethylhexanoate and Pt acetylacetonate as Pt−Ba precursor.[87] The Al and Pt−Ba precursors were sprayed from the separate nozzles with 5 and 3 mL min^{-1} feed, respectively. Both the sprays were surrounded and ignited by a small flame ring. The flames were operated in an open air environment, reaching a maximum flame temperature of up to 2500 °C, and the product particles were collected on a glass fiber filter. As the temperature during the synthesis is so high, usually the product formed is the thermodynamically most favorable. As we have discussed earlier (section 4.2.1), the flame spray pyrolysis made catalysts showed a higher percentage of monoclinic $BaCO_3$ and, at higher Ba loading, flame made catalysts were virtually free of orthorhombic $BaCO_3$, whereas, in corresponding wet impregnated catalyst, there was a higher concentration of orthorhombic $BaCO_3$ (e.g., for 25 wt % Ba loading in wet impregnated catalyst, orthorhombic $BaCO_3$ was 32% and monoclinic $BaCO_3$ was 56%, whereas, for the flame made catalyst at the same Ba loading, monoclinic

$BaCO_3$ was 48% with no orthorhombic $BaCO_3$). Because of a higher concentration of monoclinic $BaCO_3$ as well as a higher surface area of the catalyst synthesized by flame spray pyrolysis, the NO_x storage was higher compared to that of corresponding conventionally wet impregnated Pt−$BaCO_3$/Al_2O_3 (e.g., for 25 wt % Ba loading, flame made catalyst stored 1.65×10^{-3} mol of NO per g of catalyst, whereas the wet impregnated catalyst stored 1.32×10^{-3} mol of NO per g of catalyst).[86,272]

Pt−$BaCO_3/Al_2O_3$ synthesized recently by using triblock copolymer P123 as template exhibited higher Pt dispersion, higher surface area and porosity, as well as better thermal stability compared to the catalyst prepared by a conventional wet impregnation method.[123] For this synthesis, with the aqueous solution of the template P123 calculated amounts of $Ba(NO_3)_2$ and Al(O-i-Pr)$_3$ were taken. $(NH_4)CO_3$ was added dropwise to this solution to precipitate Ba^{2+} into $BaCO_3$. The $BaCO_3$ phase in this mesoporous catalyst after calcination was monoclinic, which has better NO_x adsorption properties compared to orthorhombic-whiterite $BaCO_3$.[86] The catalyst prepared by the impregnation method for comparison showed a higher concentration of orthorhombic-whiterite $BaCO_3$. The sulfur removal occurred also at lower temperature over this uniquely synthesized catalyst due to a higher dispersion of Ba and smaller Pt particles.

The coprecipitation is a simple and rapid preparation method with easy control of particle size. Synthesis of Ba/Al_2O_3 from the precursors $Ba(NO_3)_2$ and $Al(NO_3)_3 \cdot 6H_2O$ involved precipitation by $(NH_4)_2CO_3$ in acidic medium and eventually calcination at 1000 °C, which resulted in higher NO_x storage due to formation of a $BaAl_2O_4-Al_2O_3$ phase.[77] An advantage of coprecipitation synthesis of the nanocomposite of $Al_2O_3-ZrO_2-TiO_2$ for NO_x storage over the conventional physical mixture of oxide has been nicely demonstrated by Imagawa et al.[235] After thermal treatment at 1000 °C, the aggregation of ZrO_2-TiO_2 particles in the nanocomposite of Al_2O_3 and ZrO_2-TiO_2 was inhibited relative to that in the physically mixed Al_2O_3 and ZrO_2-TiO_2 because Al_2O_3 particles act as a diffusion barrier to ZrO_2-TiO_2 particles in the nanocomposite oxide. This helped in storing 55 μmol of NO per gram of coprecipitated nanocomposite of $Al_2O_3-ZrO_2-TiO_2$ compared to 40 μmol of NO per gram of the physical mixture of $Al_2O_3-ZrO_2-TiO_2$. Hydrotalcite-like compounds synthesized by coprecipitation have shown good NSR activity.[213,264] The Mg/Ru−Al hydrotalcite-like compounds synthesized by constant-pH coprecipitation were made from $Mg(NO_3)_2 \cdot 6H_2O$, $Al(NO_3)_2 \cdot 9H_2O$, and $RuCl_3 \cdot 3H_2O$ as precursors.[264] The as-prepared compound showed a single phase hydrotalcite structure, whereas when calcined at 600 °C for 6 h, it produced MgO and the spinel phase $Mg(Al,Ru)_2O_4$. However, no RuO_x was formed, indicating a high dispersion via this synthesis. Due to this high dispersion of Ru and consequent oxidation of NO to NO_2, the catalyst showed a high NO_x storage capability of 220 μmol g^{-1}.

From the above discussion, we can conclude that the synthesis method applied to prepare the catalyst plays a very important role in the NSR catalysis. The various preparation methods control the noble metal and storage site dispersion, their structural behavior, as well as the storage and regeneration chemistry. However, there is no unique way of synthesis which can conclusively be claimed as the best synthetic route for preparation of the catalyst.

4.6. Influence of Remote Control

We have considered in section 3 the different steps of the NSR mechanism, comprising the oxidation of NO_x, storage and reduction (catalyst regeneration), and also the intimate relation between the noble metal and the storage component in terms of spillover and reverse spillover phenomena. The geometric proximity between the noble metal and the storage component plays a significant role in the mechanism and overall activity of the catalyst.[273,274] Mahzoul et al., in their pioneering work on remote control, discovered two kinds of Pt sites working differently based on the distance from the Ba sites.[266] They proposed that Pt sites close to BaO crystallites are active for $Ba(NO_3)_2$ formation and involved in the spillover reaction, while the Pt sites which are located far from the BaO crystallites only help in oxidation of NO to NO_2. Later, Epling et al. concluded that it is not the Pt sites; rather two different kinds of Ba sites are present in the Pt−Ba/Al_2O_3 catalyst depending on the distance from the Pt sites.[112] The proximal Ba sites store NO_2 as nitrates with participation of Pt and O_2 as an oxidant. The remote Ba sites, where NO_2 is the more preferable source of oxygen, rely on the disproportionation mechanism to store NO_x as nitrates. Indpendent of whether there are two kinds of Pt sites or Ba sites, it is clear that the proximity of the Pt and Ba plays a significant role, as Uy et al. showed the closeness of Pt and Ba sites in the fresh catalyst enhanced NO_x storage capacity compared to the aged catalyst where Pt and Ba are not proximal sites.[158] Nova and co-workers investigated the exact effect of the geometric proximity on the NSR mechanism and arrived at an almost similar conclusion.[46,116,275] During a regeneration process over Pt−Ba/Al_2O_3, the stored nitrates were readily reduced to N_2 and NH_3, which indicated the reduction of the stored $Ba(NO_3)_2$ through a Pt-catalyzed surface reaction unlike thermal decomposition of stored $Ba(NO_3)_2$ from the Pt free surface.[275] Such results indicated the reverse spillover phenomena between Pt and Ba sites and the importance of their close proximity. This was confirmed further when different products were obtained with the regeneration experiment over the physical mixture of Pt/Al_2O_3 and Ba/Al_2O_3. Similar kinds of experiment designed to elucidate the spillover phenomena on Pt−BaO/Al_2O_3 prepared by impregnation and a physical mixture of Pt/SiO_2 and Ba/Al_2O_3 revealed that the rate of isotopic exchange between ^{15}NO and stored NO_x under storage conditions was more than five times faster in the former catalyst compared to the later, demonstrating spillover of NO_x species between Pt and BaO in close proximity.[52] The closeness of Pt and Ba sites also plays an important role in desulfation of the catalyst.[217,276] In sulfated Pt−Ba/Al_2O_3, most of the sulfate is reduced to H_2S during reduction, which contributes to the removal of sulfur.

$$BaSO_4 + 4H_2 \rightarrow Ba(OH)_2 + H_2S + 2H_2O \quad (24)$$

$$BaSO_4 + CO_2 + 4H_2 \rightarrow BaCO_3 + H_2S + 3H_2O \quad (25)$$

(CO_2 is also present in the exhaust)

Platinum has a good H_2 activation ability, and it enhances the rate of the above-mentioned reactions if it is placed near to Ba sites. In a recent study on the importance of the proximity of Pt and Ba controlled deposition of Pt clusters on $BaCO_3$ or Al_2O_3, a two-nozzle flame spray pyrolysis method was applied.[271] During storage, the beneficial role of a close interaction of Pt and Ba for NO_x uptake was

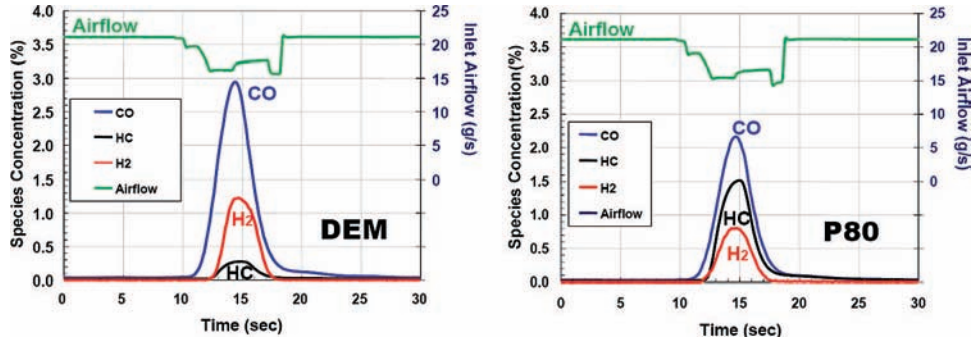

Figure 18. Reductant concentrations during two different regeneration strategies: delayed and extended main (DEM) and post-80 injection (P80). In DEM the extra fuel is injected near main injection timing to achieve rich conditions, whereas in P80 the extra fuel is injected after the main injection later in the cycle to achieve rich conditions. Reprinted with permission from ref 277.

confirmed. However, Pt on Al_2O_3 exhibited a better NO oxidation, which was the rate limiting step for the overall NO storage process at low temperatures (300 °C). During regeneration, Pt on Ba showed much better activity than Pt on Al_2O_3, which was attributed to the important reverse spillover phenomenon. However, at higher temperatures (>350 °C) the location of Pt barely affected the performance during storage and reduction.

Interesting results about the lowering of the performance of the NSR catalyst due to close contact between Pt and Ba have also been reported. According to Dawody et al., the close contact between Pt and Ba might promote electronic interaction and could suppress the NSR catalytic activity, and they demonstrated that if Pt particles were preferably anchored close to Al_2O_3 rather than to $BaCO_3$ surface particles, the catalytic activity was higher.[85]

To sum up, the proximity and the spatial distribution of the noble metal and storage sites seem to play an important role for achieving high NSR activity. However, systematic investigations on the optimum distance between the two components and exploiting this remote control phenomenon for gaining higher activity are still needed.

5. Influence of Exhaust Gas Composition

The composition of real engine exhaust gas is rather intricate and depends on many factors, such as type of fuel, engine type, and air/fuel ratio used. This, together with the different cycling times used for lean and reach periods, renders comparison of the catalyst behaviors reported in the literature often quite difficult. A possible way to alleviate this problem is the use of model gas compositions which closely mimic the composition of real engine exhaust gas. Unfortunately, even these model gas compositions vary in the literature, which makes comparison between the various studies and the drawing of general conclusions concerning the influence of gas composition even more difficult. CO/H_2 can vary from 3 to 2 in the engine exhaust, depending on the fuel injection (Figure 18).[13,277] In the real exhaust, other carbonaceous reductants such as CO and hydrocarbons (C_3H_6, C_3H_8) as well as soot deposits are also present and affect the regeneration step of NSR.[278−281] Epling et al. showed that, from a 1.7 L diesel engine, the maximum amount of H_2 and CO were listed as 4.1% and 8.2%, respectively.[13] A mixture of C4 and C5 hydrocarbons was also observed in the exhaust when the engine exhaust was cycling between lean (normal) and rich conditions.

In many of the studies, H_2 was used as a reductant because of the relative simplicity of the reaction mechanism and detection. H_2 can be produced on board via steam reforming, water gas shift reaction, partial oxidation, or autothermal reforming. Some typical reactions of diesel fuels are

$$C_{12.31}H_{22.17} + 12.31H_2O \rightarrow 12.31CO + 23.4H_2 \quad (26)$$

$$CO + H_2O \rightarrow CO_2 + H_2 \quad (27)$$

$$C_{12.31}H_{22.17} + 6.15O_2 \rightarrow 12.31CO + 11.08H_2 \quad (28)$$

$$C_{12.31}H_{22.17} + 5.65O_2 + H_2O \rightarrow 12.31CO + 12.08H_2 \quad (29)$$

Most attention has been devoted to the mechanism describing NO_x storage without H_2O and CO_2 in the gas feed. However, since H_2O and CO_2 are major components in the exhaust gas (reactions 30 and 31), it is important to understand how these exhaust gas components affect the storage and regeneration of NSR catalysts.

$$CO + H_2O \rightarrow CO_2 + H_2 \quad (30)$$

$$C_{12.31}H_{22.17} + 17.85O_2 \rightarrow 12.31CO_2 + 11.08H_2O \quad (31)$$

Under exhaust gas conditions, $Ba(OH)_2$ and $BaCO_3$ are thermodynamically favored over BaO; therefore, NO_x storage may take place with displacement of water or CO_2 rather than by simple nitrate formation. In X-ray photoelectron spectroscopy studies of the exposure of a BaO(110) surface on a Cu(111) substrate to water vapor, even at very low exposure, a second O(1s) peak, denoted O (531), became evident at ca. 531.5 eV (Figure 19a).[282] As the exposure was increased, this new peak increased in intensity while the original O (1s) peak decreased in intensity. The O (1s) binding energy of 531.0−531.4 eV, after H_2O exposure, confirmed $Ba(OH)_2$ formation. As a result of CO_2 exposure of a BaO(110) surface, the Ba $3d_{5/2}$ peak maximum was gradually shifted by ca. 0.6−0.8 eV to higher binding energy, confirming formation of $BaCO_3$ (Figure 19b).

The following section summarizes the impact of different reducing gases and the role of CO_2 and H_2O in the NSR storage and regeneration mechanism.

5.1. Reducing Gas

Fridell et al. in the early days of NSR were probably the first researchers who reported a study in which they systematically utilized different feed gases such as H_2, CO, C_3H_6, and C_3H_8 during storage of NO_x; however, they did not find any marked difference between the different reducing agents.[263] But with the increase in CO_2 concentration in the

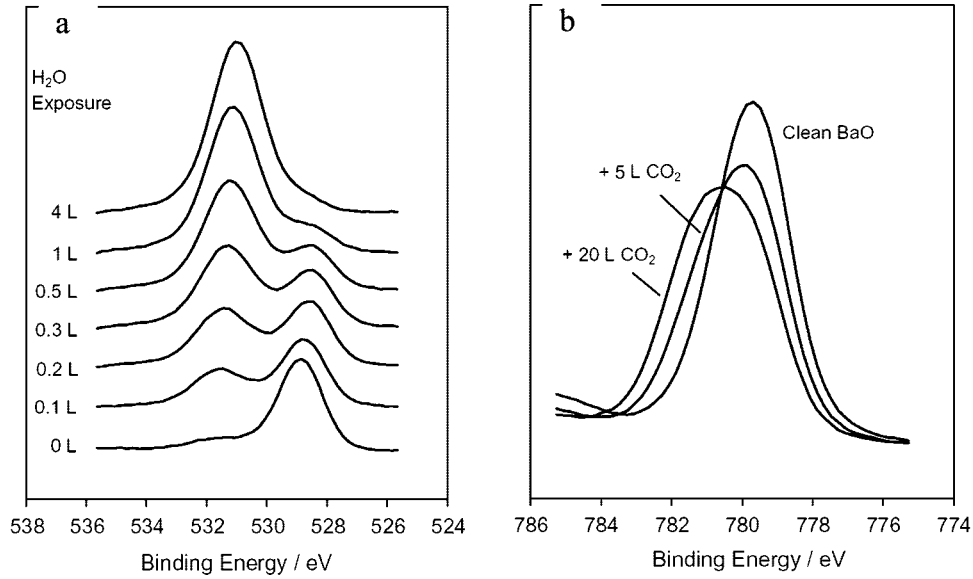

Figure 19. (a) O (1s) XP spectra of BaO after exposures to H_2O at room temperature. (b) Effect of CO_2 exposure on the Ba $3d_{5/2}$ XP spectra. XPS studies were carried out by dosing H_2O, and CO_2 from the background, and these exposures are quoted in Langmuirs (1 Langmuir = 10^{-6} Torr s). XPS were calibrated using the Cu $2p_{3/2}$ and Cu 3p peaks (with assigned binding energies of 932.66 and 75.13 eV, respectively) of the Cu(111) substrate. Reprinted with permission from ref 282. Copyright 2006 Elsevier B.V.

feed gas, the NO_x storage was affected significantly, whereas an increase in C_3H_8 concentration did not considerably affect the storage. Erkfeldt et al. demonstrated that CO and C_3H_6 play opposite roles in storage of NO_x.[283] It is well believed that NO_2 is a preferential sorbate compared to NO, and in the presence of CO, NO_2 is reduced to NO ($CO + NO_2 \rightarrow CO_2 + NO$) and the storage is inhibited. On the other hand, C_3H_6 in the feed gas stopped the NO_2 reduction by CO and thus promoted storage. Following this work, many studies making use of different reducing agents for the regeneration step appeared in the literature. H_2 was the most effective reductant for stored NO_x in $Pt-BaO/Al_2O_3$ catalyst at low temperatures (100 °C) followed by CO, whereas C_3H_6 and C_3H_8 showed activity only at higher temperatures.[39] The findings were confirmed later by a detailed investigation on $Pt-BaO/Al_2O_3$ from Abdulhamid et al.; however, C_3H_8 did not work for this catalyst even at higher temperature (350 °C).[37] They observed NH_3 formation when H_2 was used as a reductant, whereas N_2O was a major product when using CO as reductant. Later they showed that the different reducing agents behaved differently with changing of the noble metals (Figure 20). The trend in the ability of NO_x reduction of the reductants was also similar with $Pd-BaO/Al_2O_3$ except that the Pd-containing catalyst was able to reduce stored NO_x with C_3H_8 at 350 °C.[29] Over $Rh-BaO/Al_2O_3$, CO showed the maximum NO_x reduction at 250 and 350 °C (Figure 20b).

Further investigations showed that CO and hydrocarbons (C_2H_4, C_3H_6) poisoned the Pt surface of $Pt-Ba/Al_2O_3$ in the regeneration step of NSR by carbon deposition on Pt sites, which hindered the NO dissociation, eventually making the carbonaceous reductants poorer than H_2.[89,284−286] CO can be deposited on Pt sites (*) according to the following reaction: $CO + * \rightarrow CO*$ and $CO* + * \rightarrow C* + O*$. C_2H_4, on the other hand, over Pt sites, at first lead to di-σ ethylene, followed by conversion of di-σ-ethylene to π-ethylene, and then followed the reaction leading to deposition of C on the Pt sites: $C_2H_4* + 4O \rightarrow CO_2 + 2H_2O + C*$.[285] $Pt-Ba/Al_2O_3$ is a potential catalyst for soot oxidation also (diesel particulate NO_x reduction; DPNR).[287−292] NO in the lean phase can remove the deposited C on Pt sites by two ways: (i) direct reaction, $C* + NO \rightarrow CO + N*$ followed by $N* + 2O \rightarrow NO_2$, and (ii) oxidation of NO to NO_2 on Pt sites and reaction of the formed NO_2 with C, leading to the formation of CO_2 and NO.[285,293−295] A detail discussion will follow in section 5.4. Liu and Anderson also found the order of efficiency in terms of conversion of stored NO_x to N_2 to follow $H_2 > CO > C_3H_6$, and the use of H_2 led to the lowest NO_2/NO ratio.[296] On a Pt−Rh based catalyst, the steam reforming and water gas shift reactions were promoted by Rh to convert less active CO and HC into more active H_2, thus reducing the negative effects of CO and HC.[35] Koci et al. with the help of experiments and mathematical simulations on a Pt−Rh and Ba-containing $Al_2O_3-CeO_2$ monolith catalyst showed that the oxygen storage capacity of CeO_2 played an important role by affecting the water gas shift reaction, steam reforming reaction, and oxidation of H_2, CO, and C_3H_6 and thus regulating the regeneration step by different reductants.[84,297] On sulfated $Pt-BaO/Al_2O_3$ catalyst, H_2 was by far the best reductant among the three reductants (H_2, CO, C_3H_6).[298] The mechanism of $BaSO_4$ reduction by H_2 involves Pt-promoted reduction to produce either BaO, SO_2, and H_2O or BaO, H_2S, and H_2O. Irrespective of the mechanism involved, sulfate reduction by H_2 may lead to sulfur deposited on the Pt under O_2 deficient conditions. However, Liu and Anderson showed that O_2 in the rich mixture was important, as it oxidized S deposited on Pt to SO_2 or if O_2 was consumed by H_2 to form H_2O, which was able to hydrolyze sulfur compounds deposited on Pt.[298] The removal of NO_x from the $Pt-BaO/Al_2O_3$ catalyst was very effective when both H_2 and CO were used as reducing agents; the rate of removal was lower than that in the presence of only H_2 but higher than that in the presence of only CO.[81,299] Szailer et al. observed intermediate species such as isocyanates bound to the oxide components of $Pt-BaO/Al_2O_3$ during reduction with CO.[81] According to them, at low temperatures, H_2 was the primary reducing agent, whereas, at high temperatures, NCO reacted directly with NO_x to form N_2 and CO_2. On the contrary, Scholz et al. showed the

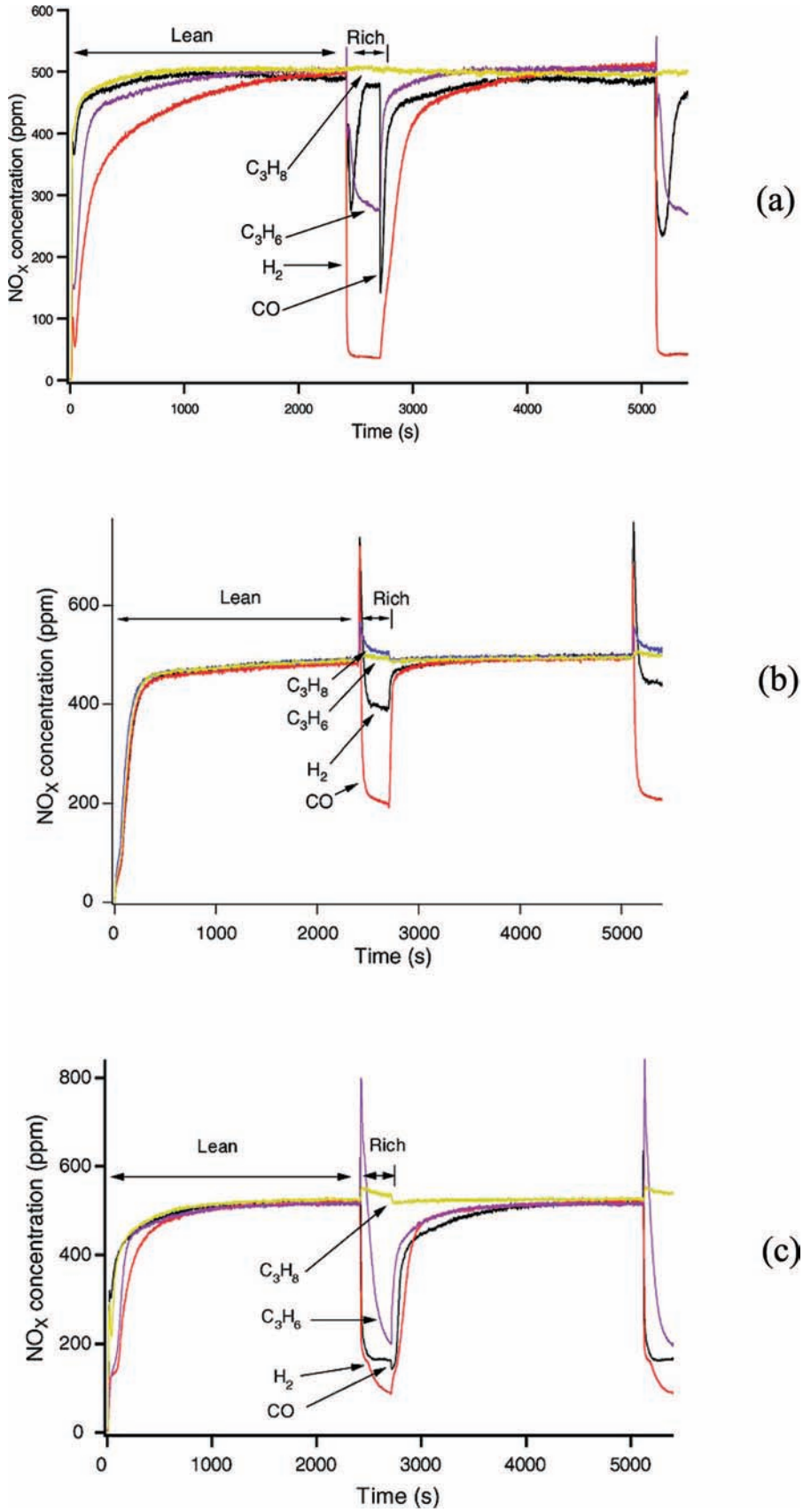

Figure 20. NO_x signal for storage and reduction of NO_x for (a) Pt−BaO/Al_2O_3, (b) Rh−BaO/Al_2O_3, and (c) Pd−BaO/Al_2O_3 at 250 °C using either CO, H_2, C_3H_6, or C_3H_8 as reducing agent. All the catalysts were first reduced in 3% H_2/Ar at 400 °C for 30 min and then stabilized in a gas mixture of 8% O_2, 400 ppm C_3H_6, 500 ppm NO_2 balanced with Ar at 500 °C for 30 min. For the lean period, the catalysts were exposed to 500 ppm NO_2 in Ar for 40 min to ensure complete saturation with NO_x. The lean period was followed by a rich period consisting of 500 ppm NO_2 and 2000 ppm CO, 2000 ppm H_2, 222 ppm C_3H_6, and 200 ppm C_3H_8 balanced with Ar for 5 min. The total flow rate during the lean and rich cycles was 1730 mL min^{-1}, corresponding to a space velocity of 52,000 h^{-1}. Reprinted with permission from ref 29 (Copyright 2006 Elsevier B.V.) and ref 37 (Copyright 2004 Plenum Publishing Corporation).

detrimental role of NCO (from the reducing gas CO), which was strongly bound to Ba sites and stopped NO_x reduction.[285]

From the results discussed, it can be concluded that depending on the noble metal and the supporting oxide, the reducing agent behaves differently. As Pt activates H_2 very easily, H_2 in all above examples has been found to be the best reducing agent at low temperature. However, over the desulfated or sulfated Pt free catalysts (BaO/Al_2O_3) under dry conditions, CO emerged as the more effective reductant than H_2.[298,300]

5.2. Water

H_2O has been shown to play a preliminary role in the storage step of NSR as a competitor for sorption sites (formation of hydroxyls) and/or influences the oxidation of NO to NO_2. Many investigations have been carried out, aiming to clarify whether H_2O plays a beneficial role or not in the overall mechanism, and plenty of mechanistic details have come out in the process. There could be a role of H_2O during regeneration also.

Lietti et al. investigated the influence of H_2O on the NO_x storage at 200, 300, and 400 °C during the lean phase for the $Pt-Ba/Al_2O_3$ catalyst.[118] The presence of H_2O in the gas phase transformed the Ba component into $Ba(OH)_2$, and the storage followed, releasing H_2O according to the stoichiometric equations:

$$Ba(OH)_2 + {}^1/_2O_2 + 2NO \rightarrow Ba(NO_2)_2 + H_2O \quad (32)$$

$$Ba(OH)_2 + {}^1/_2O + 2NO_2 \rightarrow Ba(NO_3)_2 + H_2O \quad (33)$$

$$2Ba(OH)_2 + 2N_2O_4 \rightarrow Ba(NO_2)_2 + Ba(NO_3)_2 + 2H_2O \quad (34)$$

They found that water had a promoting action at low temperature (200 °C) and a negative effect at high temperature on the reactions involved in the NO_x storage process (the net amount of NO_x stored up to catalyst saturation in the presence of water was lower by 20−40% at higher temperatures). However, in the presence of H_2O, the reduction was fast with high selectivity. Epling et al. found that different feed concentrations of H_2O affect in different ways the trapping chemistry of the NSR mechanism; however, it did not affect the regeneration of the catalyst.[112,301] According to them, two kinds of mechanism operate in the trapping process over $Pt-Ba/Al_2O_3$: a rapid and complete sorption of NO_x and a slower rate of NO_x sorption with a longer time period. H_2O shortened the time of complete trapping at lower operating temperatures (175−200 °C). They further concluded that H_2O and NO_x compete for the same adsorption site on Al_2O_3 and the presence of H_2O essentially eliminated NO_x adsorption on the sites associated with Al_2O_3.[112,178] Lindholm et al. later reached the same conclusion that the presence of H_2O affected the storage sites on Al_2O_3 but not the Ba sites.[302] It has been well proved that NO_2 is adsorbed better than NO itself, or NO_2 is a better precursor to sorption. In the presence of H_2O, $NO \rightarrow NO_2$ oxidation is hindered and so is the NO_x storage on the Ba component.[69,303,304] Cant and Patterson also concluded that the presence of H_2O reduced the NO_x storage.[300]

From the above discussion it emerges that water plays an unfavorable role in the lean phase of NSR. However, Kim et al. demonstrated that H_2O was essential in formation of the bulk $Ba(NO_3)_2$ phase, which otherwise was not feasible with NO_2 preadsorbed thermally aged $Pt-BaO/Al_2O_3$ samples, irrespective of Ba loading.[305] Fourier transform infrared spectroscopy along with time-resolved synchrotron X-ray diffraction techniques revealed that, in the presence of water, surface Ba nitrates converted to bulk nitrates and water facilitated the formation of large $Ba(NO_3)_2$ particles; this surface to bulk conversion was totally reversible and the total amount of stored NO_x was unaffected by H_2O.[306,307] The presence of water in the rich phase prevented poisoning of the catalyst from CO and hydrocarbons.[285] It is well established that the presence of H_2O in the feed gas enhances the soot oxidation; the NO_2 with H_2O forms some HNO_2 or HNO_3 in the gas phase which then reacts directly with the carbon on the surface.[308,309] Conflicting results about NH_3 formation in the regeneration process in the presence of H_2O have been reported. While some researchers reported no NH_3 formation in the presence of H_2O (as H_2O covered the Pt sites, resulting in reduced H coverage),[43,285] Chen and Schwank observed over $Pt-Ba/Al_2O_3$ in the presence of H_2O under rich conditions NH_3 as one of the major products.[310] They made use of the NH_3 by positioning a Co^{2+} exchanged beta zeolite in the downstream bed for reducing NO_x to N_2. A slightly different water treatment on BaO/Al_2O_3 samples at room temperature had shown formation of bulk $BaCO_3$ components (carbonation reaction) from $BaO/BaCO_3$ or $BaAl_2O_4$ via dissolution/reprecipitation processes which in turn showed enhanced NO_x uptake due to a promotion of Pt−Ba contact caused by morphological and structural rearrangements of the barium species (Figure 21).[120,153,311] However, at lower temperature (200 °C) the trend was opposite, which behavior was not addressed by the authors.

5.3. Carbon Dioxide

CO_2 originates from fuel combustion and from oxidation of CO in real gas exhaust. Therefore, the key question is what kind of role does CO_2 play? Is it beneficial or detrimental for NSR activity over conventional $Pt-Ba/Al_2O_3$ catalyst and how does it act over other catalysts? In the following section, we will witness the different roles CO_2 plays in different steps (storage and regeneration) of NSR catalysis.

It is well-known that CO_2 adsorbs specifically on basic sites of metal oxides, both hydroxyl groups and oxygen ions, giving rise to bicarbonate-like species and to a variety of carbonate-like species. In fact, CO_2 adsorption on $Pt-Ba/Al_2O_3$ catalyst showed the presence of linear CO_2 coordinated to Ba^{2+} ions and also the presence of a large variety of surface carbonate-like species (bridged, chelating, and very small amounts of monodentate carbonates on Ba sites).[128] Hodjati et al. were among the first researchers who addressed the effect of CO_2 in the storage step, and strong monodentate and bidentate carbonate formation was observed on bulk BaO, hindering the NO_x sorption because of the high stability of the carbonates over nitrates, whereas, on the other hand, CO_2 had no impact on $BaAl_2O_4$.[160] Formation of $BaAl_2O_4$ from $Pt-Ba/Al_2O_3$ during NSR operation is a common phenomenon, which we have discussed in section 3.2. Casapu et al., in this regard, also showed that even though CO_2 did not react with $BaAl_2O_4$, $BaCeO_3$ (formed from $Pt-Ba/CeO_2$) on treatment with 20% CO_2/He decomposed into $BaCO_3$ and CeO_2 between 400 and 980 °C, thus playing a beneficial role in NSR chemistry of $Pt-Ba/CeO_2$ catalysts.[126] In a study

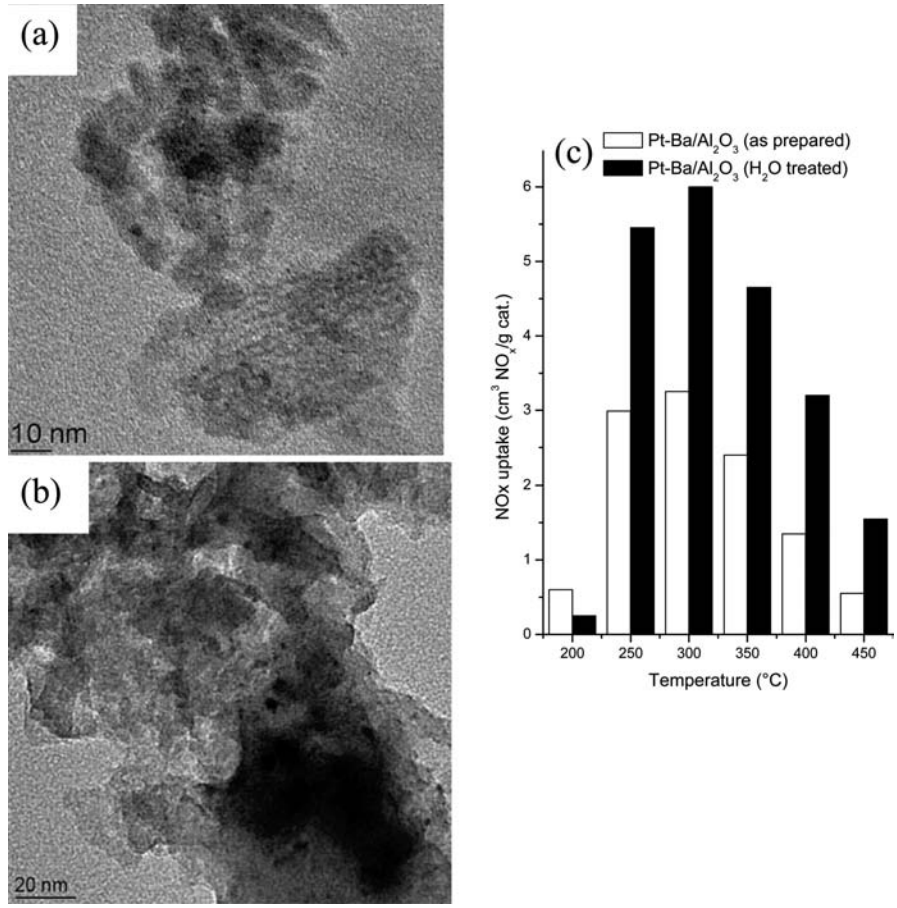

Figure 21. (a) TEM micrograph of an as prepared Pt−BaO/Al_2O_3 sample with highly dispersed Pt clusters smaller than 2 nm; (b) water treated Pt−BaO/Al_2O_3; (c) NO_x uptake of as-prepared and water treated Pt−Ba/Al_2O_3 as a function of temperature. The rich period was 1 min, and the lean period was 4 min. Lean period: 200 ppm NO, 12% O_2. Rich period: 200 ppm NO, 1.33% H_2, 4% CO, 1330 ppm C_3H_6. In both periods, H_2O and CO_2 were 10%. Reprinted with permission from ref 120. Copyright 2008 Springer Science & Business Media, LLC.

on storage of NO_x, Lietti et al. observed over Pt−Ba/Al_2O_3 the net quantity of NO_x stored at 300 °C was less in the presence of CO_2 (4.46×10^{-4} mol/g catalyst in the presence of 0.3% CO_2 while the sorption amount was 5.81×10^{-4} mol/g catalyst in the absence of CO_2), concluding an inhibiting effect of CO_2 on NO_x storage.[118] Fridell et al. also showed a similar effect of CO_2 on NO_x storage, although the storage amount was quite high (21.6×10^{-6} mol of NO_x in the absence of CO_2 and 16.1×10^{-4} mol of NO_x in the presence of 12% CO_2).[263] Over Al_2O_3 and Al_2O_3−SiO_2 supported catalyst, the detrimental effect of CO_2 increased with both Ba loading and storage temperature, whereas, over Pt−Ba/$Ce_{0.7}Zr_{0.3}O_2$ catalyst, there was no significant CO_2 effect related with Ba loading or temperature.[312]

Balcon et al. observed that CO_2 in the reducing gas mixture on Pt−Ba/Al_2O_3 helped to release more NO_2 in the regeneration phase concluding to the equilibrium: $CO_{2,gas} + {}^*NO_{2,stored} \leftrightarrow {}^*CO_{2,stored} + NO_{2,gas}$.[160,313] Later, Amberntsson and co-workers also supported formation of surface Ba-carbonates which replaced the nitrates and promoted the NO_x release in the rich phase (Figure 22).[314] Contradictory results showed that there was an inhibiting effect of CO_2 in the regeneration process, and above 300 °C, once all the stored reactive NO_x had been reduced by H_2, CO was formed through the reverse WGS reaction ($CO_2 + H_2 \leftrightarrow CO + H_2O$).[118] Lietti and co-workers recently showed that the reduction of NO_x by H_2 over Pt−Ba/Al_2O_3 consists of two steps (reduction of nitrates to NH_3 by H_2 followed by

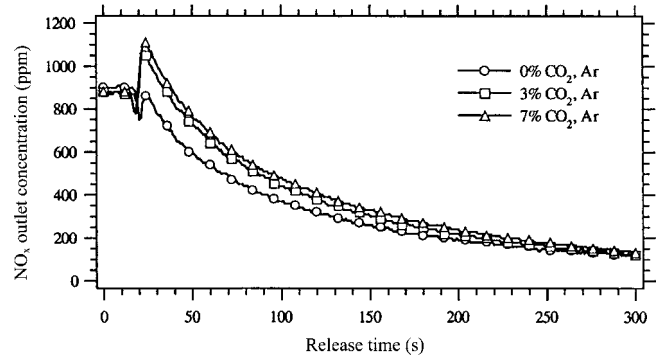

Figure 22. Release of NO_x at different CO_2 concentrations. The sample was a commercial monolith catalyst (cylindrical, ϕ = 2:0 cm, L = 3:3 cm) containing noble metals (NM) and BaO (washcoat loading 160 mg/cm^3). The lean mode was performed in a mixture of 10% O_2, 5% CO_2, 475 ppm NO, and 475 ppm NO_2 balanced to 100% with Ar. In rich mode, CO_2 was varied from 0 to 7% CO_2 with 5% H_2O. The space velocity was 10,000 h^{-1}. Reprinted with permission from ref 314. Copyright 2001 Elsevier B.V.

reduction of nitrates to N_2 by NH_3) and CO_2 inhibited both reduction steps by poisoning the Pt sites with the CO formed by the reverse WGS reaction.[315] The lesser production of NH_3 in the reduction of nitrates to NH_3 by H_2 in the regeneration period of NSR was also observed with Mg based catalysts.[316] Epling et al. also showed that the presence of CO_2 decreased the trapping ability of the Pt−Ba/Al_2O_3 catalyst by producing thermally and chemically more stable

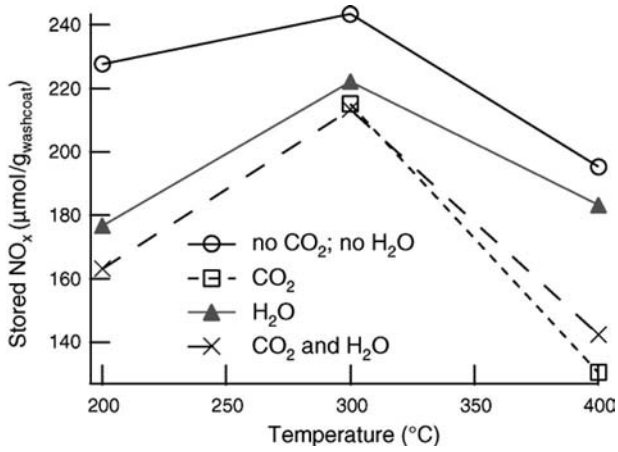

Figure 23. Different amounts of stored NO_x in the presence and/or absence of CO_2 and H_2O from one lean cycle conducted over $Pt-Ba/Al_2O_3$. The gas composition was 300 ppm NO and 8% O_2; 3%CO_2 and/or 3% H_2O. The duration of the lean period was 10 min. Reprinted with permission from ref 302. Copyright 2007 Elsevier B.V.

bulklike $BaCO_3$ as well as affected the regeneration phase at higher temperatures. They observed formation of stable bidentate carbonate species up to 500 °C, and at higher temperatures, the bidentate carbonate species transformed into unidentate species.[13,112,130,301]

Finally, it emerges from the above discussion that, in the storage step, CO_2 has a detrimental role in NO_x sorption over $Pt-Ba/Al_2O_3$ and a beneficial role for $Pt-Ba/CeO_2$. In the regeneration step, the role of CO_2 is quite diversified, as reported. Desulfurization was conducted by researchers with CO_2 in the regeneration phase; however, the exact role of CO_2 was not addressed.[180,220]

Much evidence showed the combined effect of CO_2 and H_2O on the NSR mechanism over $Pt-Ba/Al_2O_3$. Recently, kinetic modeling showed NO_x adsorption decreased from 29.7 to 12.6 mol/m^3 when $CO_2 + H_2O$ were present in the feed stream.[317] Both of these feed components have a negative impact on the storage propertiy; there seems to be no synergistic effect, but H_2O had a stronger effect compared to CO_2.[318] In the presence of both CO_2 and H_2O in the feed, the NO → NO_2 oxidation was stopped and the multiple storage sites (surface and bulk Ba sites and γ-Al_2O_3) became inactive and NO was adsorbed only on surface $BaCO_3$ sites, resulting in only 30% barium utilization.[69,285,304] Lindholm et al. clarified that H_2O had an effect only on Al_2O_3 while the storage of Ba was solely influenced by CO_2 (Figure 23).[302] Recently, they proposed a detailed kinetic model in accordance with their experimental findings.[319] According to Lindholm et al., during the regeneration period, NH_3 formation is promoted by the presence of CO_2; however, Mulla and co-workers did not find any role of CO_2 in NH_3 formation.[83,302] Thus, it seems that more clarifying research is needed here for giving a final answer.

5.4. Impact of Soot

The presence of soot obstructs NSR catalytic activity primarily by two ways. Carbon deposition on noble metal sites from CO and hydrocarbons blocking its oxidation activity has been briefly discussed in section 5.1. The diesel particulate filter (DPF) system, which is in use today for achieving low soot emission by diesel engines, is based on the oxidation of deposited soot either by O_2 and/or by the gas mixture NO_2/O_2.[320] Incidentally, the soot oxidation reaction rates are found to be in the order of $NO_2 > N_2O \approx NO \approx O_2$.[321] In the temperature range of 250−450 °C, soot is oxidized by O_2 and NO_2, with the latter leading to CO_2 and NO formation, which in turn is likely to lower NO_2 storage efficiency.

$$C + 2NO_2 \rightarrow CO_2 + 2NO \quad (35)$$

$$C + NO_2 \rightarrow CO + NO \quad (36)$$

$$C + NO + {}^1/_2O_2 \rightarrow CO_2 + NO \quad (37)$$

Atribak et al. in this regard showed that NO_x is stored in CeO_2, and once NO_2 is produced by CeO_2, there was a competition between the NO_2-soot reaction and NO_x storage on the catalyst. $Ce_{0.76}Zr_{0.24}O_2$ and CeO_2 were more active than TiO_2 and ZrO_2 for soot oxidation and mainly yielded CO_2 (reactions 35 and 37), whereas TiO_2 and ZrO_2 catalyzed soot oxidation leading to higher percentages of CO (reaction 36).[322,323] The DPNR technique developed by the Toyota group consists of soot oxidation and a NSR catalyst, which has the unique ability to remove simultaneously both soot and NO_x.[287,324] Soot abatement occurs under lean conditions; soot removal is however claimed to occur during the rich phase as well.[293,324] $Pt-Ba/Al_2O_3$ in cyclic lean/rich conditions was able to simultaneously remove both soot and NO_x, and when CO_2 was present in the feed stream, the presence of soot did not significantly affect the activity in the NO_x storage-reduction of the $Pt-Ba/Al_2O_3$ catalyst.[293] Potassium, when replaced with Ba, showed a higher soot oxidation property ($Pt-K/Al_2O_3$ decreased the soot ignition temperature by 100−150 °C compared to $Pt-Ba/Al_2O_3$) but had comparable NO_x storage capacity.[288,325] These soot oxidations are generally carried out by mixing the soot with the catalyst by physical mixing or an impregnation technique. Matarrese et al. observed the presence of a synergistic effect in $Pt-K/Al_2O_3$ despite the mixing, which is thought to be the key factor of enhanced soot oxidation ability.[326] Simultaneously, high soot combustion ability and NO_x storage capacity were also demonstrated by 4.5−10 wt % K loading on La_2O_3 or $Cu-CeO_2-Al_2O_3$ catalyst.[327,328]

However, one of the very few reports of the detrimental effects of soot combustion to NSR activity was by Krishna and Makkee, who have reported that the NO_x storage capacity of NSR materials decreased upon aging under soot oxidizing conditions.[288] Sullivan et al. demonstrated that the presence of soot is detrimental to the performance of a NO_x trap, since it offers another reaction route for the utilization of NO_2 rather than the desired formation of $Ba(NO_3)_2$ and also the trapping BaO component with a Pt active phase does not promote carbon combustion.[295]

6. Theoretical and Surface Science Studies

Theoretical and surface science studies on well-defined model catalysts have brought important insight into various aspects of NSR catalysis such as the nature of molecular interactions, structural properties, and details of the reaction kinetics. Some interesting findings emerging from these studies will be addressed in the following.

6.1. Theoretical Studies

Theoretical studies on NSR catalysis can be divided into two major segments: (1) studies of important molecular

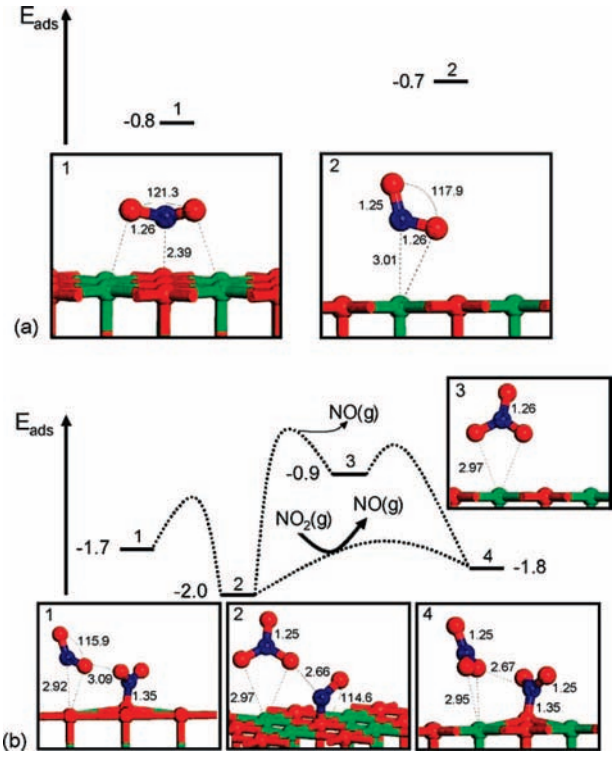

Figure 24. Potential energy diagram for the xNO$_2$/BaO(100) system calculated using the slab representation of the BaO(100) surface. (a) Single NO_2 adsorption over a surface oxygen site and a surface barium site. (b) Pairwise NO_2 adsorption on the BaO(100) surface. Color code: green is barium, red is oxygen, and blue is nitrogen. Reprinted with permission from ref 330. Copyright 2004 Elsevier B.V.

interactions (e.g., NO_2 adsorption on BaO(111)) and structural properties using density functional theory (DFT), and (2) ab initio and other computational techniques and kinetic modeling.

DFT has grown into the standard theoretical framework for large scale first principles calculations.[132,329−331] To model the BaO(100) surface (the lowest energy surface), a two-layer slab was cleaved from the geometry optimized bulk structure and modeled by a periodic supercell.[132] Following the usual convention, the adsorption energies E_{ads} were calculated according to the following expression:

$$E_{ads} = E_{slab+molecule} - (E_{slab} + E_{molecule}) \qquad (38)$$

where $E_{molecule}$ is the energy of the isolated adsorbate in its equilibrium configuration, E_{slab} is the total energy of the isolated slab, and $E_{slab+molecule}$ is the total energy of the adsorbate and slab. Single and pairwise NO_2 adsorptions were explored, allowing the NO_2 molecules to fully relax.[330,331] In Figure 24a and b, the structural results for single and pairwise NO_2 adsorption on the BaO(100) surface are shown. Two adsorption sites are atop barium and atop oxygen, respectively. The calculated adsorption energies for NO_2 over these sites are similar, −0.8 and −0.7 eV. However, despite the similar adsorption energetics, the two adsorption configurations differ significantly in chemical interaction. Single NO_2 adsorption on BaO produced nitrite species by abstraction of an electron from surface oxygen ions; thus, a delocalized electron hole is created in the surface O(2p) states, activating oxygen toward further NO_2 adsorption. The second NO_2 molecule approaches the surface with the nitrogen end and is adsorbed on the activated surface, making a nitrite−nitrate pair. Electron−hole separation implied a nonlocal mechanism for pair formation. Eventually, by heterogeneous oxidation, the remaining nitrites form an all-nitrate final product.[332] In section 4.2.1 we have also discussed the NO_2 sorption on a BaO surface using periodic supercell DFT within the gradient corrected local density approximation.[131,133] Schneider et al. examined the NO_2 adsorption on BaO(100) films supported on Pt and observed that the metal stabilized NO_2 adsorption on the BaO surface.[333] NO_2 adsorption stabilized the bonding combinations of these orbitals (the bonding Pt (d_{z^2}) + O (p_z) state was peaked at −3.5 eV below the Fermi level for BaO/Pt, whereas, in the case of NO_2/BaO/Pt, this combination is located at −4 eV). The authors described the NO_x sorption to alkaline earth metals as a Lewis base interaction.[334,335] They demonstrated the NO_x chemisorption on MO to occur via one-electron oxidations or reductions that produce strong Lewis acids and bases (M is the alkaline earth metal).

Kinetic modeling provides better insight into the interdependencies of the different experimental parameters and their influence on the performance of the NSR system. If based on intrinsic kinetic parameters, the ideal plug flow reactor model for powder catalysts in NSR can also give insight into the reaction mechanism. In section 3.1 we have discussed the NO oxidation revealed by kinetic modeling. Probably the most detailed kinetic model to describe NO_x storage and reduction was developed by Scholz et al.[69,285,304,336,337] The plug flow reactor model used a global reaction kinetic model, which considered that NO_x storage occurs on three different types of barium sites: surface, semibulk, and bulk sites. Surface sites were considered to be the most reactive, followed by semibulk sites, whereas bulk sites were not active in NO_x trapping. It was assumed for the reactor to model that (i) the pressure was uniform and equal to ambient throughout the packed bed, (ii) external and internal diffusion limitations were absent, and (iii) diffusion of the gas-phase components was considered only from the external surface of the barium clusters to the interior of the barium clusters. The gas bulk in the packed bed reactor was considered in axial direction z, and the gas in the spherical barium clusters with the partial coordinate ξ. The change in the concentration of the different components as a function of time at each axial position was described by eq 39,

$$\varepsilon_b \frac{\partial C_i}{\partial t} = \frac{F_v}{A_r}\frac{\partial C_i}{\partial z} - D_{eff} A_{Ba} \frac{\partial C_i}{\partial \xi}\Big|_{\xi=R} + L_{Pt}\sum_j \nu_{i,j} R_{Pt,j} + L_{Ba,surf}\sum_k \nu_{i,k} R_{Ba,surf,k}$$

Accumulation of moles in gas phase; Convective flow transport through reactor; Diffusional transport in radial direction in Ba clusters; Reactions involved on Pt sites; Reactions involved on Ba sites

(39)

where ε_b is the bed porosity, C_i is the gas-phase concentration of component i (NO, NO_2, O_2, H_2, and N_2), t is time, F_v is the volumetric flow rate, A_r is the surface area of the reactor, z is the axial length, D_{eff} is the effective gas diffusion coefficient, A_{Ba} is the specific Ba surface area, ξ is the radial direction in the Ba clusters, L_{Pt} is the specific number of moles of active Pt surface sites, R_{Pt} is the NO reduction rate, $L_{Ba,surf}$ is the specific number of moles of active Ba surface sites, and $R_{Ba\_surf,k}$ is the NO_x storage and regeneration rate

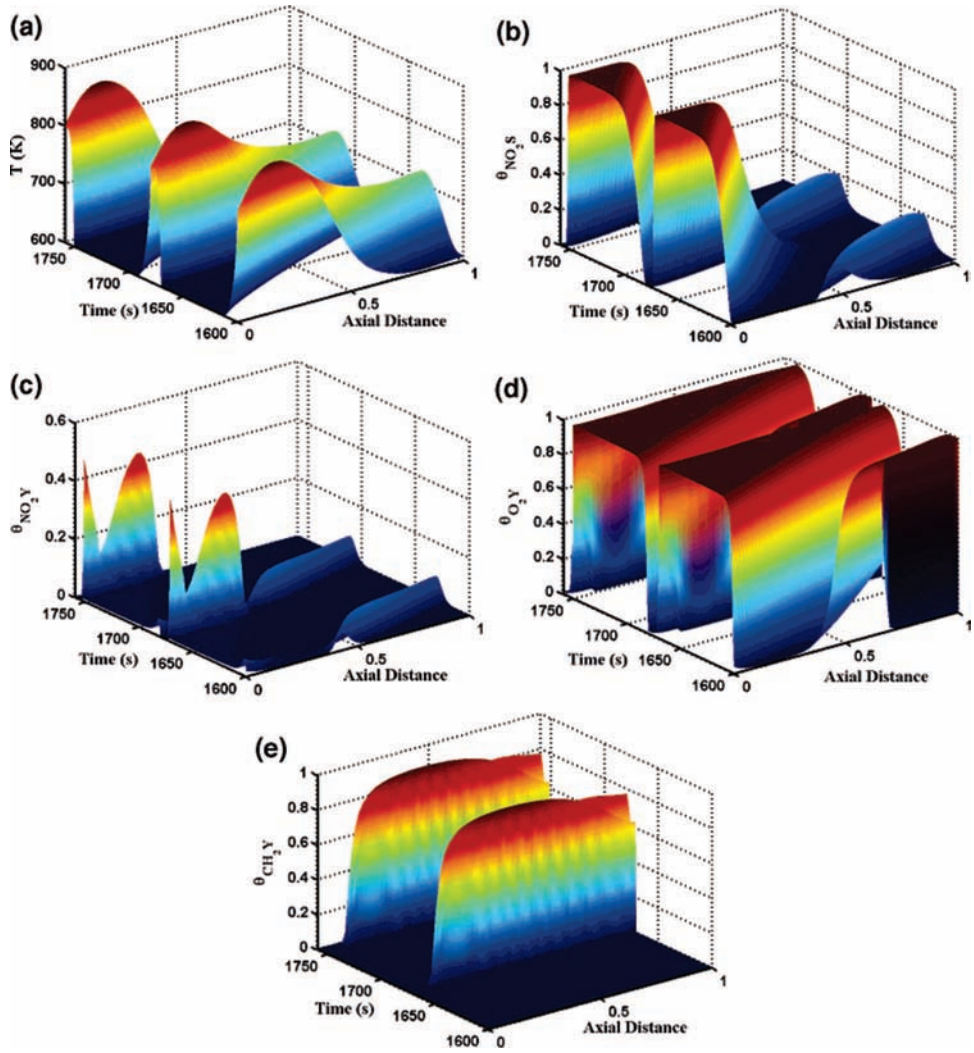

Figure 25. (a) Reactor temperature profile. (b) Fractional coverage profile of NO_x (NO_2) on storage sites (BaO). (c) Fractional coverage profile of NO_x (NO_2) on platinum sites (Y sites). (d) Fractional coverage profile of oxygen (O) on platinum sites (Y sites). (e) Fractional coverage profile of reductant (CH_2) on platinum sites (Y sites). Feed, hydrocarbon during rich phase is 1.3% and during lean phase is 0%; the feed temperature is 330 °C; feed NO_2 is 500 ppm and feed oxygen is 5%. Lean phase time is 70 s, and rich phase time is 10 s. Reprinted with permission from ref 348. Copyright 2005 American Chemical Society.

at Ba surface sites. By solving the equation using gPROMS (Process Systems Enterprise) software and by fitting it to observed experimental findings, the authors could reach the conclusion of involvement of the three types of Ba storage sites. Mostly, surface barium sites contribute significantly in NO trapping and only a small fraction of the total barium participates in NO storage. Many researchers have studied the dispersion of the noble metals and storage sites by kinetic modeling and fitting the data with the experimental observation.[42,338]

We discussed the synthesis of the monoliths (the border between "catalyst" and "reactor" vanishes in these reaction systems) in section 4.5; now we will address the issues attached with the modeling of catalytic monolith converters, which have drawn attention in NO_x abatement techniques.[339−341] A one-dimensional mathematical modeling of NO oxidation and NO_x storage on Pt−BaO/Al_2O_3 monolith catalysts often requires assumptions such as: (i) uniform radial flow distribution and no gas phase accumulation, i.e. constant gas velocity and no pressure drop along the reactor, (ii) no axial diffusion, dispersion in the gas phase, (iii) no diffusion barrier in the washcoat, and assuming an isothermal monolith reactor.[342] Recently, Xu et al. found that external mass transfer had significant effects on the concentrations of the reactants in the washcoat of a catalytic monolith reactor and has to be considered when estimating kinetic parameters and for interpretation of the results.[343] Mathematical modeling could evaluate the 28 step NSR reaction mechanism[344] and could reveal the importance of Pt and Ba geometrical proximity[342] and also the sulfur deactivation.[345,346] Koci et al. developed a spatially pseudo-1D, multiphase model of an adiabatic catalytic monolith and fitted it to the experimental data.[347] NO_x were stored on the washcoat surface during the lean phase, and the storage centers were gradually saturated from the front to the rear part of the converter. Due to the high concentrations of combustibles and the exothermicity of the reactions, additional heat was generated within the rich phase and the temperature of the monolith increased. Subsequently, during the lean phase, the temperature of the monolith decreased back to its original value, gradually from the front to the rear part of the reactor. Later, the authors showed that the storage and reduction depend on the lean/rich phase duration, monolith length, reaction temperature, and nature of the reductants.[297] Based on a similar hypothesis, Sharma et al. further showed the washcoat temperature (Figure 25a), where

with the introduction of hydrocarbon, ignition occurs at the front entrance, while there was a rapid cooling when the hydrocarbon pulse was stopped. Space−time profiles of NO_2 coverage on BaO and Pt sites (Figures 25b and c) concluded that, during the rich pulse, there was a corresponding rapid decrease in the coverage of NO_2 on BaO storage sites due to the local temperature increase. Figures 25d and e show the O_2 and hydrocarbon (CH_2) coverage on Pt sites over two complete cycles after the reactor has reached a periodic state.[348]

Independent computational calculations such as DFT or ab initio or kinetic modeling tagged with experimental results helped us determine and understand the mechanistic aspect.

6.2. Studies on Well-Defined Model Catalysts

A relatively recent approach to gain fundamental insight into NSR catalysis uses well-defined model catalyst systems. In the present review, many times during the discussion of the NSR mechanism and morphology of Ba during the storage process, we have hit the issue of material properties of NSR catalysts originating from such studies, since these well-defined model systems enable important insights regarding the structure−functionality relationships. While most of these studies have been performed under UHV conditions, studies have also been performed at normal pressure. High-field, high-resolution solid-state ^{27}Al MAS NMR showed penta-coordinated Al^{3+} sites of γ-Al_2O_3 in BaO/Al_2O_3 model powder catalysts, and ^{15}N solid state NMR spectroscopy showed the distinct bulk and surface nitrate species on the model catalyst.[142,349]

Impressive UHV studies[350−352] have been performed in a combined ultrahigh vacuum (UHV) surface analysis chamber and elevated pressure reactor system equipped with powerful and high resolution surface probes such as X-ray photoelectron spectroscopy (XPS), Auger electron spectroscopy (AES), low-energy electron diffraction (LEED), low-energy ion scattering spectroscopy (LEISS), quadrupole mass spectroscopy (QMS), and an infrared reflection absorption spectroscopy (IRAS) setup. For a model BaO/θ-Al_2O_3/NiAl(100) catalyst, θ-Al_2O_3 ultrathin films were grown with a thickness of 6 ± 2 Å. The surface was prepared by carrying out Ba deposition and subsequent oxidation in a stepwise fashion.[350−352] Figure 26 shows the stepwise formation of the model catalyst.[143] Many critical mechanistic aspects, such as (i) the formation of a $BaAl_2O_4$ phase during the storage step, (ii) involvement of the Al_2O_3 phase in the reaction mechanism, (iii) formation of condensed D_{2h}-N_2O_4 (O_2N-NO_2) layers, where the N−N bond is oriented parallel to the alumina surface, or (iv) nitrite−nitrate pair formation or decomposition of nitrites, leaving one O atom behind that helped formation of BaO_2, were probed by surface techniques over the model catalysts.[143,144,152,161,353] Combination of surface science experiments on model catalysts with periodic DFT calculations developed a clear understanding of the nature of both the surface and bulk types of nitrates during NO_x storage.

Combination of DFT with MB/IRAS (molecular beam/time-resolved IR reflection absorption spectroscopy) to investigate surface nitrate formation on model BaO/Al_2O_3 thin films prepared on a NiAl(110) single-crystal surface resulted in a different dimension from the work of Desikusumastuti et al.[95,138,140,146] The MB/IRAS experiments were performed in an UHV (ultrahigh vacuum) apparatus equipped with four effusive molecular beams and one supersonic molecular beam to be superimposed on the sample surface. The system was also equipped with a FTIR spectrometer, a beam monitor for alignment and intensity calibration of the beams, two quadrupole mass spectrometers (QMS), a vacuum transfer system with a high pressure cell, and necessary preparation tools such as evaporators, a gas doser, a quartz microbalance, an LEED/Auger, an ion gun, etc. The NO_2 beam was generated from an effusive beam doser and modulated by a valve system. The DFT calculations were applied with the gradient corrected exchange correlation functional. To synthesize the model catalyst, two cycles of oxidation in 10^{-6} mbar O_2 and UHV annealing were carried out, resulting in an Al_2O_3 film on NiAl(110). For BaO deposition, the Ba source was calibrated using a quartz microbalance and Ba was deposited at room temperature at typical rates of 1.0×10^{13} atoms cm^{-2} s^{-1} and subsequently oxidized by exposure to 6×10^{-7} mbar O_2, for 900 s. At low NO_2 exposure, the formation of surface nitrites prevailed for both the Al_2O_3/NiAl(110) support and the BaO/Al_2O_3/NiAl(110) (Figure 27). With continuing exposure, surface nitrates also were formed, followed by ionic nitrates in the limit of high exposure and temperature. All the IR spectra were confirmed by the DFT calculations. It was observed that, over Al_2O_3/NiAl(110) at low temperature, NO_2 adsorbed under formation of the D_{2h} dimer (N_2O_4), whereas, at higher temperature, there was no molecular species, but only bridging nitrates, which increased with higher NO_2 exposure. On the other hand, over BaO/Al_2O_3/NiAl(110) at low temperature NO_2 exposure, there was simultaneous formation of nitrite and nitrate, and with increased temperature, both bridged and monodentate nitrates were observed.

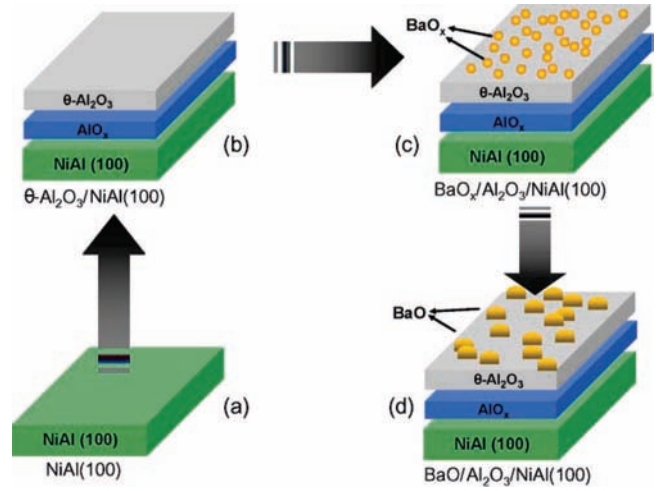

Figure 26. Preparation protocol that is followed to synthesize the BaO/θ-Al_2O_3/NiAl-(100) model system: (a) clean NiAl(100) bimetallic substrate; (b) θ-Al_2O_3 ultrathin film grown on NiAl(100); (c) Ba deposition on θ-Al_2O_3/NiAl(100) in UHV at room temperature; (d) BaO/θ-Al_2O_3/NiAl(100) model system obtained after stepwise Ba deposition/oxidation (O_2(g) was introduced into the chamber at room temperature). The sample temperature was quickly increased to 525 °C in the presence of O_2(g), and the sample was annealed at 525 °C for 15 min. These dosing and annealing sequences were repeated for each Ba deposition step (total number of deposition/oxidation steps = 8; total time of Ba deposition = 50 min). Reprinted with permission from ref 143. Copyright 2006 Elsevier Inc.

7. Reactor Configuration

When considering the different reactor configurations which are employed for NSR, we have to distinguish between

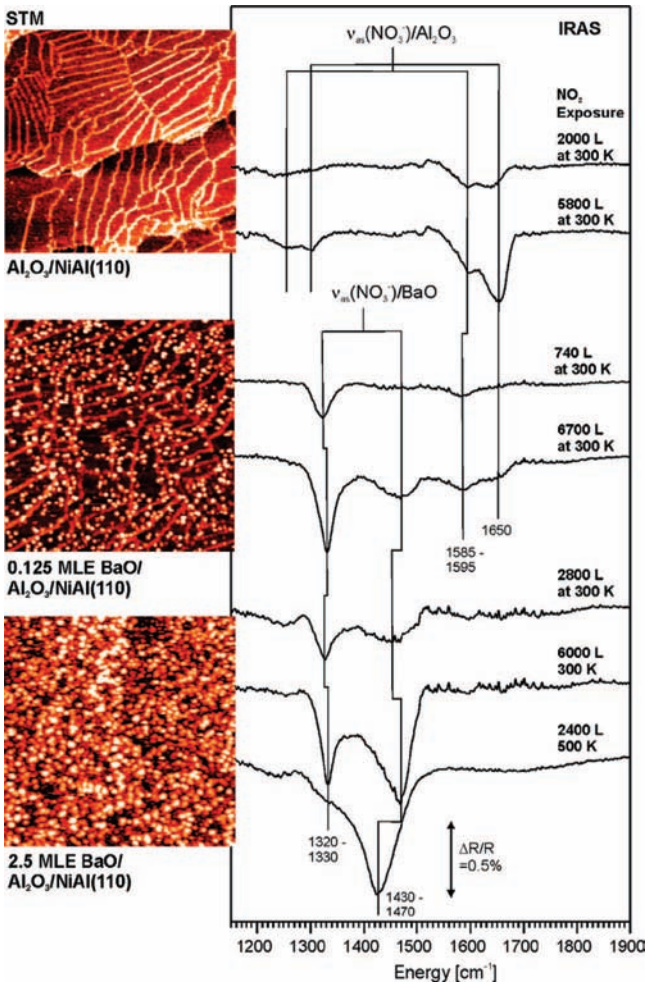

Figure 27. Structure and vibrational properties of the model systems for NO_x storage. Left: STM images (200 × 200 nm^2), showing the pristine Al_2O_3 film on NiAl(110) (top), smaller BaO particles on the Al_2O_3 film (middle, 0.125 MLE BaO, 1.8 nm BaO particles), and larger BaO nanoparticles on the Al_2O_3 film (bottom, 2.5 MLE BaO, 4.6 nm BaO particles). Right: IRAS of the NO stretching frequency region after exposure to different doses of NO_2. Reprinted with permission from ref 141. Copyright 2008 Elsevier Inc.

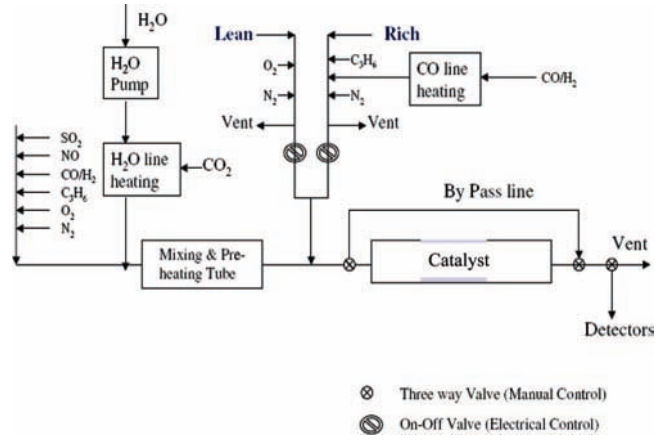

Figure 28. Schematic representation of a typcal laboratory flow reactor. Pulsed gases pass through a catalyst in a quartz tube to the detector. Reprinted with permission from ref 354. Copyright 2007 Springer Science & Business Media, LLC.

research reactors and technical reactors. Research reactors range from laboratory microreactors to bench scale reactors. The latter allow a better adaptation to the conditions encountered in technical reactors but are considerably more complex and are preferably connected to an engine providing real exhaust gas as feed gas to the reactor. Figure 28 shows schematically a reactor setup for laboratory research.[354] For laboratory investigations, a typical flow type reactor consists of a quartz tube horizontally or vertically placed inside an electric furnace (horizontally in Figure 28). Normally, the measured and preheated gases are fed into the flow reactor tube and the effluent is analyzed by MS or GC.[304,337,355] Specific reactors have been designed to carry out *operando* spectroscopy (e.g., *in situ* FTIR,[94,356,357] Raman[358]) for the analysis of chemisorbed species and reaction intermediates on the catalyst surface as well as in the gas phase at working conditions.

Although reactor optimization is normally not a big issue in laboratory research reactors, it needs to be kept in mind that reaction engineering parameters such as gas hourly space velocity (GHSV), retention time, and lean/rich timing span strongly influence the overall performance of the NSR system. Powders or cylindrical monolith catalysts are loaded into the flow reactors. The flow rates are varied for a wide range of space velocity of 29,000−100,000 h^{-1} at standard temperature and pressure.[337,344] Gas hourly space velocity (GHSV) is a crucial parameter controlling NSR kinetics and efficiency. At high space velocities, kinetic limitations reduce the NO conversion and NO_x trapping efficiency. Higher trapping efficiencies are achieved at lower space velocities when the NO oxidation approaches the equilibrium conversion limit.[359]

Figure 29 shows a schematic representation of a bench laboratory flow reactor setup connected to an operating engine. This setup allows to simulate the real technical NSR conditions. Desulfurization, which is a common occurrence, normally takes place every few hours in the case of low sulfur (<50 ppm) fuels, and for diesel fuels with a more regular sulfur level (300 ppm), the desulfurization must be performed more frequently. This higher temperature (650−750 °C) desulfurization process uses a large amount of secondary energy that has a deleterious impact on the overall engine efficiency. The bench scale NSR system shown in Figure 29 allows for studying the desulfurization step.[360−362] The system utilizes a rotating monolithic catalytic cartridge to divide the exhaust flow into two streams. The partial flow NO_x desorption can be optimized to a higher temperature window and at a lower space velocity. This setup has the potential to be energy efficient as a result of (i) the partially restricted flow, saving supplemental energy during NO_x trap regeneration/desulfurization, and (ii) the periodic flow reversal for exhaust energy recovery during oxidation.

Another conceptionally different technique which has been employed to study NSR is the temporal analysis of products (TAP), which measures and analyzes the products of a transient catalysis reaction and was originally developed by Gleaves et al.[363] The basic working principle of the TAP involves the transient assessment of a catalyst through various reactant feed protocols, including single reactant pulsing, dual reactant pulsing, and pulsing-probing. TAP operation is carried out at low pressure (ca. 10^{-5} to 10^{-7} Torr), and the primary gas phase transport process is Knudsen diffusion type. While the transient total pressure is higher during the pulsing, a pulse of sufficiently small intensity ensures operation in the Knudsen regime. The TAP affords the ability to measure transient kinetics at prescribed catalyst states. In the context of NSR, this corresponds to extracting kinetics

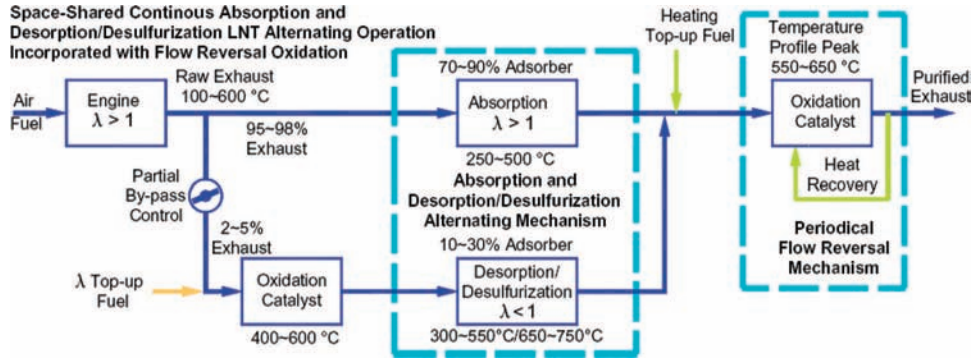

Figure 29. Schematic representation of a bench NSR laboratory reactor setup connected to an engine. Reprinted with permission from ref 360. Copyright 2004 Elsevier Ltd.

at a precise degree of nitration, as convincingly demonstrated by Harold and co-workers, and focuses on storage.[273] In a TAP reactor setup, a catalyst sample is usually set in a tube under vacuum conditions (in a chamber that is coupled to a large-capacity pump for differential pumping) in the temperature controlled catalytic microreactor and small amounts of gas are pulsed over the bed of the catalyst with the help of a high-speed pulse valve assembly. The response of product and reactant gas at the outlet of the reactor is measured by a mass spectrometer with high time resolution.[273] TAP avoids the disadvantages of traditional flow and integral reactors, and it affords the ability to conduct transient experiments under constant catalyst state conditions, which provided crucial kinetic data on the highly complex NSR process. Medhekar et al. by NO pulses and NO/H_2 pump−probe at 350 °C revealed the closely coupled Pt/Ba interfacial mechanism in NSR.[70] Sakamoto et al. using a TAP reactor observed that the release of NO_x from $Pt-K/Al_2O_3$ was faster than that from $Pt-Ba/Al_2O_3$ in the NO_x regeneration process.[181]

Combinatorial or high throughput analytical techniques are also used for studying the NSR activity.[364,365] High throughput experimentation has also been applied for studying the NSR catalysis over a wide range of reaction conditions and catalyst compositions. It is based on a guiding principle of collection of modular traditional plug flow reactors.[366] A rapid switching four-way valve system is used to alternate between the lean and rich gas mixtures so that the lean/rich/lean transitions in these experiments are almost instantaneous.[367] Hendershot et al. carried out high throughput experimentation with 16 vertical parallel flow-through reactors with catalyst powder supported on a stainless steel frit and multiple mass flow controllers to explore a wide range of feed gas concentrations, compositions, and flow rates.[203,364,365,368,369] Each reactor contained a thermocouple in the catalyst bed, and the temperatures of all 16 reactors were continuously displayed and recorded by software. The reaction products from all 16 reactors were analyzed simultaneously using FTIR imaging. A linear model was developed relating a performance criterion (Y) to the parameters of interest (X_1, X_2, X_3,...) in the form of

$$Y = C + \alpha_1 X_1 + \alpha_2 X_2 + \alpha_3 X_3 + ... + \alpha_{12} X_1 X_2 + \alpha_{13} X_1 X_3 + ... + \alpha_{123} X_1 X_2 X_3 + ... \quad (40)$$

where C is a constant and α_i are coefficients fitted to the experimental data. The authors studied the reactions with respect to performance criteria: (i) saturation NO_x storage capacity, (ii) total N_2O production, and (iii) the steady state lean NO_x reduction to both partially reduced N_2O and fully reduced N_2 as a function of NO_x concentration, O_2 concentration, reductant concentration, reductant type, and space velocity. When the saturation NO_x storage capacity was plotted as a function of Pt and Ba weight loading (Figure 30), it was observed that the predicted maximum in saturation NO_x storage capacity occurred at a catalytic composition of 0.63% w/w Pt and 9.1% w/w Ba.

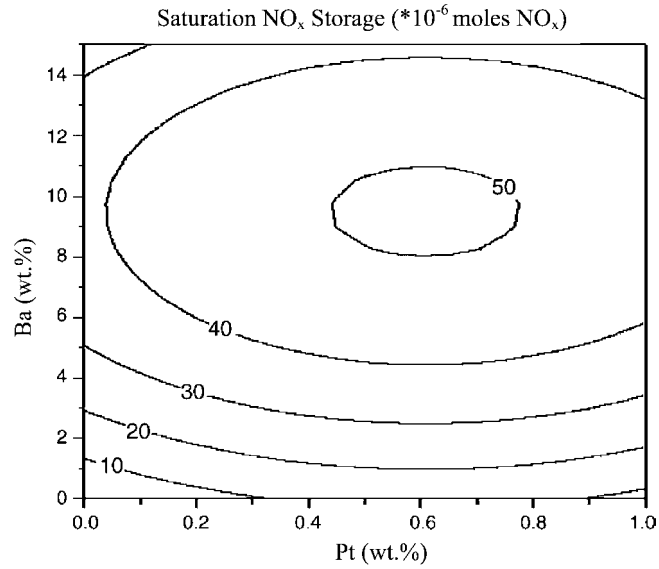

Figure 30. Model prediction showing the saturation NO_x storage as a function of Pt and Ba weight loading. The maximum saturation NO_x storage is predicted at 0.63 wt % Pt and 9.1 wt % Ba. The inlet lean concentration was 2000 ppm NO, 8% O_2, and 1% CO at a temperature of 325 °C and a space velocity of 42,500 h^{-1}. Reprinted with permission from ref 364. Copyright 2004 Elsevier B.V.

A critical reaction engineering parameter is the time span for the lean and rich phase which controls the cyclic steady state. Muncrief et al. evaluated that the periodic addition of reductant (here, C_3H_6) to the catalyst bed could result in time-averaged NO_x conversion approaching the rich conversion limit obtained under steady state conditions. In addition, the C_3H_6 injection policy (feed composition, reductant pulse duration, overall cycle time, and temperature) had an effect on NO_x conversion.[370] They showed that, to achieve a high time-averaged NO_x conversion, the gas composition during the reductant (C_3H_6) injection should be net reducing and C_3H_6 pulses should be short. According to them, cycle times of very short or very long duration do not exploit the benefits of lean/rich cycling. For shorter cycle times, the time-averaged conversion approaches a steady-state conversion as if the lean and rich streams had been premixed; for much

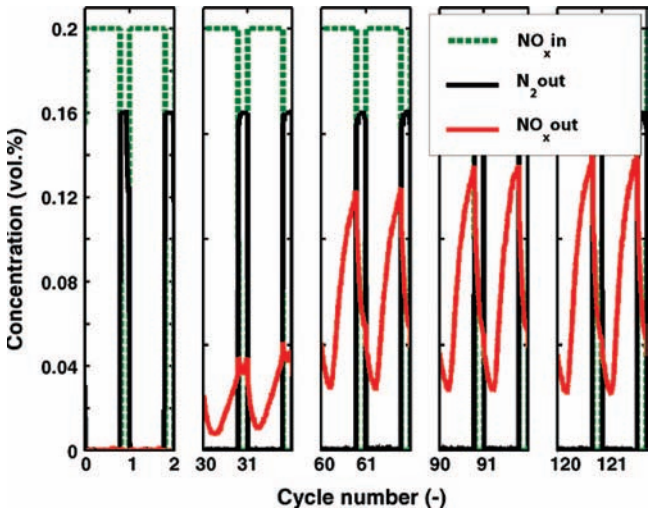

Figure 31. Outlet NO_x and N_2 concentrations during lean/rich cycling starting with a pretreated catalyst. Selected cycles out of a series of 200 cycles are shown. Lean: 0.2 vol % NO, 4 vol % O_2, and 1 vol % Ar in He, 60 s. Rich: 0.8 vol % H_2 and 1 vol % Ar in He, 15 s. $T = 350$ °C. Reprinted with permission from ref 337. Copyright 2007 Elsevier B.V.

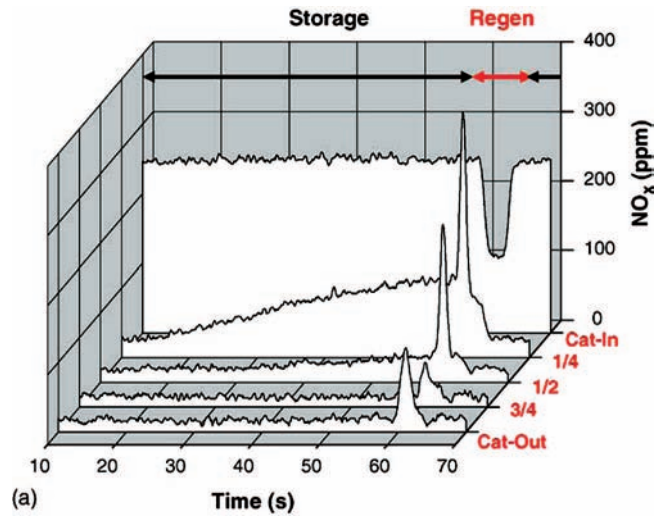

Figure 32. NO_x removal performance of a 3-in.-long Pt−K/Al_2O_3-washcoated monolith during 54-s storage/4-s regeneration cycling. Storage gas: 250 ppm NO, 8% O_2, 5% H_2O, and N_2 balance. Regeneration gas: 4% CO, 1% O_2, 5% H_2O, and N_2 balance. Catalyst midbed $T = 430$ °C. NO_x breakthrough profiles at different axial locations obtained by SpaciMS. Reprinted with permission from ref 372. Copyright 2006 Elsevier B.V.

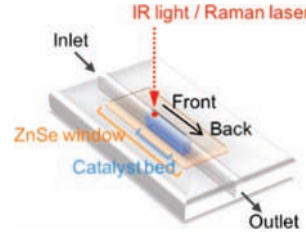

Figure 33. Schematic illustration of the cell, applicable to space- and time-resolved DRIFTS-Raman experiments. Reprinted with permission from ref 374. Copyright 2008 Wiley-VCH Verlag GmbH & Co. KGaA, Weinheim.

longer cycle times, the time-averaged conversion is a weighted average (by duty fraction) of the steady-state conversions obtained with the lean and rich feeds. Figure 31 shows selected NO_x storage and reduction data out of a series of 200 cycles with a lean flow of 60 s and a rich flow of 15 s at 350 °C. During the catalyst regeneration period, N_2 formation and NO_x desorption were observed. From the N balance per complete cycle, it was observed that NO_x stored during each lean period was not fully reduced during the subsequent rich period and consequently nitrates accumulated in the Pt−Ba/Al_2O_3 and no steady state was reached. It was found that lean/rich timing of 240 s/60 s reached the steady state immediately, whereas lean/rich timing of 120 s/30 s and 60 s/15 s took 24 and 120 cycles, respectively, to achieve the steady state.[337]

An experimental technique known as spatially resolved capillary-inlet mass spectrometry (SpaciMS) to observe the evolution of multiple species inside the channels of a monolithic NSR catalyst has made a striking consideration.[286,355,371,372] A minimally invasive capillary inlet system was employed to transport time-varying species pools to the mass spectrometer for analysis. The capillary probe was introduced from the reactor inlet and positioned at one of the five reactor locations along the 9.2-cm-long core (catalyst-inlet, $^1/_4$ length, $^1/_2$ length, $^3/_4$ length, catalyst outlet). Figure 32 shows NO_x breakthrough profiles for a representative 56-s storage/4-s regeneration cycle. During the lean phase, major NO_x uptake occurred in the first $^1/_4$ of the catalyst bed with some NO_x slip to the downstream locations. Residual NO_x of 15−20 ppm passed through the second $^1/_2$ of the catalyst without measurable storage. Upon switching to the regeneration gas stream, a NO_x pulse appeared over the first 2 s of the 4-s regeneration. The amplitude of this pulse was largest at the $^1/_4$ axial position and decreased continually until the $^3/_4$ position.

In a spatial- and time-resolved study, temperature distributions over a Pt−Ba/Al_2O_3 catalyst using infrared thermography showed that there was more nitrate formation at upstream positions relative to downstream, or from front to back of the catalyst, with short trapping times. However, as more NO_x was trapped on the catalyst during longer trapping times, it was observed that the largest amount of NO_x was trapped slightly downstream of the inlet.[373] A combined DRIFTS-Raman approach elucidated the position-dependent bulk utilization of the storage component, which greatly affects the efficiency of the NO_x storage process. Using a specially designed reactor setup (Figure 33), Urakawa et al. observed that the formation of nitrites and nitrates was significantly delayed and the band intensities decreased considerably, moving from the front to the back position of the catalyst bed.[374] The nitrite band was detected immediately at the front position but delayed by 70 and 120 s at the middle and back positions, respectively, as shown by the DRIFT spectra in Figure 34. Conversely, nitrates were formed from the beginning of lean periods, independently of the bed position, because of more complete NO oxidation to NO_2 over Pt toward the end of the bed (back position). During the rich period, nitrites were first reduced or desorbed from the surface and then the reduction of nitrates followed, as clearly indicated by a significant delay of the corresponding signals at the middle and back positions.

In conclusion, we can state that the results emerging from the various studies performed with different reactor types as well as from the time- and space-resolved spectroscopic studies clearly indicate that the integral consideration of an NSR reactor performance can lead to superficial conclusions as regards structure−activity relationships due to significant structural and temperature gradients which can occur in an

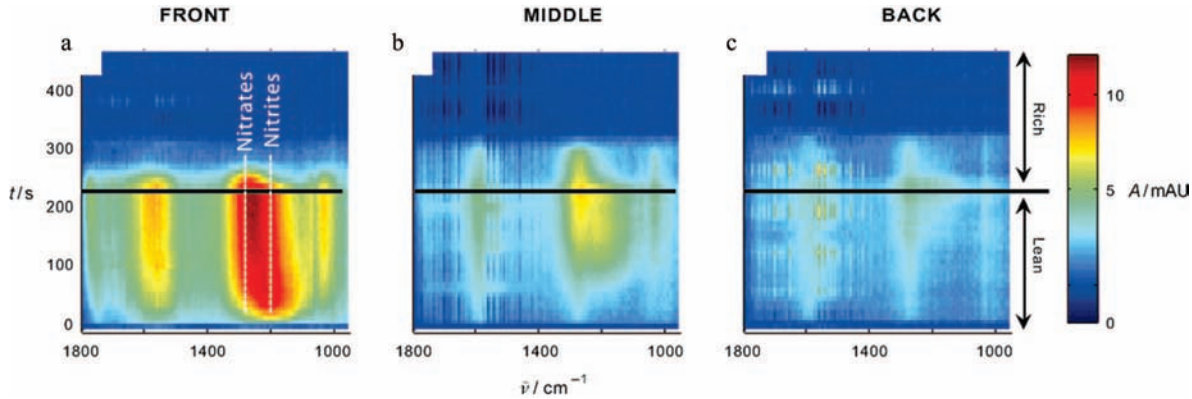

Figure 34. Time-resolved DRIFT spectra during NSR at the front, middle, and back positions of the catalyst bed. The catalyst was first activated by a number of (minimum of 8) lean (0.42 vol % NO, 3.3 vol % O_2, balance He) and rich (3.3 vol % H_2, balance He) cycles, to attain steady-state (stable-response) conditions at 350 °C. Reprinted with permission from ref 374. Copyright 2008 Wiley-VCH Verlag GmbH & Co. KGaA, Weinheim.

integral reactor setup during lean/reach cycling. Thus, time- and space-resolved information is required for a comprehensive understanding of such reactors.

8. Conclusions and Outlook

Since the introduction of the NO_x storage-reduction (NSR) concept in 1995 by Toyota until today, many investigations have been carried out in the pursuit to gain a better understanding of the NSR mechanism and in the search for more efficient materials and improved engine control for the NO_x abatement. In this review we first addressed the mechanistic aspects of the NSR, followed by concentrating on decisive investigations of the structural and morphological aspects of the catalyst on the reaction mechanism and involvement of the precious metals, alkali/alkaline earth metals, and supporting oxides and their promoting role in storage and reduction steps. We dealt with the different catalyst synthesis methods and the reactor configurations used in research and technical applications and their influence on NSR performance. The ongoing research on theoretical calculations, kinetic modeling, and surface science studies to probe the NSR mechanism has also been addressed. Important facets characterizing the state of the art of NSR research may be summarized as follows:

(i) Although there is a wide general agreement concerning the overall NSR mechanism consisting of primarily five steps, diversified and sometimes contradictory results also have been reported mainly due to different experimental conditions used by the various researchers, such as different lean and regeneration periods, different reducing gas, different catalyst preparation and pretreatment, and different mass- and heat-transfer conditions (different reactors). The Langmuir−Hinshelwood or the Eley−Rideal mechanism; which is the pathway for NO oxidation, is still under debate. The NO_x sorption, on the other hand, is a sequential process (initially nitrite and eventually nitrate formation), which still does not clearly state the nature of the Ba species or does not account for the NO_x slip during the storage process. The NO_x reduction mechanism and the product selectivity under rich conditions are dependent on the reductants. NH_3, which is recently believed to be an intermediate reductant, has not been universally observed and accepted by the researchers.

(ii) The noble metal Pt is widely used by the researchers for the oxidation of NO and the subsequent reduction of the stored NO_x. However, the nature of the Pt particles, the loading, the dispersion, the size and the morphology, and the metal−support effect influencing the catalytic activity are still a matter of debate. There is still no conclusive proof about the optimum loading, shape, and dispersion of Pt particles for the best catalytic activity. Investigations have been carried out with other noble metals, such as Pd and Rh, to find out the appropriate one, and still the question remains whether the combination of more than one metal performs better? Furthermore, the potential of metal alloys needs to be explored.

(iii) The storage component best investigated and commonly used is Ba; however, the nature of the storage component is still ill-defined. According to some researchers, $BaCO_3$ is the dominant storage component under real conditions, whereas some others claim that BaO, due to its higher basicity, should be a more potential storage component than $BaCO_3$. Researchers revealed that the proximity of Ba and the noble metal is important in the storage process; however, systematic investigations are still lacking regarding this aspect. Overall, it is accepted that $BaAl_2O_4$ is formed at higher temperature during NSR operation, although the exact role of $BaAl_2O_4$ is still unknown. Storage materials, other than Ba, such as K, Mg, and Ca, showed promising performance in the storage step and less sulfur poisoning, which needs to be explored more profoundly.

(iv) Besides stabilizing the dispersed noble metal particles, the support material can also affect the oxidation state of the noble metal and the spillover process, which in turn has an effect on the oxidation, storage, and regeneration (reduction) steps and thus overall performance of the NSR catalyst. For Ba-based lean traps the NO_x storage capacity seems to follow the basicity of the oxide support, while the rate of NO_x reduction tends to decrease with stronger basicity of the support. An open question is the role of the support in the spillover processes occurring in the NSR system. Furthermore, for a deeper understanding of the surface processes during NSR, the structure and the chemistry of the interfaces of the support with catalytic (noble metals) and storage components (alkali and alkaline earth metals) need to be investigated more thoroughly, particularly under dynamic conditions.

(v) A wide variety of promoters have been used for betterment of NSR performance, which act either as chemical or as structural promoters. The latter enhance the lifetime by increasing the stability of the dispersed noble metal, storage components, and support. Systematic studies on the role of promoters are still scarce and may provide an interesting potential for further improvement of NSR catalysts.

(vi) Various synthetic methods of preparing the NSR catalysts have been approached in the literature. Wet-impregnation is the most popular method of synthesis; however, there are plenty of investigations which report that sol−gel synthesis and flame spray pyrolysis have beneficial effects over wet-impregnation synthesis.
(vii) Several inconsistencies in the literature are due to the fact that inappropriate reaction conditions have been used in the investigations. In real engine exhaust gas, the presence of H_2, CO, hydrocarbons, H_2O, and CO_2 in the rich phase can vary depending on the engine operating conditions, whereas model synthetic gas mixtures as mostly used in laboratory scale investigations are normally simpler. This discrepancy of real exhaust to the model gas mixtures sometimes causes considerable uncertainty concerning the practical conclusions which can be drawn from the experiments. The exact roles played by CO_2 and H_2O in the mechanism and for the activity are still underdeveloped. Systematic investigations are needed to elucidate the exact role played by the CO_2 and H_2O.
(viii) Laboratory scale reactor or practical aftertreatment technologies are a separate branch of research for NSR catalysis. Different kinds of reactors and experimental techniques, such as TAP reactor, spatiotemporal product analysis, time- and space-resolved spectroscopic studies, and high throughput experimentation significantly enhanced the present knowledge about NSR. However, a great variety of experimental conditions often renders drawing of general conclusions difficult. A new impetus for gaining a better understanding of the different surface processes of NSR may come from pertinent surface science studies, as recent investigations indicate.
(ix) Special care has to be taken when extracting structure−performance relationships from integral reactor types due to large gradients in structure and temperature which can occur along the catalyst bed, as recent space- and time-resolved spectroscopic investigations revealed.
(x) The rapid development of theoretical calculations is gaining importance in NSR research as a potential tool for supporting experimental results and for giving answers to fundamental questions which are difficult or impossible to access by experimental research. Furthermore, the development of global kinetic models considering the interplay between chemical processes and mass and heat transfer may provide a solid basis for optimizing the overall efficiency of technical storage−reduction systems.

An overall conclusion emerging from this survey is that the conventional $Pt-Ba/Al_2O_3$ catalyst which has been used for so long needs to be improved using a more potential catalyst, which allows NO_x removal at low temperatures (<150 °C) and can cope with undesired input components such as SO_2, CO_2, and H_2O. It remains a challenge to find new more efficient materials which are specifically designed for the various functions needed for NO_x removal. A better understanding of the mechanism of NSR gained by *in situ* characterization may help in pursuing this aim.

Finally, it has to be stressed that only an integrated approach, including the development of new efficient materials as well as proper engine control strategies and reaction engineering, will allow us to meet future increasingly stringent emission regulations.

9. Acknowledgments

Financial support of this work by ETH Zurich (TH-0906-2) is kindly acknowledged. A.B. thanks past and present co-workers for their valuable contributions, their enthusiasm, and perseverance, which have greatly stimulated our research. Their names appear in the reference list.

10. References

(1) Klingstedt, F.; Arve, K.; Eranen, K.; Murzin, D. Y. *Acc. Chem. Res.* **2006**, *39*, 273–282.
(2) Helms, G. T.; Vitas, J. B.; Nikbakht, P. A. *Water Air Soil Pollut.* **1993**, *67*, 207–216.
(3) http://www.dieselnet.com/standards/.
(4) Lox, E. S. J. *Handb. Heterog. Catal.* **2008**, *5*, 2274–2277.
(5) Webb, C. C.; Weber, P. A.; Thornton, M. J. *SAE Tech. Pap. Ser.* **2004**, 2004−01−0585.
(6) Iwamoto, M.; Yokoo, S.; Sakai, K.; Kagawa, S. *J. Chem. Soc., Faraday Trans. 1* **1981**, *77*, 1629–1638.
(7) Iwamoto, S.; Kon, S.; Yoshida, S.; Inui, T. In Progress in Zeolite and Microporous Materials, Parts A−C; 1997; Vol. 105.
(8) Burch, R. *Catal. Rev.−Sci. Eng.* **2004**, *46*, 271–333.
(9) Pârvulescu, V. I.; Grange, P.; Delmon, B. *Catal. Today* **1998**, *46*, 233–316.
(10) Busca, G.; Larrubia, M. A.; Arrighi, L.; Ramis, G. *Catal. Today* **2005**, *107−08*, 139–148.
(11) Roy, S.; Viswanath, B.; Hegde, M. S.; Madras, G. *J. Phys. Chem. C* **2008**, *112*, 6002–6012.
(12) Centi, G.; Arena, G. E.; Perathoner, S. *J. Catal.* **2003**, *216*, 443–454.
(13) Epling, W. S.; Campbell, L. E.; Yezerets, A.; Currier, N. W.; Parks, J. E. *Catal. Rev.−Sci. Eng.* **2004**, *46*, 163–245.
(14) Kanazawa, T. *Catal. Today* **2004**, *96*, 171–177.
(15) Forzatti, P.; Castoldi, L.; Lietti, L.; Nova, I.; Tronconi, E. *Stud. Surf. Sci. Catal.* **2007**, *171*, 175–208.
(16) Brogan, M. S.; Clark, A. D.; Spencer, M. J.; Brisley, R. J. *SAE Tech. Pap. Ser.* **1998**, 980933.
(17) Narula, C. K.; Moses, M. J.; Allard, L. F. *SAE Tech. Pap. Ser.* **2006**, 2006−01−3420.
(18) Miyoshi, N.; Matsumoto, S.; Katoh, K.; Tanaka, T.; Harada, J.; Takahashi, N.; Yokota, K.; Sugiura, M.; Kasahara, K. *SAE Tech. Pap. Ser.* **1995**, 950809.
(19) Matsumoto, S. *Catal. Today* **1996**, *29*, 43–45.
(20) Takahashi, N.; Shinjoh, H.; Iijima, T.; Suzuki, T.; Yamazaki, K.; Yokota, K.; Suzuki, H.; Miyoshi, N.; Matsumoto, S.; Tanizawa, T.; Tanaka, T.; Tateishi, S.; Kasahara, K. *Catal. Today* **1996**, *27*, 63–69.
(21) Alkemade, U. G.; Schumann, B. *Solid State Ionics* **2006**, *177*, 2291–2296.
(22) Kim, D. H.; Chin, Y. H.; Muntean, G.; Yezerets, A.; Currier, N.; Epling, W.; Chen, H. Y.; Hess, H.; Peden, C. H. F. *Ind. Eng. Chem. Res.* **2007**, *46*, 2735–2740.
(23) Roedel, E.; Urakawa, A.; Kureti, S.; Baiker, A. *Phys. Chem. Chem. Phys.* **2008**, *10*, 6190–6198.
(24) Epling, W. S.; Kisinger, D.; Everest, C. *Catal. Today* **2008**, *136*, 156–163.
(25) Lesage, T.; Saussey, J.; Malo, S.; Hervieu, M.; Hedouin, C.; Blanchard, G.; Daturi, M. *Appl. Catal., B: Environ.* **2007**, *72*, 166–177.
(26) Lesage, T.; Verrier, C.; Bazin, P.; Saussey, J.; Malo, S.; Hedouin, C.; Blanchard, G.; Daturi, M. *Top. Catal.* **2004**, *30−31*, 31–36.
(27) Verrier, C.; Kwak, J. H.; Kim, D. H.; Peden, C. H. F.; Szanyi, J. *Catal. Today* **2008**, *136*, 121–127.
(28) Kobayashi, H.; Ohkubo, K. *Appl. Surf. Sci.* **1997**, *121*, 111–115.
(29) Abdulhamid, H.; Fridell, E.; Skoglundh, M. *Appl. Catal., B: Environ.* **2006**, *62*, 319–328.
(30) Kim, J. G.; Lee, H. M.; Lee, M. J.; Lee, J. H.; Kim, J. G.; Jeon, J. Y.; Jeong, S. K.; Yoo, S. J.; Kim, S. S. *J. Ind. Eng. Chem.* **2008**, *14*, 841–846.
(31) Amberntsson, A.; Fridell, E.; Skoglundh, M. *Appl. Catal., B: Environ.* **2003**, *46*, 429–439.
(32) Breen, J. P.; Burch, R.; Fontaine-Gautrelet, F.; Hardacre, C.; Rioche, C. *Appl. Catal., B: Environ.* **2008**, *81*, 150–159.
(33) Forzatti, P.; Castoldi, L.; Nova, I.; Lietti, L.; Tronconi, E. *Catal. Today* **2006**, *117*, 316–320.
(34) Li, Y.; Roth, S.; Dettling, J.; Beutel, T. *Top. Catal.* **2001**, *16*, 139–144.
(35) Takahashi, N.; Yamazaki, K.; Sobukawa, H.; Shinjoh, H. *Appl. Catal., B: Environ.* **2007**, *70*, 198–204.
(36) Epling, W. S.; Yezerets, A.; Currier, N. W. *Catal. Lett.* **2006**, *110*, 143–148.
(37) Abdulhamid, H.; Fridell, E.; Skoglundh, M. *Top. Catal.* **2004**, *30−31*, 161–168.
(38) Epling, W. S.; Yezerets, A.; Currier, N. W. *Appl. Catal., B: Environ.* **2007**, *74*, 117–129.

(39) Poulston, S.; Rajaram, R. R. *Catal. Today* **2003**, *81*, 603–610.
(40) Al-Harbi, M.; Epling, W. S. Catal. Lett., http://dx.doi.org/10.1007/s10562-009-9912-3.
(41) Olsson, L.; Westerberg, B.; Persson, H.; Fridell, E.; Skoglundh, M.; Andersson, B. *J. Phys. Chem. B* **1999**, *103*, 10433–10439.
(42) Olsson, L.; Persson, H.; Fridell, E.; Skoglundh, M.; Andersson, B. *J. Phys. Chem. B* **2001**, *105*, 6895–6906.
(43) Crocoll, M.; Kureti, S.; Weisweiler, W. *J. Catal.* **2005**, *229*, 480–489.
(44) Mulla, S. S.; Chen, N.; Cumaranatunge, L.; Blau, G. E.; Zemlyanov, D. Y.; Delgass, W. N.; Epling, W. S.; Ribeiro, F. H. *J. Catal.* **2006**, *241*, 389–399.
(45) Schmitz, P. J.; Baird, R. J. *J. Phys. Chem. B* **2002**, *106*, 4172–4180.
(46) Nova, I.; Castoldi, L.; Lietti, L.; Tronconi, E.; Forzatti, P.; Prinetto, F.; Ghiotti, G. *J. Catal.* **2004**, *222*, 377–388.
(47) Nova, I.; Castoldi, L.; Prinetto, F.; Dal Santo, V.; Lietti, L.; Tronconi, E.; Forzatti, P.; Ghiotti, G.; Psaro, R.; Recchia, S. *Top. Catal.* **2004**, *30*−*31*, 181–186.
(48) Olsson, L.; Fridell, E.; Skoglundh, M.; Andersson, B. *Catal. Today* **2002**, *73*, 263–270.
(49) Olsson, L.; Jozsa, P.; Nilsson, M.; Jobson, E. *Top. Catal.* **2007**, *42*−*43*, 95–98.
(50) Anastasiadou, T.; Loukatzikou, L. A.; Costa, C. N.; Efstathiou, A. M. *J. Phys. Chem. B* **2005**, *109*, 13693–13703.
(51) Elizundia, U.; Lopez-Fonseca, R.; Landa, I.; Gutierrez-Ortiz, M. A.; Gonzalez-Velasco, J. R. *Top. Catal.* **2007**, *42*−*43*, 37–41.
(52) Cant, N. W.; Liu, I. O. Y.; Patterson, M. J. *J. Catal.* **2006**, *243*, 309–317.
(53) Kwak, J. H.; Kim, D. H.; Szailer, T.; Peden, C. H. F.; Szanyi, J. *Catal. Lett.* **2006**, *111*, 119–126.
(54) Tonkyn, R. G.; Disselkamp, R. S.; Peden, C. H. F. *Catal. Today* **2006**, *114*, 94–101.
(55) Sakamoto, Y.; Motohiro, T.; Matsunaga, S.; Okumura, K.; Kayama, T.; Yamazaki, K.; Tanaka, T.; Kizaki, Y.; Takahashi, N.; Shinjoh, H. *Catal. Today* **2007**, *121*, 217–225.
(56) Pihl, J. A.; Parks, J.; Daw, C. S. *SAE Tech. Pap. Ser.* **2006**, 2006-01-3441.
(57) Parks, J. E.; Huff, S.; Pihl, J. A.; Choi, J. S.; West, B. H. *SAE Tech. Pap. Ser.* **2005**, 2005-01-3876.
(58) Clayton, R. D.; Harold, M. P.; Balakotaiah, V. *Appl. Catal., B: Environ.* **2008**, *84*, 616–630.
(59) Parks, J.; Watson, A.; Campbell, G.; Epling, W. S. *SAE Tech. Pap. Ser.* **2002**, 2002-01-2880.
(60) Faou, P. L.; Guyon, M.; Bert, C. *SAE Tech. Pap. Ser.* **1998**, 982607.
(61) Li, J.; Theis, J. R.; W., C.; Goralski, C. T.; Kudla, R. J.; Watkins, W. L.; Chattha, M.; Hurley, R. G. *SAE Tech. Pap. Ser.* **2001**, 2001-01-2503.
(62) Theis, J. R.; Li, J.; Hurley, R. G.; Ura, J. A. *SAE Tech. Pap. Ser.* **2002**, 2002−01−0733.
(63) Abdulhamid, H.; Fridell, E.; Dawody, J.; Skoglundh, M. *J. Catal.* **2006**, *241*, 200–210.
(64) Amberntsson, A.; Skoglundh, M.; Ljungstrom, S.; Fridell, E. *J. Catal.* **2003**, *217*, 253–263.
(65) Kim, D. H.; Kwak, J. H.; Szanyi, J.; Cho, S. J.; Peden, C. H. F. *J. Phys. Chem. C* **2008**, *112*, 2981–2987.
(66) Huang, H. Y.; Long, R. Q.; Yang, R. T. *Energy Fuels* **2001**, *15*, 205–213.
(67) Efthimiadism, E. A.; Lionta, G. D.; Christoforou, S. C.; Vasalos, I. A. *Catal. Today* **1998**, *40*, 15–26.
(68) Toubeli, E. A. E. A.; Vasalos, I. A. *Catal. Lett.* **2000**, *69*, 157–164.
(69) Scholz, C. M. L.; Gangwal, V. R.; de Croon, M.; Schouten, J. C. *Appl. Catal., B: Environ.* **2007**, *71*, 143–150.
(70) Medhekar, V.; Balakotaiah, V.; Harold, M. P. *Catal. Today* **2007**, *121*, 226–236.
(71) Nova, I.; Lietti, L.; Forzatti, P. *Catal. Today* **2008**, *136*, 128–135.
(72) Lee, J. H.; Kung, H. H. *Catal. Lett.* **1998**, *51*, 1–4.
(73) Denton, P.; Giroir-Fendler, A.; Praliaud, H.; Primet, M. *J. Catal.* **2000**, *189*, 410–420.
(74) Kim, D. H.; Chin, Y. H.; Muntean, G. G.; Yezeretz, A.; Currier, N. W.; Epling, W. S.; Chen, H. Y.; Hess, H.; Peden, C. H. F. *Ind. Eng. Chem. Res.* **2006**, *45*, 8815–8821.
(75) Schmitz, P. J.; Kudla, R. J.; Drews, A. R.; Chen, A. E.; Lowe-Ma, C. K.; McCabe, R. W.; Schneider, W. F.; Goralski, C. T. *Appl. Catal., B: Environ.* **2006**, *67*, 246–256.
(76) Anderson, J. A.; Bachiller-Baeza, B.; Fernandez-Garcia, M. *Phys. Chem. Chem. Phys.* **2003**, *5*, 4418–4427.
(77) Li, X. G.; Meng, M.; Lin, P. Y.; Fu, Y. L.; Hu, T. D.; Xie, Y. N.; Zhang, J. *Top. Catal.* **2003**, *22*, 111–115.
(78) Su, Y.; Amiridis, M. D. *Catal. Today* **2004**, *96*, 31–41.
(79) Dutta, G.; Waghmare, U. V.; Baidya, T.; Hegde, M. S. *Chem. Mater.* **2007**, *19*, 6430–6436.
(80) Abdulhamid, H.; Dawody, J.; Fridell, E.; Skoglundh, M. *J. Catal.* **2006**, *244*, 169–182.
(81) Szailer, T.; Kwak, J. H.; Kim, D. H.; Hanson, J. C.; Peden, C. H. F.; Szanyi, J. *J. Catal.* **2006**, *239*, 51–64.
(82) Olsson, L.; Fridell, E. *J. Catal.* **2002**, *210*, 340–353.
(83) Mulla, S. S.; Chaugule, S. S.; Yezerets, A.; Currier, N. W.; Delgass, W. N.; Ribeiro, F. H. *Catal. Today* **2008**, *136*, 136–145.
(84) Koci, P.; Plat, F.; Stepanek, J.; Kubicek, M.; Marek, M. *Catal. Today* **2008**, *137*, 253–260.
(85) Dawody, J.; Skoglundh, M.; Wall, S.; Fridell, E. *J. Mol. Catal. A: Chem.* **2005**, *225*, 259–269.
(86) Piacentini, M.; Strobel, R.; Maciejewski, M.; Pratsinis, S. E.; Baiker, A. *J. Catal.* **2006**, *243*, 43–56.
(87) Strobel, R.; Madler, L.; Piacentini, M.; Maciejewski, M.; Baiker, A.; Pratsinis, S. E. *Chem. Mater.* **2006**, *18*, 2532–2537.
(88) Lee, F.; Wilson, K.; Lambert, R.; Hubbard, C. P.; Hurley, R. G.; McCabe, R. W.; Gandhi, H. S. *J. Catal.* **1999**, *184*, 491–498.
(89) Salasc, S.; Skoglundh, M.; Fridell, E. *Appl. Catal., B: Environ.* **2002**, *36*, 145–160.
(90) McCabe, R. W.; Usmen, R. K. In 11th International Congress on Catalysis−40th Anniversary, Parts A and B; 1996; Vol. 101.
(91) Bera, P.; Patil, K. C.; Jayaram, V.; Subbanna, G. N.; Hegde, M. S. *J. Catal.* **2000**, *196*, 293–301.
(92) Roy, S.; Hegde, M. S. *Catal. Commun.* **2008**, *9*, 811–815.
(93) Datye, A. K.; Bravo, J.; Nelson, T. R.; Atanasova, P.; Lyubovsky, M.; Pfefferle, L. *Appl. Catal., A: Gen.* **2000**, *198*, 179–196.
(94) Su, Y.; Kabin, K. S.; Harold, M. P.; Amiridis, M. D. *Appl. Catal., B: Environ.* **2007**, *71*, 207–215.
(95) Desikusumastuti, A.; Qin, Z.; Staudt, T.; Happel, M.; Lykhach, Y.; Laurin, M.; Shaikhutdinov, S.; Libuda, J. Surf. Sci., http://dx.doi.org/10.1016/j.susc.2008.11.003.
(96) Breen, J. P.; Burch, R.; Lingaiah, N. *Catal. Lett.* **2002**, *79*, 171–174.
(97) Brosius, R.; Arve, K.; Groothaert, M. H.; Martens, J. A. *J. Catal.* **2005**, *231*, 344–353.
(98) Shimizu, K.; Shibata, J.; Satsuma, A. *J. Catal.* **2006**, *239*, 402–409.
(99) Breen, J. P.; Burch, R.; Hill, C. J. Catal. Today, http://dx.doi.org/10.1016/j.cattod.2008.05.016.
(100) Haneda, M.; Yoshinari, T.; Sato, K.; Kintaichi, Y.; Hamada, H. *Chem. Commun.* **2003**, *22*, 2814–2815.
(101) Wogerbauer, C.; Maciejewski, M.; Baiker, A. *J. Catal.* **2002**, *205*, 157–167.
(102) Wogerbauer, C.; Maciejewski, M.; Baiker, A.; Gobel, U. *J. Catal.* **2001**, *201*, 113–127.
(103) Amberntsson, A.; Westerberg, B.; Engstrom, P.; Fridell, E.; Skoglundh, M. In Catalyst Deactivation 1999 1999; Vol. 126.
(104) Olsson, L.; Monroe, D.; Blint, R. J. *Ind. Eng. Chem. Res.* **2006**, *45*, 8883–8890.
(105) Olsson, L.; Blint, R. J.; Fridell, E. *Ind. Eng. Chem. Res.* **2005**, *44*, 3021–3032.
(106) Schmeissesr, V.; Tuttlies, U.; Eigenberger, G. *Top. Catal.* **2007**, *42*−*43*, 77–81.
(107) Theis, J. R.; Ura, J. A.; McCabe, R. W. *SAE Tech. Pap. Ser.* **2007**, 2007-01-1055.
(108) Lesage, T.; Verrier, C.; Bazin, P.; Saussey, J.; Daturi, M. *Phys. Chem. Chem. Phys.* **2003**, *5*, 4435–4440.
(109) Jelic, J.; Meyer, R. J. *Catal. Today* **2008**, *136*, 76–83.
(110) Jelic, J.; Meyer, R. J. Abstracts of Papers, 235th ACS National Meeting, United States, 2008.
(111) Sedlmair, C.; Seshan, K.; Jentys, A.; Lercher, J. A. *J. Catal.* **2003**, *214*, 308–316.
(112) Epling, W. S.; Parks, J. E.; Campbell, G. C.; Yezerets, A.; Currier, N. W.; Campbell, L. E. *Catal. Today* **2004**, *96*, 21–30.
(113) Cant, N. W.; Patterson, M. J. *Catal. Today* **2002**, *73*, 271–278.
(114) Kabin, K. S.; Muncrief, R. L.; Harold, M. P. *Catal. Today* **2004**, *96*, 79–89.
(115) Laurent, F.; Pope, C. J.; Mahzoul, H.; Delfosse, L.; Gilot, P. *Chem. Eng. Sci.* **2003**, *58*, 1793–1803.
(116) Castoldi, L.; Nova, I.; Lietti, L.; Forzatti, P. *Catal. Today* **2004**, *96*, 43–52.
(117) Kwak, J. H.; Kim, D. H.; Szanyi, J.; Szailer, T.; Peden, C. H. F. *Abstr. Pap. Am. Chem. Soc.* **2005**, *229*, U876−U876.
(118) Lietti, L.; Forzatti, P.; Nova, I.; Tronconi, E. *J. Catal.* **2001**, *204*, 175–191.
(119) Szailer, T.; Kwak, J. H.; Kim, D. H.; Szanyi, J.; Wang, C. M.; Peden, C. H. F. *Catal. Today* **2006**, *114*, 86–93.
(120) Kim, D. H.; Chin, Y. H.; Kwak, J. H.; Peden, C. H. F. *Catal. Lett.* **2008**, *124*, 39–45.
(121) Basile, F.; Fornasari, G.; Gambatesa, A.; Livi, M.; Vaccari, A. *Catal. Today* **2007**, *119*, 59–63.
(122) Shimizu, K.; Saito, Y.; Nobukawa, T.; Miyoshi, N.; Satsuma, A. *Catal. Today* **2008**, *139*, 24–28.
(123) Luo, J. Y.; Meng, M.; Li, X. G.; Zha, Y. Q. *Microporous Mesoporous Mater.* **2008**, *113*, 277–285.
(124) Malpartida, I.; Vargas, M. A. L.; Alemany, L. J.; Finocchio, E.; Busca, G. *Appl. Catal., B: Environ.* **2008**, *80*, 214–225.

(125) Piacentini, M.; Maciejewski, M.; Burgi, T.; Baiker, A. *Top. Catal.* **2004**, *30*−*31*, 71–80.
(126) Casapu, M.; Grunwaldt, J. D.; Maciejewski, M.; Wittrock, M.; Gobel, U.; Baiker, A. *Appl. Catal., B: Environ.* **2006**, *63*, 232–242.
(127) Piacentini, M.; Maciejewski, M.; Baiker, A. *Appl. Catal., B: Environ.* **2005**, *59*, 187–195.
(128) Frola, F.; Manzoli, M.; Prinetto, P.; Ghiotti, G.; Castoldi, L.; Lietti, L. *J. Phys. Chem. C* **2008**, *112*, 12869–12878.
(129) Rodrigues, F.; Juste, L.; Potvin, C.; Tempere, J. F.; Blanchard, G.; Djega-Mariadassou, G. *Catal. Lett.* **2001**, *72*, 59–64.
(130) Epling, W. S.; Peden, C. H. F.; Szanyi, J. *J. Phys. Chem. C* **2008**, *112*, 10952–10959.
(131) Broqvist, P.; Panas, I.; Gronbeck, H. *J. Phys. Chem. B* **2005**, *109*, 9613–9621.
(132) Broqvist, P.; Panas, I.; Fridell, E.; Persson, H. *J. Phys. Chem. B* **2002**, *106*, 137–145.
(133) Broqvist, P.; Panas, I.; Gronbeck, H. *J. Phys. Chem. B* **2005**, *109*, 15410–15416.
(134) Prinetto, F.; Ghiotti, G.; Nova, I.; Lietti, L.; Tronconi, E.; Forzatti, P. *J. Phys. Chem. B* **2001**, *105*, 12732–12745.
(135) Hess, C.; Lunsford, J. H. *J. Phys. Chem. B* **2002**, *106*, 6358–6360.
(136) Hess, C.; Lunsford, J. H. *J. Phys. Chem. B* **2003**, *107*, 1982–1987.
(137) Westerberg, B.; Fridell, E. *J. Mol. Catal., A: Chem.* **2001**, *165*, 249–263.
(138) Desikusumastuti, A.; Happel, M.; Dumbuya, K.; Staudt, T.; Laurin, M.; Gottfried, J. M.; Steinrück, H. P.; Libuda, J. *J. Phys. Chem. C* **2008**, *112*, 6477–6486.
(139) Yi, C. W.; Szanyi, J. J. Phys. Chem. C, http://dx.doi.org/10.1021/jp806854y.
(140) Desikusumastuti, A.; Staudt, T.; Gronbeck, H.; Libuda, J. *J. Catal.* **2008**, *255*, 127–133.
(141) Desikusumastuti, A.; Laurin, M.; Happel, M.; Qin, Z.; Shaikhutdinov, S.; Libuda, J. *Catal. Lett.* **2008**, *121*, 311–318.
(142) Szanyi, J.; Kwak, J. H.; Kim, D. H.; Burton, S. D.; Peden, C. H. F. *J. Phys. Chem. B* **2005**, *109*, 27–29.
(143) Ozensoy, E.; Peden, C. H. F.; Szanyi, J. *J. Catal.* **2006**, *243*, 149–157.
(144) Ozensoy, E.; Peden, C. H. F.; Szanyi, J. *J. Phys. Chem. B* **2005**, *109*, 15977–15984.
(145) Staudt, T.; Desikusumastuti, A.; Happel, M.; Vesselli, E.; Baraldi, A.; Gardonio, S.; Lizzit, S.; Rohr, F.; Libuda, J. *J. Phys. Chem. C* **2008**, *112*, 9835–9846.
(146) Desikusumastuti, A.; Staudt, T.; Happel, M.; Laurin, M.; Libuda, J. *J. Catal.* **2008**, *260*, 315–328.
(147) Kwak, J. H.; Mei, D.; Yi, C. W.; Kim, D. H.; Peden, C. H. F.; Allard, L. F.; Szanyi, J. J. Catal. , http://dx.doi.org/10.1016/j.jcat.2008.10.016.
(148) Bowker, M. *Chem. Soc. Rev.* **2008**, *37*, 2204–2211.
(149) Szanyi, J.; Kwak, J. H.; Hanson, J.; Wang, C. M.; Szailer, T.; Peden, C. H. F. *J. Phys. Chem. B* **2005**, *109*, 7339–7344.
(150) Xie, S.; Mestl, G.; Rosynek, M. P.; Lunsford, J. H. *J. Am. Chem. Soc.* **1997**, *119*, 10186–10191.
(151) Fridell, E.; Persson, H.; Westerberg, B.; Olsson, L.; Skoglundh, M. *Catal. Lett.* **2000**, *66*, 71–74.
(152) Yi, C. W.; Kwak, J. H.; Szanyi, J. *J. Phys. Chem. C* **2007**, *111*, 15299–15305.
(153) Kim, D. H.; Chin, Y. H.; Kwak, J. H.; Szanyi, J.; Peden, C. H. F. *Catal. Lett.* **2005**, *105*, 259–268.
(154) Balint, I.; You, Z.; Aika, K. *Phys. Chem. Chem. Phys.* **2002**, *4*, 2501–2503.
(155) Camby, L. P.; Thomas, G. *Solid State Ionics* **1997**, *93*, 315–320.
(156) Casapu, M.; Grunwaldt, J. D.; Maciejewski, M.; Baiker, A.; Wittrock, M.; Gobel, U.; Eckhoff, S. *Top. Catal.* **2007**, *42*−*43*, 3–7.
(157) Elbouazzaoui, S.; Courtois, X.; Marecot, P.; Duprez, D. *Top. Catal.* **2004**, *30*−*31*, 493–496.
(158) Uy, D.; O'Neill, A. E.; Li, J.; Watkins, W. L. H. *Catal. Lett.* **2004**, *95*, 191–201.
(159) Hodjati, S.; Bernhardt, P.; Petit, C.; Pitchon, V.; Kiennemann, A. *Appl. Catal., B: Environ.* **1998**, *19*, 209–219.
(160) Hodjati, S.; Bernhardt, P.; Petit, C.; Pitchon, V.; Kiennemann, A. *Appl. Catal., B: Environ.* **1998**, *19*, 221–232.
(161) Yi, C. W.; Kwak, J. H.; Peden, C. H. F.; Wang, C.; Szanyi, J. *J. Phys. Chem. C* **2007**, *111*, 14942–14944.
(162) Arena, G. E.; Capito, L.; Centi, G. In Oxide Based Materials: New Sources, Novel Phases, New Applications; 2005; Vol. 155.
(163) Engstrom, P.; Amberntsson, A.; Skoglundh, M.; Fridell, E.; Smedler, G. *Appl. Catal., B: Environ.* **1999**, *22*, L241−L248.
(164) Limousy, L.; Mahzoul, H.; Brilhac, J. F.; Garin, F.; Maire, G.; Gilot, P. *Appl. Catal., B: Environ.* **2003**, *45*, 169–179.
(165) Sedlmair, C.; Seshan, K.; Jentys, A.; Lercher, J. A. *Catal. Today* **2002**, *75*, 413–419.
(166) Schreier, E.; Eckelt, R.; Richter, M.; Fricke, R. *Catal. Commun.* **2005**, *6*, 409–414.
(167) Elbouazzaoui, S.; Corbos, E. C.; Courtois, X.; Marecot, P.; Duprez, D. *Appl. Catal., B: Environ.* **2005**, *61*, 236–243.
(168) Kim, D. H.; Szanyi, J.; Kwak, J. H.; Szailer, T.; Hanson, J.; Wang, C. M.; Peden, C. H. F. *J. Phys. Chem. B* **2006**, *110*, 10441–10448.
(169) Han, P. H.; Lee, Y. K.; Han, S. M.; Rhee, H. K. *Top. Catal.* **2001**, *16*, 165–170.
(170) Huang, H. Y.; Long, R. Q.; Yang, R. T. *Energy Fuels* **2001**, *15*, 205–213.
(171) Takeuchi, M.; Matsumoto, S. *Top. Catal.* **2004**, *28*, 151–156.
(172) Karlsen, E. J.; Nygren, M. A.; Pettersson, L. G. M. *J. Phys. Chem. B* **2003**, *107*, 7795–7802.
(173) Basile, F.; Fomasari, G.; Grimandi, A.; Livi, M.; Vaccari, A. *Appl. Catal., B: Environ.* **2006**, *69*, 58–64.
(174) Konsolakis, M.; Yentekakis, I. V. *Appl. Catal., B: Environ.* **2001**, *29*, 103–113.
(175) Konsolakis, M.; Vrontaki, M.; Avgouropoulos, G.; Ioannides, T.; Yentekakis, I. V. *Appl. Catal., B: Environ.* **2006**, *68*, 59–67.
(176) Dou, D.; Balland, J. *SAE Tech. Pap. Ser.* **2002**, 2002-01-0734.
(177) Toops, T. J.; Smith, D. B.; Partridge, W. P. *Appl. Catal., B: Environ.* **2005**, *58*, 245–254.
(178) Toops, T. J.; Smith, D. B.; Epling, W. S.; Parks, J. E.; Partridge, W. P. *Appl. Catal., B: Environ.* **2005**, *58*, 255–264.
(179) Iwata, N.; Suzuki, Y.; Kato, H.; Takeuchi, M.; Sugiura, M. *SAE Tech. Pap. Ser.* **2004**, 2004-01-1494.
(180) Toops, T. J.; Pihl, J. A. *Catal. Today* **2008**, *136*, 164–172.
(181) Sakamoto, Y.; Matsunaga, S.; Okumura, K.; Kayama, T.; Yamazaki, K.; Takahashi, N.; Tanaka, T.; Kizaki, Y.; Motohiro, T.; Shinjoh, H. *Chem. Eng. Sci.* **2008**, *63*, 5028–5034.
(182) Liu, Y.; Meng, M.; Zou, Z. Q.; Li, X. G.; Zha, Y. Q. Catal. Commun., http://dx.doi.org/10.1016/j.catcom.2008.08.014.
(183) de Lucas-Consuegra, A.; Caravaca, A.; Sánchez, P.; Dorado, F.; Valverde, J. L. *J. Catal.* **2008**, *259*, 54–65.
(184) Rohart, E. *SAE Tech. Pap. Ser.* **2008**, 2008-01-0450.
(185) Belliere-Baca, V.; Harle, V.; Pitois, C.; Rohart, E. *SAE Tech. Pap. Ser.* **2007**, 2007-01-1241.
(186) Miyoshi, S.; Harada, K.; Iwakuni, H.; Yamada, H.; Tsushio, Y.; Takami, A. *SAE Tech. Pap. Ser.* **2007**, 2007-01-3732.
(187) Svedberg, P.; Jobson, E.; Erkfeldt, S.; Andersson, B.; Larsson, M.; Skoglundh, M. *Top. Catal.* **2004**, *30*−*31*, 199–206.
(188) Symalla, M. O.; Drochner, A.; Vogel, H.; Philipp, S.; Gobel, U.; Muller, W. *Top. Catal.* **2007**, *42*−*43*, 199–202.
(189) Casapu, M.; Grunwaldt, J. D.; Maciejewski, M.; Baiker, A.; Eckhoff, S.; Göbel, U.; Wittrock, M. *J. Catal.* **2007**, *251*, 28–38.
(190) Casapu, M.; Grunwaldt, J. D.; Maciejewski, M.; Krumeich, F.; Baiker, A.; Wittrock, M.; Eckhoff, S. *Appl. Catal., B: Environ.* **2008**, *78*, 288–300.
(191) Casapu, M.; Grunwaldt, J. D.; Maciejewski, M.; Baiker, A.; Hoyer, R.; Wittrock, M.; Eckhoff, S. *Catal. Lett.* **2008**, *120*, 1–7.
(192) Ji, Y.; Choi, J. S.; Toops, T. J.; Crocker, M.; Naseri, M. *Catal. Today* **2008**, *136*, 146–155.
(193) Kwak, J. H.; Kim, D. H.; Szanyi, J.; Peden, C. H. F. *Appl. Catal., B: Environ.* **2008**, *84*, 545–551.
(194) Piacentini, M.; Maciejewski, M.; Baiker, A. *Appl. Catal., B: Environ.* **2006**, *66*, 126–136.
(195) Piacentini, M.; Maciejewski, M.; Baiker, A. *Appl. Catal., B: Environ.* **2007**, *72*, 105–117.
(196) Choi, B.; Jeong, J.; Lee, C. *SAE Tech. Pap. Ser.* **2007**, 2007-01-1916.
(197) Despres, J.; Koebel, M.; Kröcher, O.; Elsener, M.; Wokaun, A. *Appl. Catal., B: Environ.* **2003**, *43*, 389–395.
(198) Yamamoto, K.; Kikuchi, R.; Takeguchi, T.; Eguchi, K. *J. Catal.* **2006**, *238*, 449–457.
(199) Dawody, J.; Skoglundh, M.; Fridell, E. *J. Mol. Catal. A: Chem.* **2004**, *209*, 215–225.
(200) Rohr, F.; Peter, S. D.; Lox, E.; Kogel, M.; Sassi, A.; Juste, L.; Rigaudeau, C.; Belot, G.; Gelin, P.; Primet, M. *Appl. Catal., B: Environ.* **2005**, *56*, 201–212.
(201) Rohr, F.; Gobel, U.; Kattwinkel, P.; Kreuzer, T.; Muller, W.; Philipp, S.; Gelin, P. *Appl. Catal., B: Environ.* **2007**, *70*, 189–197.
(202) Park, J. H.; Cho, H. J.; Park, S. J.; Nam, I. S.; Yeo, G. K.; Kil, J. K.; Youn, Y. K. *Top. Catal.* **2007**, *42*−*43*, 61–64.
(203) Vijay, R.; Snively, C. M.; Lauterbach, J. *J. Catal.* **2006**, *243*, 368–375.
(204) Hammache, S.; Evans, L. R.; Coker, E. N.; Miller, J. E. *Appl. Catal., B: Environ.* **2008**, *78*, 315–323.
(205) Fornasari, G.; Trifiro, F.; Vaccari, A.; Prinetto, F.; Ghiotti, G.; Centi, G. *Catal. Today* **2002**, *75*, 421–429.
(206) Centi, G.; Fornasari, G.; Gobbi, C.; Livi, M.; Trifiro, F.; Vaccari, A. *Catal. Today* **2002**, *73*, 287–296.
(207) Fornasari, G.; Glockler, R.; Livi, M.; Vaccari, A. *Appl. Clay Sci.* **2005**, *29*, 258–266.
(208) Kang, S. F.; Jiang, Z.; Hao, Z. P. *Acta Phys. Chim. Sin.* **2005**, *21*, 278–282.

(209) Morandi, S.; Prinetto, F.; Ghiotti, G.; Livi, M.; Vaccari, A. *Microporous Mesoporous Mater.* **2007**, *107*, 31–38.
(210) Palomares, A. E.; Uzcategui, A.; Corma, A. *Catal. Today* **2008**, *137*, 261–266.
(211) Cheng, H.; Chen, G. W.; Wang, S. D.; Wu, D. Y.; Zhang, Y.; Li, H. Q. *Korean J. Chem. Eng.* **2004**, *21*, 595–600.
(212) Takahashi, N.; Matsunaga, S.; Tanaka, T.; Sobukawa, H.; Shinjoh, H. *Appl. Catal., B: Environ.* **2007**, *77*, 73–78.
(213) Yu, J. B.; Jiang, Z.; Zhu, L.; Hao, Z. P.; Xu, Z. P. *J. Phys. Chem. B* **2006**, *110*, 4291–4300.
(214) Yu, J. J.; Tao, Y. X.; Liu, C. C.; Hao, Z. P.; Xu, Z. P. *Environ. Sci. Technol.* **2007**, *41*, 1399–1404.
(215) Yu, J. J.; Wang, X. P.; Tao, Y. X.; Hao, Z. P.; Xu, Z. P. *Ind. Eng. Chem. Res.* **2007**, *46*, 5794–5797.
(216) Yamazaki, K.; Suzuki, T.; Takahashi, N.; Yokota, K.; Sugiura, M. *Appl. Catal., B: Environ.* **2001**, *30*, 459–468.
(217) Luo, J. Y.; Meng, M.; Zha, Y. Q.; Xie, Y. N.; Hu, T. D.; Zhang, J.; Liu, T. *Appl. Catal., B: Environ.* **2008**, *78*, 38–52.
(218) Xiao, J.; Li, X.; Deng, S.; Wang, F.; Wang, L. *Catal. Commun.* **2008**, *9*, 563–567.
(219) Strobel, R.; Krumeich, F.; Pratsinis, S. E.; Baiker, A. *J. Catal.* **2006**, *243*, 229–238.
(220) Corbos, E. C.; Courtois, X.; Bion, N.; Marecot, P.; Duprez, D. *Appl. Catal., B: Environ.* **2008**, *80*, 62–71.
(221) Machida, M.; Uto, M.; Kurogi, D.; Kijima, T. *Chem. Mater.* **2000**, *12*, 3158–3164.
(222) Machida, M.; Kurogi, D.; Kijima, T. *Chem. Mater.* **2000**, *12*, 3165–3170.
(223) Machida, M.; Kurogi, D.; Kijima, T. *Catal. Today* **2003**, *84*, 201–207.
(224) Machida, M.; Kurogi, D.; Kijima, T. *J. Phys. Chem. B* **2003**, *107*, 196–202.
(225) Yamazaki, K.; Takahashi, N.; Shinjoh, H.; Sugiura, M. *Appl. Catal., B: Environ.* **2004**, *53*, 1–12.
(226) Costa, C. N.; Efstathiou, A. M. *Environ. Chem. Lett.* **2004**, *2*, 55–58.
(227) Costa, C. N.; Efstathiou, A. M. *J. Phys. Chem. C* **2007**, *111*, 3010–3020.
(228) Costa, C. N.; Efstathiou, A. M. *Appl. Catal., B: Environ.* **2007**, *72*, 240–252.
(229) Huang, H. Y.; Long, R. Q.; Yang, R. T. *Appl. Catal., B: Environ.* **2001**, *33*, 127–136.
(230) Matsumoto, S.; Ikeda, Y.; Suzuki, H.; Ogai, M.; Miyoshi, N. *Appl. Catal., B: Environ.* **2000**, *25*, 115–124.
(231) Takahashi, N.; Suda, A.; Hachisuka, I.; Sugiura, M.; Sobukawa, H.; Shinjoh, H. *Appl. Catal., B: Environ.* **2007**, *72*, 187–195.
(232) Imagawa, H.; Tanaka, T.; Takahashi, N.; Matsunaga, S.; Shinjoh, H. *Stud. Surf. Sci. Catal.* **2007**, *172*, 609–610.
(233) Ikeda, Y.; Sobue, K.; Tsuji, S.; Matsumoto, S. *SAE Tech. Pap. Ser.* **1999**, 1999-01-1279.
(234) Hachisuka, I.; Hirata, H.; Ikeda, Y.; Matsumoto, S. *SAE Tech. Pap. Ser.* **2000**, 2000-01-1196.
(235) Imagawa, H.; Tanaka, T.; Takahashi, N.; Matsunaga, S.; Suda, S.; Shinjoh, H. *J. Catal.* **2007**, *251*, 315–320.
(236) Hirata, H.; Hachisuka, I.; Ikeda, Y.; Tsuji, S.; Matsumoto, S. *Top. Catal.* **2001**, *16*, 145–149.
(237) Yazawa, Y.; Takeuchi, M.; Watanabe, M.; Imagawa, H.; Tanaka, T. *SAE Tech. Pap. Ser.* **2007**, 2007-01-1056.
(238) Zou, Z. Q.; Meng, M.; Zhou, X. Y.; Li, X. G.; Zha, Y. Q. Catal. Lett., http://dx.doi.org/10.1007/s10562-008-9775-z.
(239) Hodjati, S.; Vaezzadeh, K.; Petit, C.; Pitchon, V.; Kiennemann, A. *Appl. Catal., B: Environ.* **2000**, *26*, 5–16.
(240) Hodjati, S.; Petit, C.; Pitchon, V.; Kiennemann, A. *Appl. Catal., B: Environ.* **2001**, *30*, 247–257.
(241) Li, X. G.; Chen, J. F.; Lin, P. Y.; Meng, M.; Fu, Y. L.; Tu, J.; Li, Q. X. *Catal. Commun.* **2004**, *5*, 25–28.
(242) Zhang, W. X.; Yahiro, H.; Mizuno, M.; Izumi, J.; Iwamoto, M. *Langmuir* **1993**, *9*, 2337–2343.
(243) Arai, H.; Machida, M. *Catal. Today* **1994**, *22*, 97–109.
(244) Sultana, A.; Loenders, R.; Monticelli, O.; Kirschhock, C.; Jacobs, P. A.; Martens, J. A. *Angew. Chem., Int. Ed.* **2000**, *39*, 2935–2937.
(245) Brilhac, J. F.; Sultana, A.; Gilot, P.; Martens, J. A. *Environ. Sci. Technol.* **2002**, *36*, 1136–1140.
(246) Szanyi, J.; Kwak, J. H.; Moline, R. A.; Peden, C. H. F. *Phys. Chem. Chem. Phys.* **2003**, *5*, 4045–4051.
(247) Sultana, A.; Habermacher, D. D.; Kirschhock, C. E. A.; Martens, J. A. *Appl. Catal., B: Environ.* **2004**, *48*, 65–76.
(248) Despres, J.; Koebel, M.; Krocher, O.; Elsener, M.; Wokaun, A. *Microporous Mesoporous Mater.* **2003**, *58*, 175–183.
(249) Shinjoh, H.; Takahashi, N.; Yokota, K. *Top. Catal.* **2007**, *42*−*43*, 215–219.
(250) Corbos, E. C.; Haneda, M.; Courtois, X.; Marecot, P.; Duprez, D.; Hamada, H. *Catal. Commun.* **2008**, *10*, 137–141.
(251) Rossignol, S.; Kappenstein, C. *Int. J. Inorg. Mater.* **2001**, *3*, 51–58.
(252) Chai, M.; Machida, M.; Eguchi, K.; Arai, H. *J. Membr. Sci.* **1994**, *96*, 205–212.
(253) Schaper, H.; Doesburg, E. B. M.; Reijen, L. L. V. *Appl. Catal.* **1983**, *7*, 211–220.
(254) Ozawa, M.; Kimura, M.; Isogai, A. *J. Mater. Sci. Lett.* **1990**, *9*, 709–711.
(255) Lin, H. Y.; Wu, C. J.; Chen, Y. W.; Lee, C. H. *Ind. Eng. Chem. Res.* **2006**, *45*, 134–141.
(256) Rohart, E.; Belliere-Baca, V.; Yokota, K.; Harle, V.; Pitois, C. *Top. Catal.* **2007**, *42*−*43*, 71–75.
(257) Liotta, L. F.; Macaluso, A.; Arena, G. E.; Livi, M.; Centi, G.; Deganello, G. *Catal. Today* **2002**, *75*, 439–449.
(258) Liu, Y.; Meng, M.; Li, X. G.; Guo, L. H.; Zha, Y. Q. *Chem. Eng. Res. Des.* **2008**, *86*, 932–940.
(259) Nguyen, K.; Kim, H.; Bunting, B. G.; Toops, T. J.; Yoon, C. S. *SAE Tech. Pap. Ser.* **2007**, 2007-01-0470.
(260) Theis, J. R.; Ura, J. A.; Goralski, C. T.; Caine, J. J.; Davies, M.; Kay, D. D.; Todd, A.; Dinsdale, S. *SAE Tech. Pap. Ser.* **2005**, 2005-01-1117.
(261) Corbos, E. C.; Courtois, X.; Can, F.; Marécot, P.; Duprez, D. Appl. Catal., B: Environ., http://dx.doi.org/10.1016/j.apcatb.2008.05.003.
(262) Cant, N. W.; Liu, I. O. Y.; Patterson, M. J. *Appl. Catal., B: Environ.* **2007**, *77*, 12–18.
(263) Fridell, E.; Skoglundh, M.; Westerberg, B.; Johansson, S.; Smedler, G. *J. Catal.* **1999**, *183*, 196–209.
(264) Li, L. D.; Yu, J. J.; Hao, Z. P.; Xu, Z. P. *J. Phys. Chem. C* **2007**, *111*, 10552–10559.
(265) Haneda, M.; Morita, T.; Nagao, Y.; Kintaichi, Y.; Hamada, H. *Phys. Chem. Chem. Phys.* **2001**, *3*, 4696–4700.
(266) Mahzoul, H.; Brilhac, J. F.; Gilot, P. *Appl. Catal., B: Environ.* **1999**, *20*, 47–55.
(267) Piacentini, M.; Maciejewski, M.; Baiker, A. *Appl. Catal., B: Environ.* **2005**, *60*, 265–275.
(268) Mathew, S. M.; Umbarkar, S. B.; Dongare, M. K. *Catal. Commun.* **2007**, *8*, 1178–1182.
(269) Lindholm, A.; Currier, N. W.; Dawody, J.; Hidayat, A.; Li, J.; Yezerets, A.; Olsson, L. Appl. Catal., B: Environ., http://dx.doi.org/10.1016/j.apcatb.2008.10.004.
(270) Li, J.; Li, W.; Kang, S.; Ke, R. *Catal. Lett.* **2007**, *116*, 155–160.
(271) Büchel, R.; Strobel, R.; Krumeich, F.; Baiker, A.; Pratsinis, S. E. *J. Catal.* **2009**, *261*, 201–207.
(272) Symalla, M. O.; Drochner, A.; Vogel, H.; Buchel, R.; Pratsinis, S. E.; Baiker, A. Appl. Catal., B: Environ., http://dx.doi.org/10.1016/j.apcatb.2008.11.020.
(273) Kabin, K. S.; Khanna, P.; Muncrief, R. L.; Medhekar, V.; Harold, M. P. *Catal. Today* **2006**, *114*, 72–85.
(274) Nova, I.; Castoldi, L.; Lietti, L.; Tronconi, E.; Forzatti, P.; Prinetto, P.; Ghiotti, G. *SAE Tech. Pap. Ser.* **2005**, 2005-01-1085.
(275) Nova, I.; Lietti, L.; Castoldi, L.; Tronconi, E.; Forzatti, P. *J. Catal.* **2006**, *239*, 244–254.
(276) Sakamoto, Y.; Okumura, K.; Kizaki, Y.; Matsunaga, S.; Takahashi, N.; Shinjoh, H. *J. Catal.* **2006**, *238*, 361–368.
(277) Parks, J.; Huff, S.; Swartz, M.; West, B. In *10th CLEERS workshop*, Dearborn, MI, 2007.
(278) Lavy, J.; Rohr, F.; Armaroli, T.; Lambert, A.; Raux, S.; Dorge, S.; Gilot, P.; Climaud, P.; Sassi, A.; LeTallec, T. *SAE Tech. Pap. Ser.* **2006**, 2006-01-1068.
(279) Ahmadinejad, M.; Watling, T.; York, A.; Walker, A.; Chen, H. Y.; Hess, H.; Cox, J. *SAE Tech. Pap. Ser.* **2006**, 2006-01-3445.
(280) Theis, J. R.; McCabe, R. W.; Jen, H. W.; Sharma, M.; Balakotaiah, V.; Harold, M. P. *SAE Tech. Pap. Ser.* **2006**, 2006-01-1067.
(281) Lietti, L.; Nova, I.; Castoldi, L.; Tronconi, E.; Forzatti, P. *SAE Tech. Pap. Ser.* **2006**, 2006-01-1368.
(282) Tsami, A.; Grillo, F.; Bowker, M.; Nix, R. M. *Surf. Sci.* **2006**, *600*, 3403–3418.
(283) Erkfeldt, S.; Jobson, E.; Larsson, M. *Top. Catal.* **2001**, *16*, 127–131.
(284) James, D.; Fourre, E.; Ishii, M.; Bowker, M. *Appl. Catal., B: Environ.* **2003**, *45*, 147–159.
(285) Scholz, C. M. L.; Maes, B. H. W.; de croon, M. H. J. M.; Schouten, J. C. *Appl. Catal., A: Gen.* **2007**, *332*, 1–7.
(286) Choi, J. S.; Partridge, W. P.; Daw, C. S. *Appl. Catal., A: Gen.* **2005**, *293*, 24–40.
(287) Suzuki, J.; Matsumoto, S. *Top. Catal.* **2004**, *28*, 171–176.
(288) Krishna, K.; Makkee, M. *Catal. Today* **2006**, *114*, 48–56.
(289) Chimner, C. T. *SAE Tech. Pap. Ser.* **2008**, 2008-01-2641.
(290) Brilhac, J. F.; Jacquot, F.; Noirot, R. *SAE Tech. Pap. Ser.* **2004**, 2004-01-1943.
(291) Jung, J.; Song, S.; Chun, K. *SAE Tech. Pap. Ser.* **2008**, 2008-01-0482.
(292) Kim, D. S.; Kim, M. Y.; Lee, C. S. *J. Eng. Gas Turbines Power* **2006**, *128*, 497–505.

(293) Castoldi, L.; Matarrese, R.; Lietti, L.; Forzatti, P. *Appl. Catal., B: Environ.* **2006**, *64*, 25–34.
(294) Jelles, S. J.; Krul, R. R.; Makkee, M.; Moulijn, J. A. *Catal. Today* **1999**, *53*, 623–630.
(295) Sullivan, J. A.; Keane, O.; Cassidy, A. *Appl. Catal., B: Environ.* **2007**, *75*, 102–106.
(296) Liu, Z. Q.; Anderson, J. A. *J. Catal.* **2004**, *224*, 18–27.
(297) Koci, P.; Schejbal, M.; Trdlicka, J.; Gregor, T.; Kubicek, M.; Marek, M. *Catal. Today* **2007**, *119*, 64–72.
(298) Liu, Z. Q.; Anderson, J. A. *J. Catal.* **2004**, *228*, 243–253.
(299) Breen, J. P.; Rioche, C.; Burch, R.; Hardacre, C.; Meunier, F. C. *Appl. Catal., B: Environ.* **2007**, *72*, 178–186.
(300) Cant, N. W.; Patterson, M. J. *Catal. Lett.* **2003**, *85*, 153–157.
(301) Epling, W. S.; Campbell, G. C.; Parks, J. E. *Catal. Lett.* **2003**, *90*, 45–56.
(302) Lindholm, L.; Currier, N. W.; Fridell, E.; Yezerets, A.; Olsson, L. *Appl. Catal., B: Environ.* **2007**, *75*, 78–87.
(303) Olsson, L.; Abul-Milh, M.; Karlsson, H.; Jobson, E.; Thormahlen, P.; Hinz, A. *Top. Catal.* **2004**, *30*−*31*, 85–90.
(304) Scholz, C. M. L.; Nauta, K. M.; de croon, M. H. J. M.; Schouten, J. C. *Chem. Eng. Sci.* **2008**, *63*, 2843–2855.
(305) Kim, D. H.; Kwak, J. H.; Szanyi, J.; Burton, S. D.; Peden, C. H. F. *Appl. Catal., B: Environ.* **2007**, *72*, 233–239.
(306) Szanyi, J.; Kwak, J. H.; Kim, D. H.; Wang, X. Q.; Chimentao, R.; Hanson, J.; Epling, W. S.; Peden, C. H. F. *J. Phys. Chem. C* **2007**, *111*, 4678–4687.
(307) Szanyi, J.; Kwak, J. H.; Kim, D. H.; Wang, X. Q.; Hanson, J.; Chimentao, R. J.; Peden, C. H. F. *Chem. Commun.* **2007**, 984–986.
(308) Jeguirim, M.; Tschamber, V.; Brilhac, J. F.; Ehrburger, P. *Fuel* **2005**, *84*, 1949–1956.
(309) Jacquot, F.; Logie, V.; Brilhac, J. F.; Gilot, P. *Carbon* **2002**, *40*, 335–343.
(310) Chen, X.; Schwank, J. *Top. Catal.* **2007**, *46*, 39–47.
(311) Graham, G. W.; Jen, H. W.; Theis, J. R.; McCabe, R. W. *Catal. Lett.* **2004**, *93*, 3–6.
(312) Corbos, E. C.; Courtois, X.; Bion, N.; Marecot, P.; Duprez, D. *Appl. Catal., B: Environ.* **2007**, *76*, 357–367.
(313) Balcon, S.; Potvin, C.; Salin, L.; Tempere, J. F.; Djega-Mariadassou, G. *Catal. Lett.* **1999**, *60*, 39–43.
(314) Amberntsson, A.; Persson, H.; Engstrom, P.; Kasemo, B. *Appl. Catal., B: Environ.* **2001**, *31*, 27–38.
(315) Lietti, L.; Nova, I.; Forzatti, P. *J. Catal.* **2008**, *257*, 270–282.
(316) Basile, F.; Gambatesa, A.; Fornasari, G.; Livi, M.; Vaccari, A. *Top. Catal.* **2007**, *42*−*43*, 165–169.
(317) Cao, L.; Ratts, J. L.; Yezerets, A.; Currier, N. W.; Caruthers, J. M.; Ribeiro, F. H.; Delgass, W. N. Ind. Eng. Chem. Res., http://dx.doi.org/10.1021/ie8001809.
(318) Hendershot, R. J.; Vijay, R.; Snively, C. M.; Lauterbach, J. *Appl. Surf. Sci.* **2006**, *252*, 2588–2592.
(319) Lindholm, L.; Currier, N. W.; Li, J.; Yezerets, A.; Olsson, L. *J. Catal.* **2008**, *258*, 273–288.
(320) Jeguirim, M.; Tschamber, V.; Ehrburger, P. *Appl. Catal., B: Environ.* **2007**, *76*, 235–240.
(321) Stanmore, B. R.; Tschamber, V.; Brilhac, J. F. *Fuel* **2008**, *87*, 131–146.
(322) Atribak, I.; Such-Basáñez, I.; Bueno-López, A.; Garcı´a-Garcı´a, A. *J. Catal.* **2007**, *250*, 75–84.
(323) Atribak, I.; Bueno-López, A.; Garcı´a-Garcı´a, A. *J. Catal.* **2008**, *259*, 123–132.
(324) Nakatani, K.; Hirota, S.; Takeshima, S.; Itoh, K.; Tanaka, T. *SAE Tech. Pap. Ser.* **2002**, 2002-01-0957.
(325) Matarrese, R.; Castoldi, L.; Lietti, L.; Forzatti, P. *Top. Catal.* **2007**, *42*−*43*, 293–297.
(326) Matarrese, R.; Castoldi, L.; Lietti, L.; Forzatti, P. *Catal. Today* **2008**, *136*, 11–17.
(327) Milt, V. G.; Pissarello, M. L.; Miro, E. E.; Querini, C. A. *Appl. Catal., B: Environ.* **2003**, *41*, 397–414.
(328) Wu, X.; Lin, F.; Weng, D.; Li, J. *Catal. Commun.* **2008**, *9*, 2428–2432.
(329) Broqvist, P.; Gronbeck, H.; Panas, I. *Surf. Sci.* **2004**, *554*, 262–271.
(330) Broqvist, P.; Gronbeck, H.; Fridell, E.; Panas, I. *Catal. Today* **2004**, *96*, 71–78.
(331) Broqvist, P.; Gronbeck, H.; Fridell, E.; Panas, I. *J. Phys. Chem. B* **2004**, *108*, 3523–3530.
(332) Gronbeck, H.; Broqvist, P.; Panas, I. *Surf. Sci.* **2006**, *600*, 403–408.
(333) Broqvist, P.; Gronbeck, H. *Surf. Sci.* **2006**, *600*, L214−L218.
(334) Schneider, W. F. *J. Phys. Chem. B* **2004**, *108*, 273–282.
(335) Miletic, M.; Gland, J. L.; Hass, K. C.; Schneider, W. F. *J. Phys. Chem. B* **2003**, *107*, 157–163.
(336) Scholz, C. M. L.; Gangwal, V. R.; de Croon, M. H. J. M.; Schouten, J. C. *J. Catal.* **2007**, *245*, 215–227.
(337) Scholz, C. M. L.; Gangwal, V. R.; Hoebink, J. H. B. J.; Schouten, J. C. *Appl. Catal., B: Environ.* **2007**, *70*, 226–232.
(338) Scotti, A.; Nova, I.; Tronconi, E.; Castoldi, L.; Lietti, L.; Forzatti, P. *Ind. Eng. Chem. Res.* **2004**, *43*, 4522–4534.
(339) Tomasic, V. *Catal. Today* **2007**, *119*, 106–113.
(340) Sharma, M.; Kabin, K.; Harold, M. P.; Balakotaiah, V. *SAE Tech. Pap. Ser.* **2005**, 2005-01-0972.
(341) Wickman, B.; Lundstrom, A.; Sjoblom, J.; Creaser, D. *Top. Catal.* **2007**, *42*−*43*, 123–127.
(342) Kromer, B. R.; Cao, L.; Cumaranatunge, L.; Mulla, S. S.; Ratts, J. L.; Yezerets, A.; Currier, N. W.; Ribeiro, F. H.; Delgass, W. N.; Caruthers, J. M. *Catal. Today* **2008**, *136*, 93–103.
(343) Xu, J.; Harold, M. P.; Balakotaiah, V. Appl. Catal., B: Environ., http://dx.doi.org/10.1016/j.apcatb.2008.11.017.
(344) Larson, R. S.; Pihl, J. A.; Chakravarty, V. K.; Toops, T. J.; Daw, C. S. *Catal. Today* **2008**, *136*, 104–120.
(345) Dawody, J.; Skoglundh, M.; Olsson, L.; Fridell, E. *Appl. Catal., B: Environ.* **2007**, *70*, 179–188.
(346) Asanuma, T.; Takeshima, S.; Yamashita, T.; Tanaka, T.; Murai, T.; Iguchi, S. *SAE Tech. Pap. Ser.* **1999**, 1999-01-3501.
(347) Koci, P.; Marek, M.; Kubicek, M.; Maunula, T.; Harkonen, M. *Chem. Eng. J.* **2004**, *97*, 131–139.
(348) Sharma, M.; Harold, M. P.; Balakotaiah, V. *Ind. Eng. Chem. Res.* **2005**, *44*, 6264–6277.
(349) Kwak, J. H.; Hu, J. Z.; Kim, D. H.; Szanyi, J.; Peden, C. H. F. *J. Catal.* **2007**, *251*, 189–194.
(350) Yi, C. W.; Szanyi, J. *J. Phys. Chem. C* **2009**, *113*, 716–723.
(351) Ozensoy, E.; Peden, C. H. F.; Szanyi, J. *J. Phys. Chem. B* **2006**, *110*, 17001–17008.
(352) Ozensoy, E.; Peden, C. H. F.; Szanyi, J. *J. Phys. Chem. B* **2006**, *110*, 17009–17014.
(353) Ozensoy, E.; Peden, C. H. F.; Szanyi, J. *J. Phys. Chem. B* **2006**, *110*, 8025–8034.
(354) Xu, L.; Graham, G.; McCabe, R. W. *Catal. Lett.* **2007**, *115*, 108–113.
(355) Partridge, W. P.; Storey, J. M.; Smithwick, R. A.; Devault, G. L.; Cunningham, M. J.; Currier, N. W.; Yonushonis, T. M. *SAE Tech. Pap. Ser.* **2000**, 2000-01-2952.
(356) Mosqueda-Jimenez, B. I.; Lahougue, A.; Bazin, P.; Harle, V.; Blanchard, G.; Sassi, A.; Daturi, M. *Catal. Today* **2007**, *119*, 73–77.
(357) Fang, H. L.; Huang, S. C.; Yu, R. C.; Wan, C. Z.; Howden, K. *SAE Tech. Pap. Ser.* **2002**, 2002-01-2889.
(358) Wei, X.; Liu, X.; Deeba, M. *Appl. Catal., B: Environ.* **2005**, *58*, 41–49.
(359) Kabin, K. S.; Muncrief, R. L.; Harold, M. P.; Li, Y. J. *Chem. Eng. Sci.* **2004**, *59*, 5319–5327.
(360) Zheng, M.; Reader, G. T. *Energy Convers. Manage.* **2004**, *45*, 2473–2493.
(361) Theis, J. R.; Goebel, U.; Koegel, M.; Kreuzer, T.; Lindner, D.; Lox, E. S. J.; Ruwisch, L. *SAE Tech. Pap. Ser.* **2002**, 2002-01-0057.
(362) Schenk, C.; McDonald, J.; Laroo, C. *SAE Tech. Pap. Ser.* **2002**, 2001-01-3619.
(363) Gleaves, J. T.; Ebner, J. R.; Kuechler, T. C. *Cat. Rev.—Sci. Eng.* **1988**, *30*, 49–116.
(364) Hendershot, R. J.; Rogers, W. B.; Snively, C. M.; Ogunnaike, B. A.; Lauterbach, J. *Catal. Today* **2004**, *98*, 375–385.
(365) Hendershot, R. J.; Fanson, P. T.; Snively, C. M.; Lauterbach, J. A. *Angew. Chem., Int. Ed.* **2003**, *42*, 1152–1155.
(366) Vijay, R.; Lauterbach, J. *Stud. Surf. Sci. Catal.* **2007**, *171*, 325–359.
(367) Choi, J. S.; Partridge, W. P.; Daw, C. S. *Appl. Catal., B: Environ.* **2007**, *77*, 145–156.
(368) Hendershot, R. J.; Vijay, R.; Feist, B. J.; Snively, C. M.; Lauterbach, J. *Meas. Sci. Technol.* **2005**, *16*, 302–308.
(369) Hendershot, R. J.; Vijay, R.; Snively, C. M.; Lauterbach, J. *Chem. Eng. Sci.* **2006**, *61*, 3907–3916.
(370) Muncrief, R. L.; Kabin, K. S.; Harold, M. P. *AIChE J.* **2004**, *50*, 2526–2540.
(371) West, B. H.; Huff, S. P.; Parks, J. E.; Lewis, S. A.; Choi, J. S.; Partridge, W. P.; Storey, J. M. *SAE Tech. Pap. Ser.* **2004**, 2004-01-3023.
(372) Choi, J. S.; Partridge, W. P.; Epling, W. S.; Currier, N. W.; Yonushonis, T. M. *Catal. Today* **2006**, *114*, 102–111.
(373) Aftab, K.; Mandur, J.; Budman, H.; Currier, N. W.; Yezerets, A.; Epling, W. S. *Catal. Lett.* **2008**, *125*, 229–235.
(374) Urakawa, A.; Maeda, N.; Baiker, A. *Angew. Chem., Int. Ed.* **2008**, *47*, 9256–9259.

CR800496F